博士論文

Development of DNA and RNA manipulation using ultrafast photo-cross-linking toward for nucleic acid editing

渡部　康羽

主指導教員　藤本　健造

北陸先端科学技術大学院大学

先端科学技術研究科 [マテリアルサイエンス]

令和 4 年 3 月

Table of Contents

Chapter 1: General Introduction

1.1.1 Nucleic Acid-Based Drugs

Recently, the mainstream disease treatment is antibody drugs. However, when the Human Genome Project was completed in 2003, genetic engineering developed and nucleic acid medicine attracted attention. The characteristic of nucleic acid medicine is to treat the disease at the genetic level, and it is expected to be applied to genetic diseases such as familial Alzheimer's disease. Nucleic acid drugs are classified into 4 methods. (1) Oligodeoxynucleotide (ODN) antisense method that binds to DNA and inhibits RNA transcription[1], (2) antisense method that binds to mRNA and inhibits protein translation [2], (3) RNAi method that interferes with DNA-RNA double strand and cleaves RNA[3], ④ aptamer method that binds to a specific nucleic acid or peptide[4]. Nucleic acid drugs are marketed mainly in the United States and Europe using the antisense method, RNAi method, and aptamer method. Nucleic acid drugs on the market have high immediate effects targeting mRNA and proteins. However, mRNA and protein are molecules that are constantly being produced in the body, and only temporary effects can be obtained. In other words, in order to treat a fundamental genetic disease, it is necessary to inhibit the process of transcription of mRNA from DNA.

Restriction enzymes are well-known as a tool for cleaving target DNA in genetic engineering. Restriction enzymes, however, can only recognize 6-8 bases of DNA and cannot cut genomic DNA in a precise position. The CRISPR-Cas9 [5] artificial restriction enzyme was developed in response to such conditions, making it possible to modify genomic DNA in a specific location. CRISPR-Cas9 uses a 20-mer sgRNA that can recognize genomic DNA in a specific spot and is characterized by the ease with which sgRNA may be artificially modified. Experimental procedures are simpler and less expensive than those used with artificial restriction enzymes (ZFN [6], TALEN [7]), and fluorescent dye labeling is also conceivable. It does, however, have issues with off-target effects and Cas9 delivery to the afflicted area.

As CRISPR technology improves, so does the development of genome editing approaches based on synthetic nucleic acids. PNA and LNA, for example, create a strong hybridization with DNA in a usual approach. Due to its remarkably rapid action, the antigene technique employing artificial nucleic acids has a smaller molecule than protein enzymes and is relatively straightforward to deliver into the afflicted area. It is projected to be used as a

nucleic acid medicine. Furthermore, the interaction of the synthetic nucleic acid with genomic DNA can result in the formation of a single-stranded structure. It is possible to cleave and alter single-stranded genomic DNA by combining nucleases and small compounds (Ce/ EDTA) that act particularly on single-stranded genomic DNA.

However, PNA and LNA methods have low reactivity and are difficult to use for genome manipulation. Therefore, DNA-targeted nucleic acid drugs have not yet been commercialized.

Product name	Popular name	Classification	Chemical modification	DDS	Approved country/year	Target molecule	Target disease	Administration
Vitravene	Fomivirsen	Antisense	PS (full)	Naked	America 1998 Europe 1999	CMV IE2 mRNA	CMV retinitis	Intravitreal
Macugen	Pegaptanib	Aptamer	2'-Ome, 2'-F	Naked (PEG-conjugate)	America 1998 Europe 1999 Japan 2008	VEGF165	Exudative age-related macular degeneration	Intravitreal
Kynamro	Mipomersen	Antisense	PS (full) 2'-MOE	Naked	America 2013	ApoB-100 mRNA	Homozygous familial hypercholesterolemia	Subcutaneous
Exondys 51	Eteplirsen	Antisense	Morpholino nucleic acid	Naked	America 2016	Dystrophin pre-mRNA	Duchenne muscular dystrophy	Intravenous
Spinraza	Nusinersen	Antisense	PS (full) 2'-MOE	Naked	America 2016 Europe 2017 Japan 2017	SMN2 pre-mRNA	Spinal muscular atrophy	Intramedullary cavity
HEPLISAV-B	CpG1018	CpG oligo	PS(full)	Naked	America 2017 Europe 2019	TLR9	Hepatitis B	Intramuscular
Tegsedi	Inotersen	Antisense	PS(full) 2'-MOE	Naked	America 2018 Europe 2018	TTR mRNA	Hereditary ATTR amyloidosis	Subcutaneous
Onpattro	Patisiran	siRNA	2'-OMe	LNP	America 2018 Europe 2018 Japan 2019	TTR mRNA	Hereditary ATTR amyloidosis	Intravenous
Waylivra	Volanesorsen	Antisense	PS(full) 2'-MOE	Naked	Europe 2019	ApoCIII mRNA	Familial hyperchylomicronemia	Subcutaneous
Givlaari	Givosiran	siRNA	PS(partial) 2'-MOE, 2'-F	Naked (GalNAc-conjugate)	America 2020 Europe 2020 Japan 2021	ALAS1 mRNA	Acute hepatic porphyria	Subcutaneous
Vyondys 53	Golodirsen	Antisense	Morpholino nucleic acid	Naked	America 2019	Dystrophin pre-mRNA	Duchenne muscular dystrophy	Intravenous
Vitepso	Vlitolarsen	Antisense	Morpholino nucleic acid	Naked	America 2020 Japan 2020	Dystrophin pre-mRNA	Duchenne muscular dystrophy	Intravenous
Oxlumo	Lumasiran	siRNA	PS(partial) 2'-MOE, 2'-F	Naked (GalNAc-conjugate)	America 2020 Europe 2020	HAO mRNA	Primary hyperoxalate type I	Subcutaneous
Leqvio	Inclisiran	siRNA	PS(partial) 2'-MOE, 2'-F	Naked (GalNAc-conjugate)	Europe 2020	PCSK9 mRNA	Hyperlipidemia/Mixed Dyslipidemia	Subcutaneous
Amodys 45	Casimersen	Antisense	Morpholino nucleic acid	Naked	America 2021	Dystrophin pre-mRNA	Duchenne muscular dystrophy	Intravenous

Figure 1.1. Approved Nucleic Acid Drug (May 2021)

1.1.2 DNA and RNA structure

DNA (deoxyribonucleic acid) and RNA (ribonucleic acid) are genetic information of living organisms and are widely known as blueprint for forming biological structures. This section describes the history and structure of DNA. Nucleic acid chemistry begins with Johannes Friedrich Miescher extracting nucleic acid from the cell nucleus in 1869[8]. Nucleic acids are separated into DNA and RNA and are made up of three domains: acid-base, sugar, and phosphate, according to Phoebus Levene, who discovered them in 1929. Adenine, cytosine, thymine, and guanine are 4 types of bases found in DNA, thymine is replaced by uracil in RNA [9]. Deoxyribose and ribose, respectively, are sugars found in DNA and RNA. RNA is extremely reactive and less stable than DNA because it possesses a hydroxy group as a

substituent at the 2'position of the sugar [10]. The tetranucleotide hypothesis [11] proposing a model in which four bases were combined into a single molecule was accepted at the time of nucleic acid discovery. According to the tetranucleotide hypothesis, the molar ratios of all four bases are equivalent. Erwin Chargaff later discovered that the base abundance ratio was A = T, G = C (Chargaff's rule) [12]. A double helix structure of DNA was reported in 1953 by James Dewey Watson and Francis Harry Compton Crick, proposing that DNA is genetic information [13]. The double helix of DNA has a number of properties. 1. Each polynucleotide chain in the double helix is made up of two polynucleotide chains. 2. The two polynucleotides have the same direction of travel (antiparallel). 3. The double helix has a right-handed orientation. 4. The backbone containing the phosphate group is orientated outwards, whereas the base is oriented inside the double helix. 5. The bases are joined by hydrogen bonds and are complimentary. 6. At around 10 base pairs, the double helix rotates once. 7. There are two grooves in the double helix: a major groove and a minor groove. A and T, as well as G and C, are hydrogen-bonded Watson-Crick base pairs (Fig.1.3). Hoogsteen base pairs creating triple and quadruple chains, on the other hand, have been identified. When the target sequence is a homopurine sequence, the triple chain is formed, and the quadruple chain is formed by arranging four guanines in a plane. Compared to Watson-Crick base pairs, Hoogsteen base pairs are rare, but their distinctive structure is likely to be useful in sectors like nucleic acid therapeutics and aptamers.

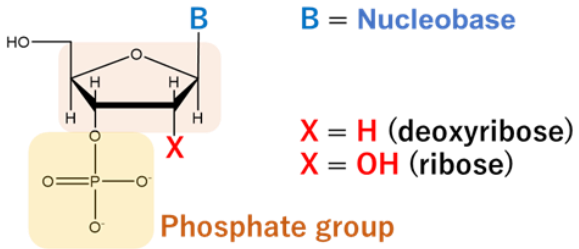

B = Nucleobase

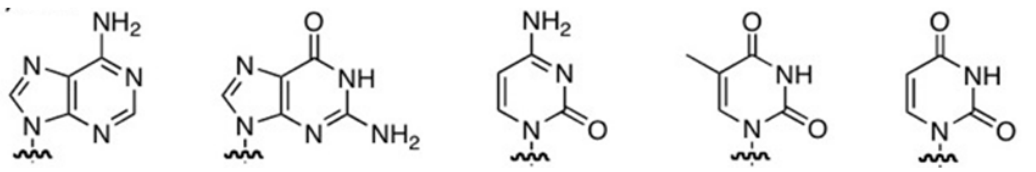

Adenine (DNA/RNA) Guanine (DNA/RNA) Cytosine (DNA/RNA) Thymine (DNA/RNA) Uracil (DNA/RNA)

Figure 1.2. Nucleic acid structure

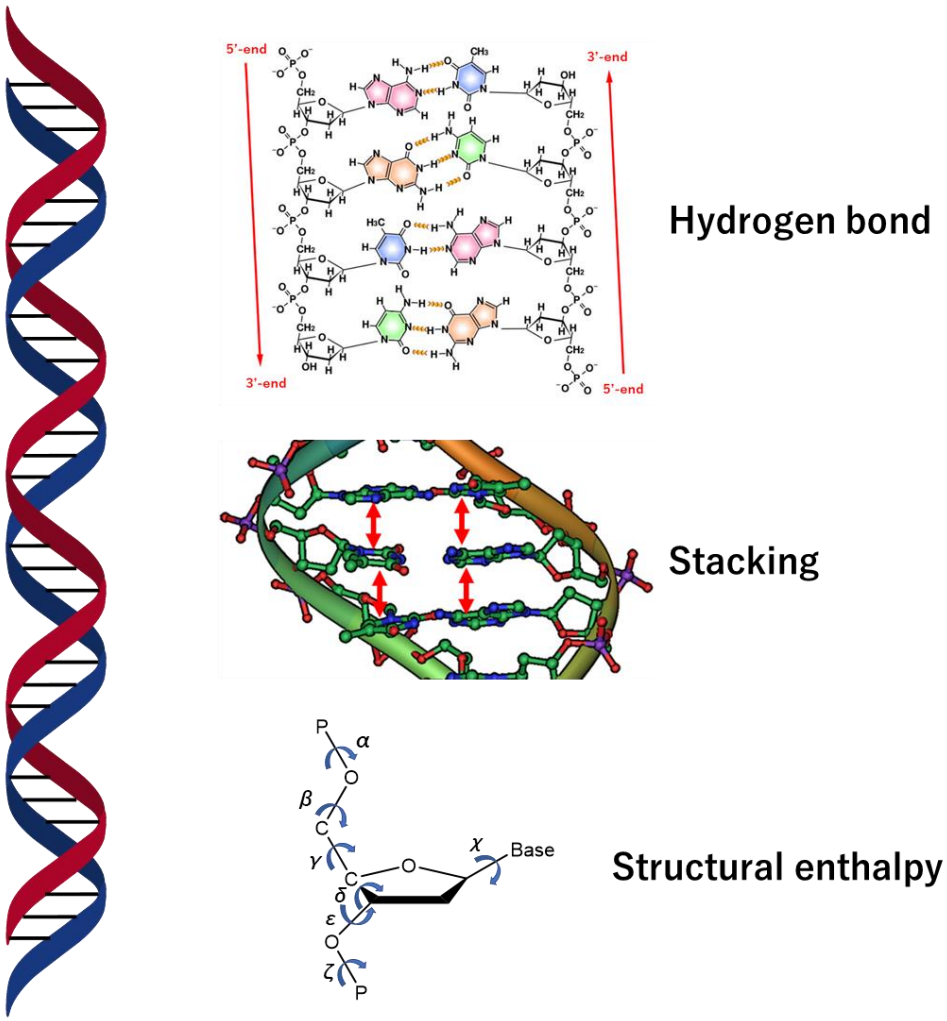

Figure 1.3. DNA double helix structure, Watson click base pair

1.1.3 Central dogma

Proteins were thought to constitute genetic information before DNA was discovered to be genetic information. Meanwhile, Torbjörn Oskar Caspersson of Sweden and Jean Louis Auguste Bracht of France stated in the early 1940s that intermediates were involved in DNA and proteins [14, 15]. Protein synthesis is now known to occur outside of the nucleus on a structure called the ribosome, which is made up of RNA and proteins [16]. In some viruses, RNA appears to carry genetic information in place of DNA, and there appears to be a strong link between DNA and RNA in the transmission of genetic information.

Based on these observations, Crick suggested the Central Dogma in 1958[17], which went

further than the adaptor molecule prediction. The genetic information is saved in DNA, which is copied into RNA, which is then translated into an amino acid sequence by some method to generate a protein. Each amino acid has been linked to an RNA [18], and transfer RNA (tRNA), which transports amino acids during protein synthesis, has also been discovered [19]. This information, however, was insufficient to explain the substance that transports DNA information from the nucleus to the ribosome. Elliot Volkin and Lazarus Astrachan infected E. coli with T2 phage and gave it radioactive phosphorus (^{32}P) to analyze the base chemically. They discovered that they could make short-lived RNA (DNA-like-RNA) that looked more like T2 phage DNA than E. coli DNA [20]. Based on their study on the enzyme -galactosidase in E. coli, Francois Jacob and Jacques Monod hypothesized that when an enzyme protein was generated from a gene, the presence of an unstable molecule X was required [21]. It was further clarified that the unstable molecule is a DNA-like-RNA found by Volkin and Astrakhan, and it is responsible for copying nuclear DNA's genetic information and transmitting it to the ribosome [22]. As a result, the intermediate material X was given the name messenger RNA (mRNA) since it communicates genetic information.

The core idea depicted in the picture is now generally known as a result of these research. Retroviruses have been found to replicate DNA by utilizing reverse transcriptase and using RNA as a template, with certain exceptions. [23] Howard M. Temin anticipated that there would be a reverse transcription phenomenon.

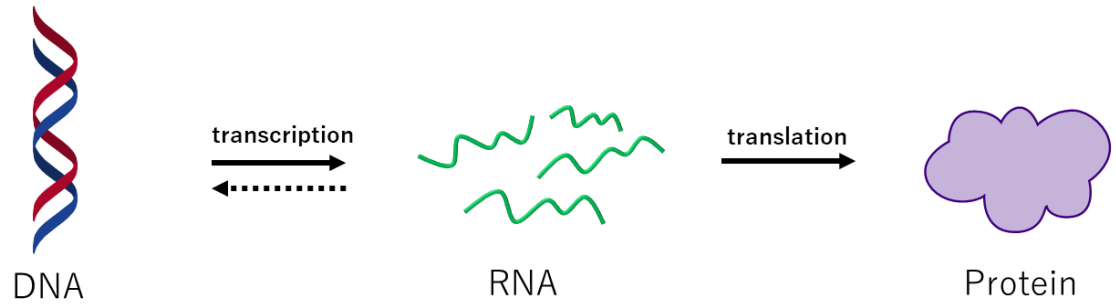

Figure 1.4. Centraldogma

1.1.4 Transcription, Translation

The following is how mRNA transcription works. 1. Transcription factors bind to the promoter region on the DNA strand. 2. The DNA double helix dissociates locally as RNA polymerase attaches to transcription factors. 3. RNA polymerase moves in the 3' 5' direction

and operates on her single strand of them. 4. RNA is produced by utilizing ribonucleotide triphosphate as a substrate at the same time. 5. The DNA bases C, T, G, and A are replicated into RNA as G, A, C, and U, which are complementary to each other. 6. From the 5'end to the 3'end, the RNA strand stretches. 7. During stretching, ribonucleotide triphosphate is added to her 3'end, and two phosphate groups are removed. A portion of RNA produced from DNA is connected to protein design (exon) and a portion is not related to protein design (intron). Splicing is the process of eliminating introns from RNA and connecting exons together [24]. Furthermore, the attachment of a methylation GTP termed 5'-Cap to the 5' end of mRNA enhances ribosome interaction and prevents ribonuclease destruction. The 5' end of mRNA contains a cap structure, whereas the 3' end has a poly A chain. The translation initiation factor eIF4E attaches to the 5'end cap structure as well as the 3'end poly A-binding protein, and the two form a complex through the translation initiation factor eIF4G, which is a scaffold protein, resulting in a cyclic structure for the mRNA [25]. Furthermore, the translation terminator eRF3 binds to PABP-eIF4G and loops out the 3'UTR [26]. Some mRNA bases are changed in the nucleus and directed out of the nucleus through nuclear pores by RNA-binding proteins. The 5'end cap structure and the 3'end poly A chain not only boost the efficiency of such translation, but they also stabilize the mRNA by blocking exonuclease degradation from the end, which improves translation efficiency. It plays an important role in the regulation of gene expression following transcription in both mRNA stabilization processes.

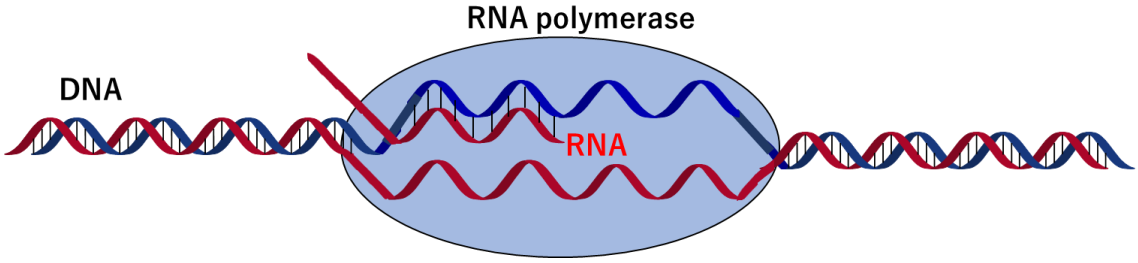

Figure 1.5. Pre-mRNA transcription by RNA polymerase

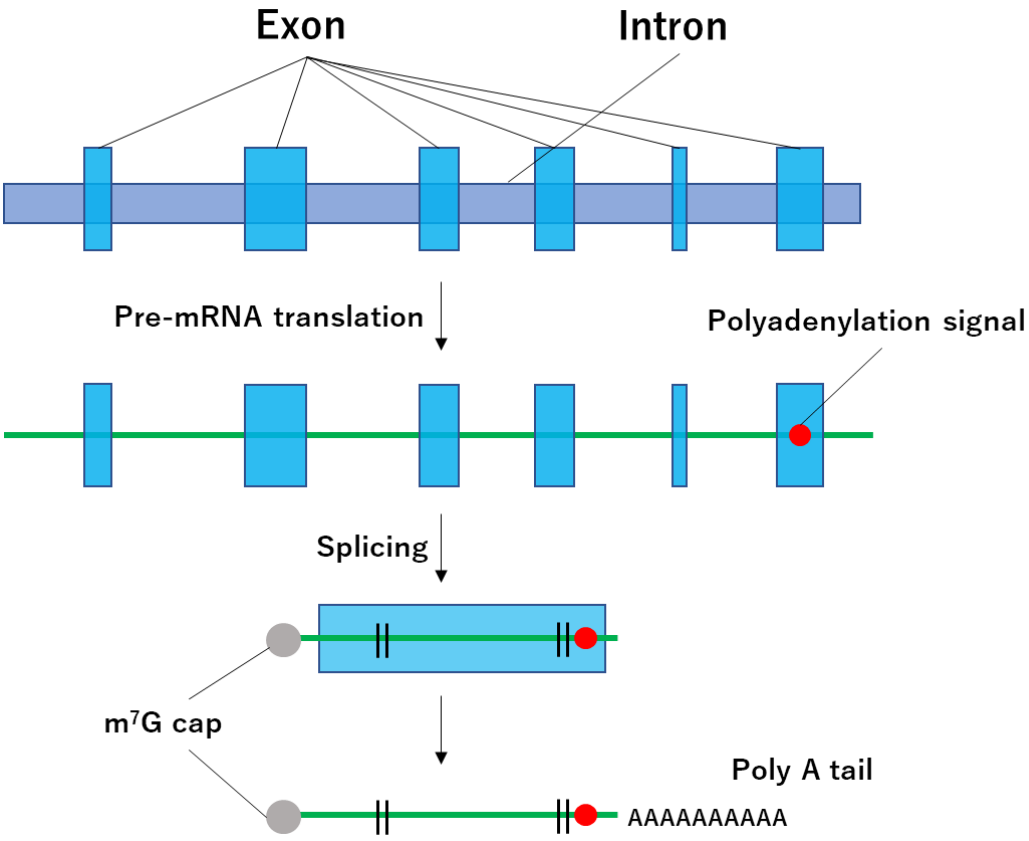

Figure 1.6. Process from transcription to splicing

To manufacture proteins, mRNA is transferred from the nucleus to the cytoplasm and binds to ribosomes, which are made up of two subunits, the large and the small subunits (translation). Ribosomes are large protein-RNA complexes, and ribosomal RNA (rRNA) is the RNA that makes up the ribosome [27]. The large subunit binds after the mRNA binds to the small subunit, and the large and small subunits travel along the mRNA toward the 3' end while binding amino acids. The amino acids corresponding to the base sequence are transported to the ribosome by transfer RNA (tRNA) [28]. The anticodon of tRNA is a triad base sequence that matches to the codon of mRNA. The aminoacyl-tRNA synthetase links the tRNA to the amino acid that corresponds to each anticodon. Aminoacyl-tRNA synthetases come in 20 different varieties, each with sites that recognize three different sorts of molecules: amino acids, tRNA, and ATP. Ribosomes have tRNA binding sites named A, P, and E, which are mostly made up of rRNA, and the catalytic site for peptide binding is a big subunit of rRNA rather than a protein. The tRNA separates from the ribosome when one amino acid is attached to the next amino acid. Peptide bonds join amino acids, and polypeptide production begins. The extended polypeptide folds into a three-dimensional structure, which can perform and performs the function of a protein.

	U		C		A		G		
U	UUU	Phe/F	UCU	Ser/S	UAU	Tyr/Y	UGU	Cys/C	U
	UUC	Phe/F	UCC	Ser/S	UAC	Tyr/Y	UGC	Cys/C	C
	UUA	Leu/L	UCA	Ser/S	UAA	Stop	UGA	Stop	A
	UUG	Leu/L	UCG	Ser/S	UAG	Stop	UGG	Trp/W	G
C	CUU	Leu/L	CCU	Pro/P	CAU	His/H	CGU	Arg/R	U
	CUC	Leu/L	CCC	Pro/P	CAC	His/H	CGC	Arg/R	C
	CUA	Leu/L	CCA	Pro/P	CAA	Gln/Q	CGA	Arg/R	A
	CUG	Leu/L	CCG	Pro/P	CAG	Gln/Q	CGG	Arg/R	G
A	AUU	Ile/I	ACU	Thr/T	AAU	Asn/N	AGU	Ser/S	U
	AUC	Ile/I	ACC	Thr/T	AAC	Asn/N	AGC	Ser/S	C
	AUA	Ile/I	ACA	Thr/T	AAA	Lys/K	AGA	Arg/R	A
	AUG	Met/M (Start)	ACG	Thr/T	AAG	Lys/K	AGG	Arg/R	G
G	GUU	Val/V	GCU	Ala/A	GAU	Asp/D	GGU	Gly/G	U
	GUC	Val/V	GCC	Ala/A	GAC	Asp/D	GGC	Gly/G	C
	GUA	Val/V	GCA	Ala/A	GAA	Glu/E	GGA	Gly/G	A
	GUG	Val/V	GCG	Ala/A	GAG	Glu/E	GGG	Gly/G	G

Figure 1.7. Genetic code table

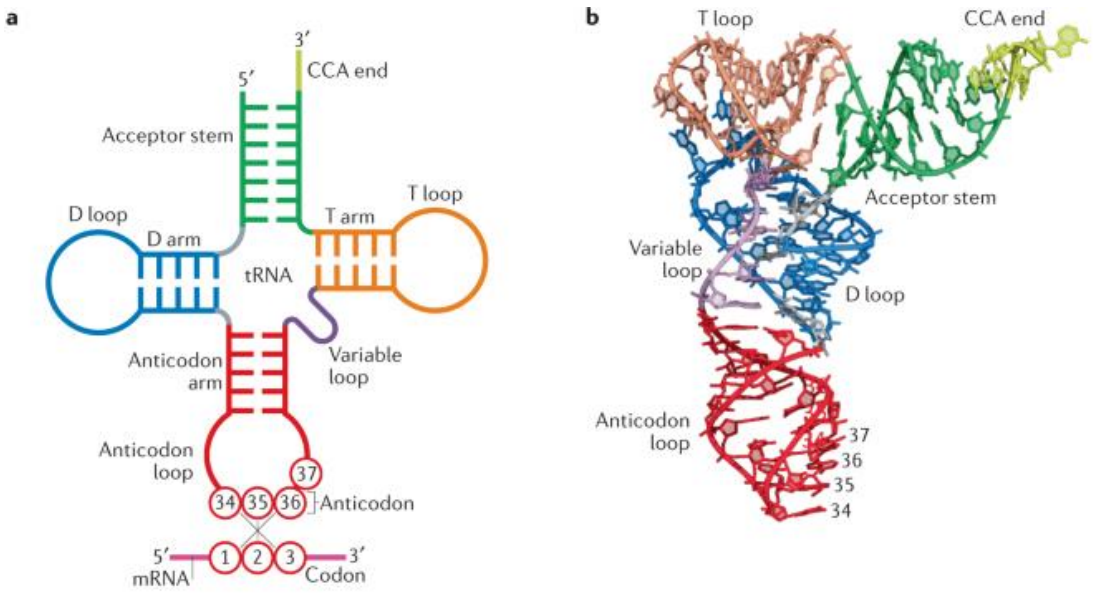

Figure 1.8. (a) Cloverleaf structure of transfer RNA (tRNA) with codon–anticodon pairing. (b) Tertiary structure of tRNA. The coordinates are obtained from Protein Data Bank entry 1EHZ. (*Nat Rev Mol Cell Biol.* **2021**, 375-392.)

Regulation of proteins that express biological functions can also be achieved by controlling transcription and translation. Artificial oligonucleotides can be used to interact with target sequences to inhibit splicing and tRNA binding.

1.1.5 Oligodeoxynucleotide synthesis

Nucleic acid (DNA, RNA) are biopolymers that can store and express genetic information, and its molecular structure has been clarified. On the other hand, from a chemical point of view, nucleic acids are biopolymers composed of carbon, hydrogen, nitrogen, oxygen, and phosphorus atoms. In other words, nucleic acids can be artificially synthesized. Nucleic acid sequences that exist in nature can be amplified by PCR [29], but specific sequences of dozens of bases are difficult to amplify. Nucleic acid synthesis has been studied since the 1950s, but the phosphate diester method (HG Khorana) [30], phosphodiester method (R. Letsinger et al. And C. Reese)[31], are only used phosphite method[31] used by around 1980. In the triester method, there are problems such as low yield and stability of the intermediate. In particular, nucleic acid synthesis requires repeated coupling reactions, so the yield should be as close to 100% as possible. Therefore, Marvin H. Caruthers developed a method for chemically synthesizing DNA using phosphoramidite [33]. Phosphoramidite is a compound in which the 3'position of a nucleoside (or deoxynucleoside), a cyanoethoxy group, and a dialkylamino group are bonded to a phosphorus atom. The steps of the phosphoramidite method are as follows. (1) Deprotection: Remove the 4,4'-dimethoxytrityl group (DMTr group) at the 5' position from the nucleoside supported on the solid phase. (2) Coupling: The nucleoside from which the DMTr group at the 5'position was removed in (1) is condensed with phosphoramidite (nucleic acid monomer) and an activator (activator). (Amidite activator) ③ Capping: In order to suppress side reactions, the 5'-hydroxyl group of the unreacted chain generated in ② is acetylated. ④ Stabilization: Converts phosphite ester to stable phosphate ester or thiophosphate ester by oxidation or sulfurization. Phosphoramidite is relatively stable and can be stored for a long period of time, and the reaction proceeds in high yield.

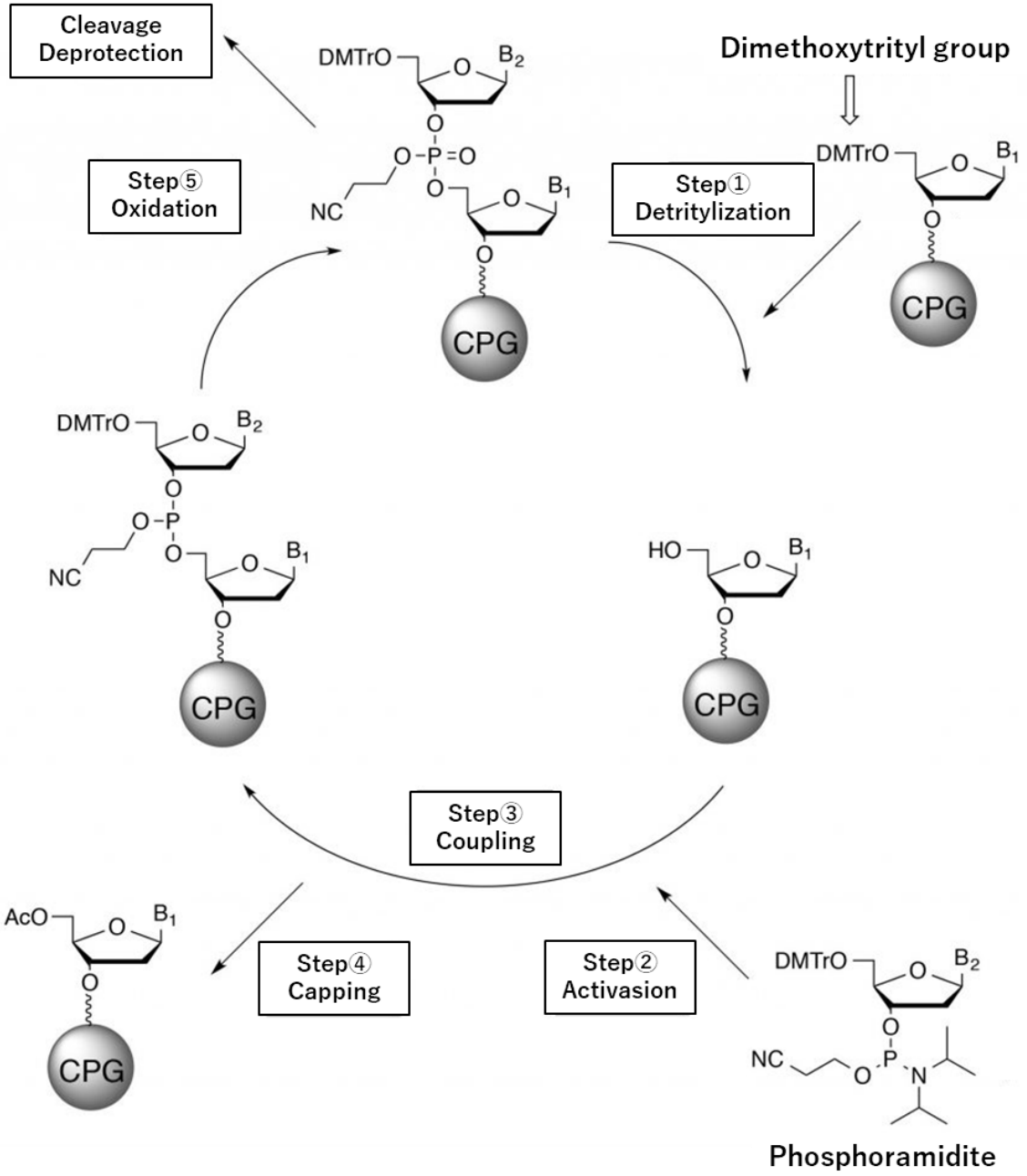

Figure 1.9. Phosphoramidite method

1.2 Antisense

ASOs are single-stranded molecules with a length of 15 to 30 nucleotides [34]. A variety of molecular modifications, similar to siRNAs, have been utilized to improve the pharmacological profile. The use of phosphorothioate as a substitute for phosphodiester connections between nucleotide bases confers resilience to nucleases and enhances binding to plasma proteins, extending plasma half-life and boosting the likelihood of target tissue uptake[35]. Other changes include, but are not limited to, substituting 20-O-methyl, 20-O-methoxyethyl, and 20-fluoro groups for the 20-hydroxyl moiety to boost resistance to nuclease-mediated destruction. ASOs affect gene expression in two ways [36]. To begin with, ASOs can occupy the target mRNA without causing it to degrade, preventing it from being translated. Changes in RNA processing and suppression of the target mRNA's interaction with critical proteins, among other methods, are used to achieve this. Second, ASOs can cause the target mRNA to be degraded by a variety of processes, one of which being RNase H1 cleavage. A DNA sequence in the middle of the ASO molecule (gap) flanked on both sides by 20 -O-methoxyethyl– modified RNA nucleotides has been found as the structure that optimally exploits this process [37, 38]. RNase H1 degradation of mRNA is selective for RNA in an RNA-DNA duplex and occurs in both the cytoplasm and the nucleus [39]. In contrast to siRNA, most ASOs prevent the translation of mRNA based on one-to-one stoichiometry. Antisense nucleic acid is the oldest developed method, and in 1998, fomivirsen (Vitravene), a treatment for cytomegalovirus retinal inflammation for AIDS patients, was approved as a nucleic acid drug for the first time [40].

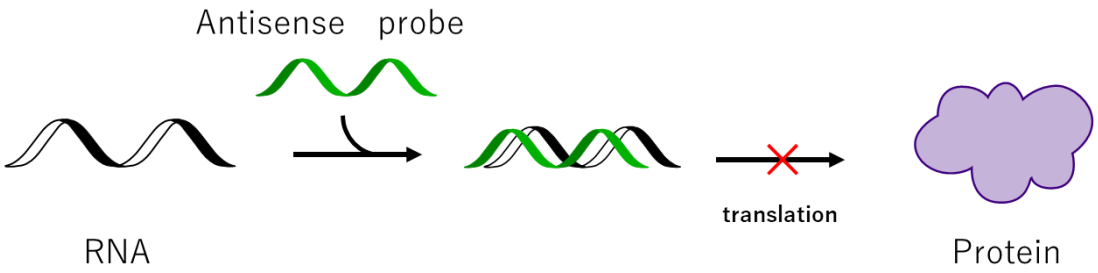

Figure 1.10. Antisense method

1.3. siRNA method

In 2006, Andrew Z. Fire and Craig C. Mello were awarded the Nobel Prize in Physiology or Medicine for the discovery of RNA interference (RNAi), in which double-stranded RNA specifically cleaves mRNA [41]. RNAi is a mechanism by which double-stranded RNA forms a complex with a protein and specifically pairs and cleaves complementary messenger RNA. Similar to ASO, it is a phenomenon that suppresses gene expression. It seems to be involved in maintaining the stability of the genome by suppressing the defense mechanism against viral infection [42] and the genes that metastasize and move on the genome [43]. In addition, it has become clear that a large number of short double stranded RNAs called microRNAs (miRNAs) are expressed *in vivo* and regulate the expression of many genes. Furthermore, RNA interference can also be applied to artificially suppress gene function, so it is attracting attention as a highly versatile tool for gene function analysis.

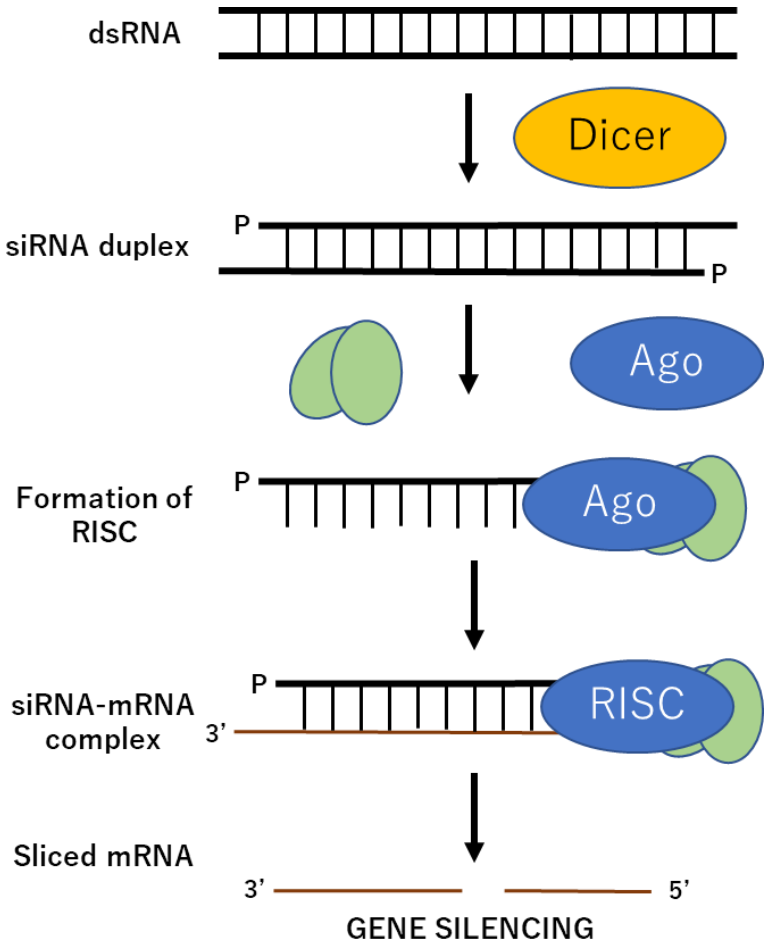

Figure 1.11 siRNA method

1.4 Ribozyme

In the body, enzymes that act as catalysts are frequently involved in chemical reactions. Nucleases, ligases, and polymerases are very important molecules that can be used as nucleic acid editing tools *in vivo*. and there are various types of enzymes such as redox, isomerization, and hydrolysis. On the other hand, it has been proven that RNA can be cleaved by the splicing process without the use of an enzyme. In 1989, Thomas Cech and Sidney Altman earned the Nobel Prize for discovering a ribozyme in which nucleic acids cleave nucleic acids [44]. The discovery of ribozymes suggests that information-holding RNA is catalytic. It was demonstrated that RNA may evolve on its own by repeated cleavage and ligation. Harry Noller et al. reported in 1992 that thermophile 23S rRNA could generate peptide linkages after being extensively deproteinized, revealing the ability of RNA to make proteins [45]. In 1998, Kimitsuna Watanabe et al. discovered that Escherichia coli's 23S rRNA catalyzes the synthesis of peptide bonds. [46] To put it another way, atomic life is thought to begin with RNA, which acts as a catalyst for protein production in order to exhibit biological functions. There are various types of ribozymes. The hammerhead ribozyme, a self-cleaving RNA, is one of them [47]. This ribozyme was identified in viroids and plant viruses' satellite RNA, which is a single-stranded RNA. When heated combined with magnesium ions, the sequence of these RNAs breaks by itself, and the secondary structure of that section is shaped like a hammerhead, hence the term hammerhead ribozyme. A hairpin ribozyme has been discovered in addition to the hammerhead ribozyme. The nucleotide sequences conserved among diverse hammerhead ribozymes were then deciphered, and it was discovered that they were split between an enzyme area and a substrate region that recognizes the sequence. Ribozymes are tiny and simple to make, and several artificial ribozymes have already been created and their activity and selectivity validated [48].

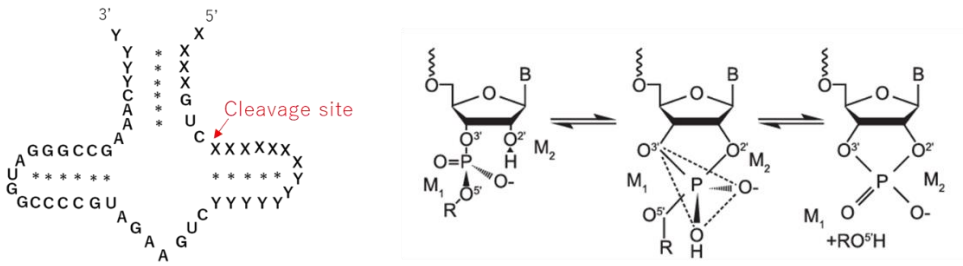

Figure 1.12 Hammerhead ribozyme secondary structure and RNA degradation scheme

1.5 DNAzyme

Ribozymes are particularly unique molecules in which nucleic acids alter RNA and are predicted to be used in domains such as nucleic acid therapy and DNA nanotechnology [49, 50, 51]. However, because ribozyme is made up of RNA, its stability is quite low. Because of its limited stability, the flaws are mitigated by a method of lipofecting a large amount of ribozyme for use as RNAi [52] and a vector that can be produced in huge amounts. As a result, DNAzyme, a nucleic acid with enzymatic activity similar to ribozyme, was discovered. DNAzyme is less likely to be degraded than RNA, which improves its stability and facilitates its use. When compared to ribozyme, DNAzyme is less likely to be destroyed, which improves stability and makes artificial synthesis easier. DNAzymes with functionalities such as target mRNA cleavage [53], ligation [54], and DNA phosphorylation [55] have been created. They were discovered using *in vitro* screening technology (the SELEX method), and they have a high structural recognition capacity [56]. Those with RNA-cleaving activity are particularly useful in cancer treatment and are receiving study interest. DNAzyme, similar to ribozyme, is separated into a substrate region and a catalytic region that recognizes sequences. The more firmly Watson-click pairing attaches to the substrate, the longer the enzyme region is. [57] Several mRNA-cleaving DNAzymes have been produced, and two varieties, 8-17 DNAzyme and 10-23 DNAzyme, have shown to have very strong cleavage activity and have been studied extensively. Cations (Mg^{2+}, Cu^{2+}, Pb^{2+}, Mn^{2+}, Na^{+}) can cleave the phosphodiester link between the unpaired purine and the paired pyrimidine [58]. DNAzyme is also used in biosensors and DNA nanotechnology since it is more stable and easier to intentionally manipulate than Ribozyme and enzyme proteins, and it has a high substrate selectivity.

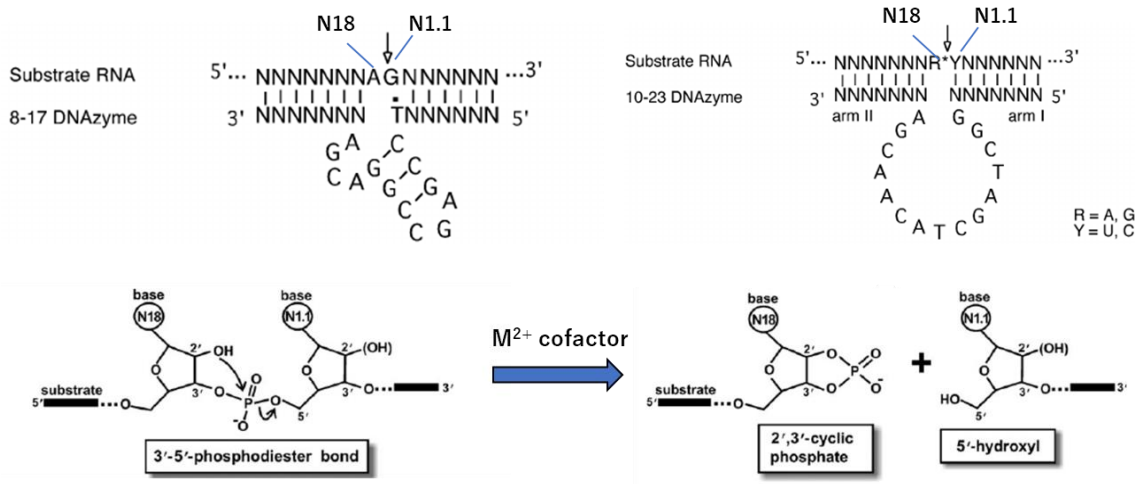

Figure 1.13 Two type DNAzymes and RNA cleavage schemes

1.6 Antigene

Recently, the majority of nucleic acid medications work by inhibiting protein translation by acting on RNA. However, because RNA is always copied from DNA, the effect of suppressing protein translation is only transitory. Inhibition of DNA-to-mRNA transcription, which is the most upstream of the basic dogma, is required for the final treatment of genetic diseases. Transcriptional suppression is particularly difficult since DNA forms a double helix structure and is more molecularly stable than RNA. Restriction enzymes are the most well-known DNA editing tool [59].

1.7 Restriction enzyme

Restriction enzymes cut DNA in bacteria to defend themselves against external foes like bacteriophage. It became possible to artificially recombine DNA, such as plasmids, after the sequence recognition bases of restriction enzymes were examined. However, restriction enzymes' sequence recognition bases are typically around 4-6 bases, making it challenging to specifically break long-chain DNA like genomic DNA. The recognition sequence of *BamH*I, for example, is GGATCC, and when it works on human and plant chromosomal DNA, it cleaves at a frequency of once every 4000-5000 base pairs and in pieces.

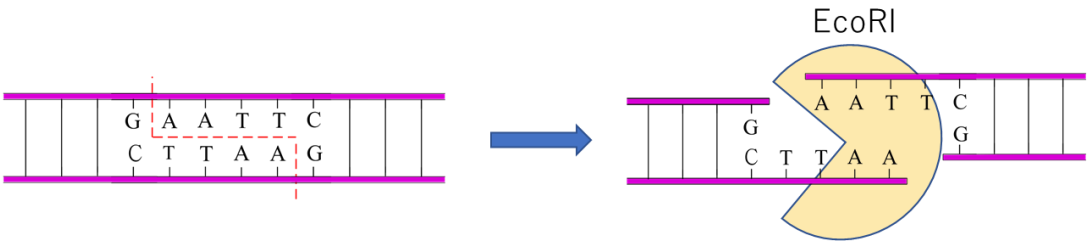

Figure 1.14 Cleavage scheme of restriction enzyme (EcoRI)

1.8 Artificial restriction enzymes

Most restriction enzymes have a recognition sequence length of 4-6 bp and are unable to cut genomic DNA in a position-specific manner. Restriction enzymes have been improved and a type that recognizes 10 bp has been developed, but it is not sufficient for application to genomic DNA. A recognition sequence of 20 bp or more is required for position-specific cleavage of genomic DNA. In this section, we will summarize the artificial restriction enzymes and show the current issues.

1.8.1. ZFN, TALEN

The first-generation zinc finger nuclease (ZFN) was discovered in 1996, and it was used to create an artificial restriction enzyme that could target genomic DNA. ZFN is a chimeric protein that has a DNA recognition and binding domain as well as a DNA cleaving domain (endonuclease FokI). In many organisms, the zinc finger is a protein found in the DNA-binding domain of transcription factors. Three bases can be recognized by one finger, and several fingers can be joined. A 4-finger ZFN, for example, can detect 12 bases, while a dimer can recognize a total of 24 bases [60]. Only one place in mammalian genomic DNA does a sequence of 24 bases appear consecutively. Among protein enzymes, ZFNs have the benefit of being tiny in size. However, the specificity of neighboring zinc fingers is affected by the zinc finger motifs ordered within the array, making the design and selection of modified zinc finger arrays more complicated and time-consuming. ZFNs with great specificity, on the other hand, are extremely difficult to make and have a high cost.

The second generation of genome editing tools, Transcription activator-like effector

nucleases (TALEN), was announced in 2010. The Transcription activator-like effector (TALE) and endonuclease FokI produced by the phytopathogenic bacterium Xanthomonas are used to create TALEN, an artificial restriction enzyme. TALE recognizes the nucleotide sequence using DNA binding repeats (TALE repeats) with 34 amino acid residues as a unit. A dimer can recognize 30-40 bases, while a TALE repeat can detect 15-20 bases [61]. Because each TALE domain's activity is confined to one nucleotide and does not impact the binding specificity of neighboring TALEs, TALEN engineering is easier than ZFN engineering.

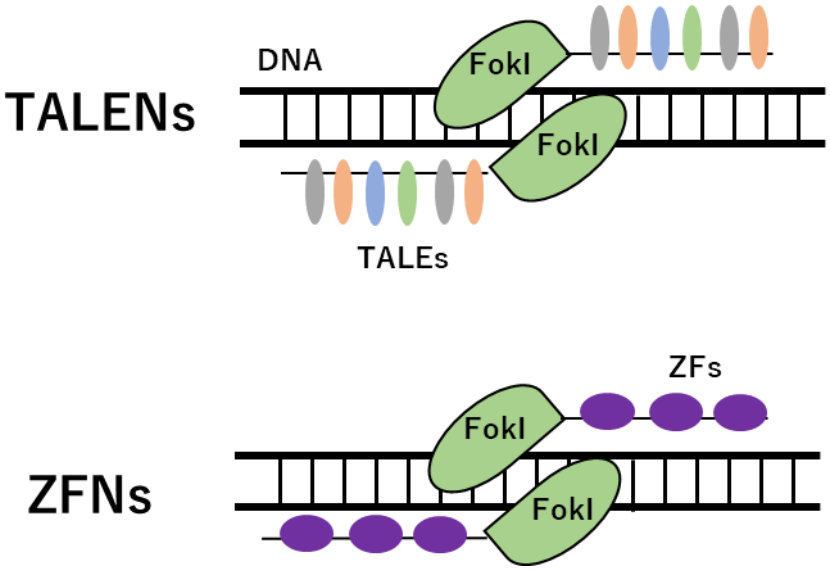

Figure 1.15 Binding to DNA by TALENs and ZFNs

ZFNs and TALENs are very useful, but have several drawbacks, including high system manufacturing costs, off-target cutting, and extensive processes that require time and effort.

1.8.2 CRISPR-Cas

Although the development of TALEN has simplified genome editing, the complexity of production and manipulation remains a hurdle. CRISPR-Cas9 is a third-generation artificial restriction enzyme that is exceedingly simple to create. It was first announced in 2012. Jennifer Doudna and Emmanuelle Charpentier collaborated to develop CRISPR-Cas9, a technology that makes use of the newly acquired immune system. [62] The viral DNA is taken

up at the CRISPR locus recently, and when it is infected again, the viral DNA is cleaved using a short RNA (single guide RNA: sgRNA) transcribed from the CRISPR locus. sgRNA is around 20 bases long and can target genomic DNA in a single location. Cas9 cleavage requires a sequence known as the PAM (protospacer flanking motif) sequence, which Cas9 recognizes in addition to sgRNA binding. 5'-NGG-3' is the normal wild Cas9 PAM recognition sequence. Because of its simplicity, the CRISPR-Cas system can be built and controlled in the laboratory, and research on it as a genome editing method is quickly expanding. Not only Cas9, but also Base Editor [63] has been developed to allow base altering (A to T, C to U). Cas12f [64], an RNA-targeting enzyme, has also been developed.

The CRISPR system is easy to modify artificially and light-triggered activity control has been reported.. The photoactivatable RNA N6-methyladenosine (m6A) editing system [65] was successfully switched from an inactive state to an active state in response to blue light. However, it requires upconversion nanoparticle membranes and multiple protein domains, which complicates design and manipulation.　The CRISPR system was originally created as a basic bacterial defensive mechanism. CRISPR, in other words, lacks a regulating mechanism. The longer CRISPR stays intracellularly for use as a nucleic acid medication, the more likely it is to be hazardous due to its off-target effect. Anti-CRISPR proteins that disable CRISPR have been developed as a solution to this problem [66]. To improve off-target impacts, 21 families have been discovered and studied so far [67].

In addition to sgRNA, PAM sequences are required, and sequence design is not completely unrestricted.

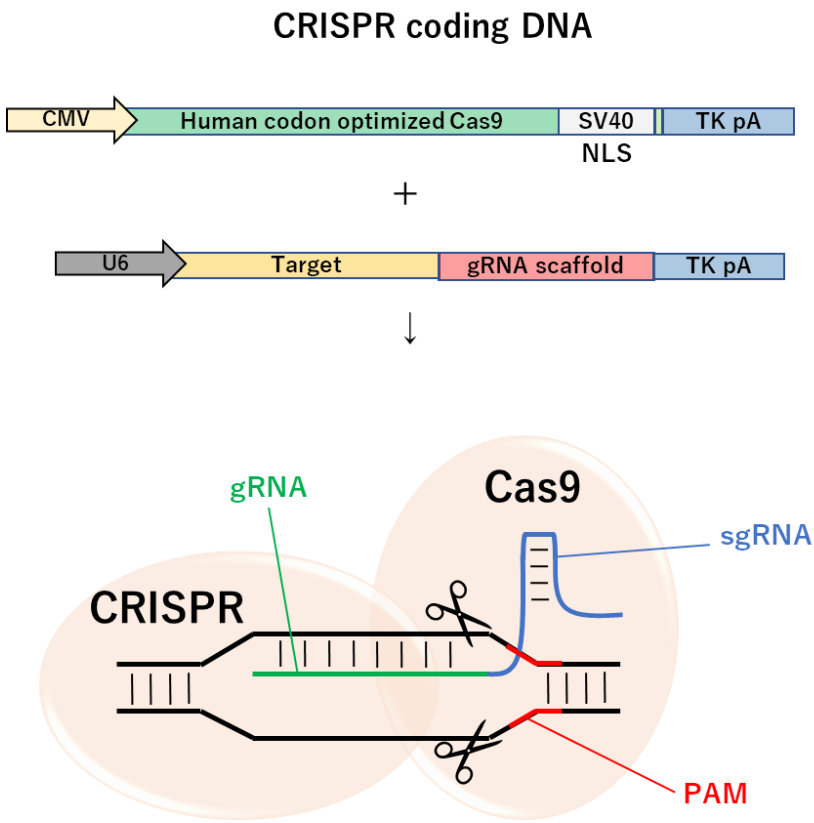

Figure 1.16 DNA cleavage scheme by CRISPR-Cas9

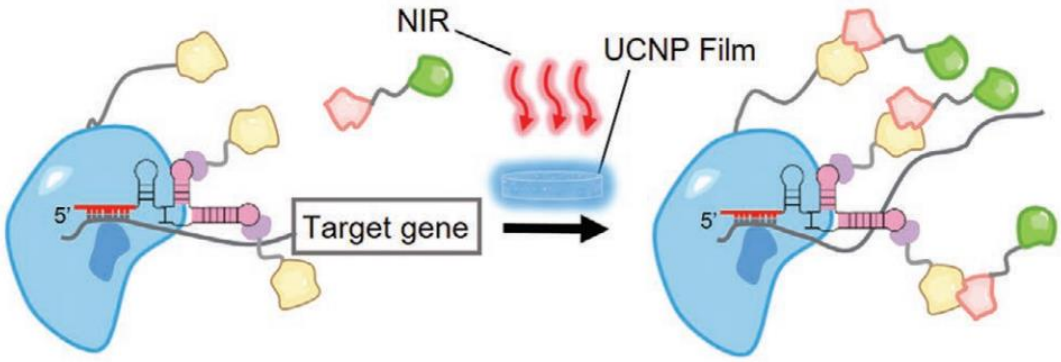

Figure 1.17 Spatiotemporal regulation of CRISPR-Cas13 by blue light irradiation

1.8.3 Peptide nucleic acids (PNA)

In addition to the three protein-based artificial restriction enzymes stated above, there are other genome editing approach using a simpler artificial nucleic acid to stop mRNA production.

Peptide nucleic acids (PNA) is a peptide-backed artificial oligonucleotide mimic [68]. PNA's most distinguishing property is that it combines the properties of both peptides and nucleic acids. The main chain of DNA and RNA is sugar, whereas of PNA is N- (2-aminoethyl) glycine. A methylene group and a carbonyl group are then used to connect a purine or pyrimidine ring matching to a nucleobase to the main chain. The effect of electrostatic repulsion is modest in PNA because it lacks the charge of the phosphate site found in DNA and RNA, and the binding of PNA/DNA is stronger than the double strand of DNA/DNA. [69, 70] However, due to its high binding force, PNA promotes the stability of PNA/PNA. To address these issues, derivatives have been developed.

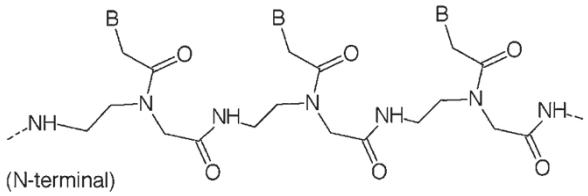

Figure 1.17 Chemical structure of PNA

The most representative derivative is pseudocomplementary PNA (pcPNA) [70, 71], which substitutes 2,6-diaminopurine (D) and 2-thiouracil (sU) for adenine and thymine, respectively. PNA / PNA was successfully destabilized due to steric hindrance between the thio group of sU and the two amino groups in the sU-D pair [72, 73]. Despite the fact that this steric hindrance destabilizes the pcPNA-pcPNA double strand, it has a greater binding force to pcPNA-DNA than unmodified PNA. Artificial nucleic acids can now invade a highly stable DNA double helix thanks to the development of pcPNA. Furthermore, by adding Lysine to the amino acid residue of PNA, chiral PNA [71] was produced, in which the PNA probe has a positive charge. The binding force of chiral PNA to the negatively charged DNA of phosphoric acid is increased electrostatically, and the PNAs repel each other with positive charges. In addition to the steric barrier of pcPNA, electrostatic contact greatly improved

invasion efficiency when compared to the DNA probe. Using pcPNA invasion, Frank-Kamenetskii et al. were able to produce a single-stranded structure in DNA and successfully detect a specific sequence [72].

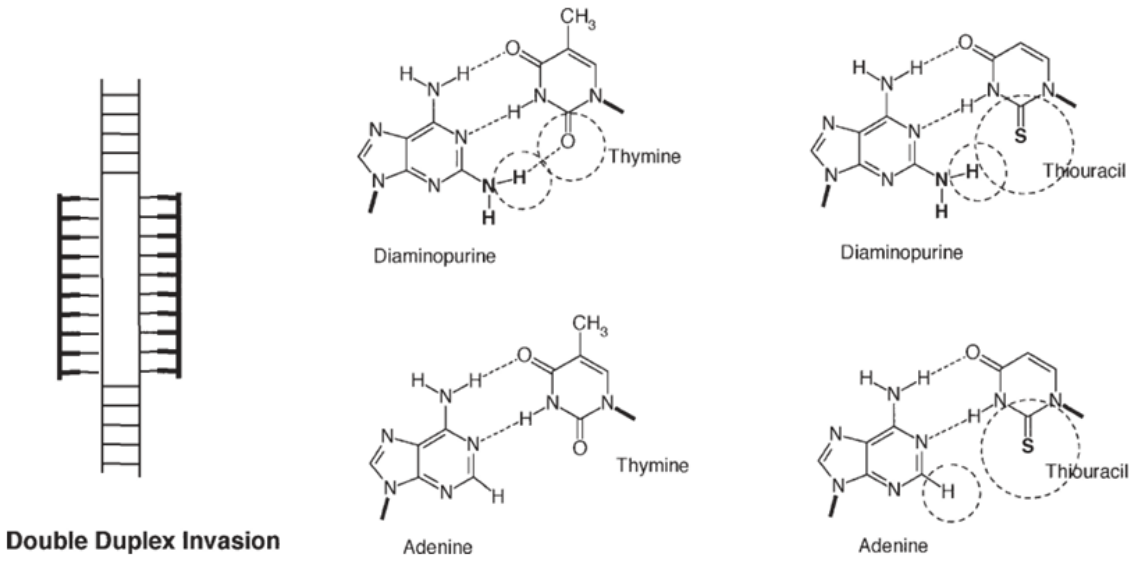

Figure 1.18 Chemical structure of pcPNA and double duplex invasion

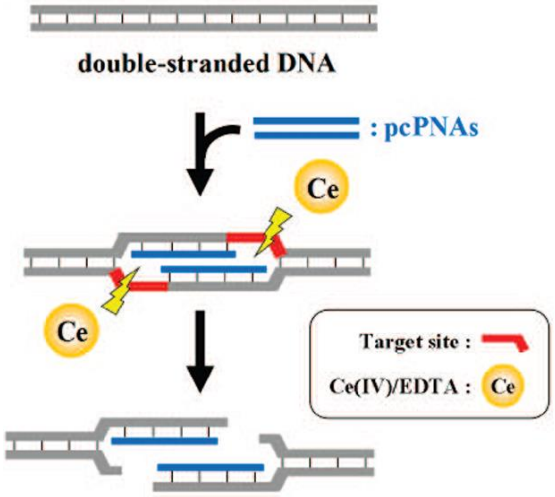

Figure 1.19 Chiral PNA chemical structure and double duplex invasion

1.8.4 Locked Nucleic Acid (LNA)

LNA [73] is an artificial nucleic acid that improves DNA stability. It has been crosslinked with 2'-O, 4'-C methylene. When the flexibility of the ribofuranose ring is limited, immobilization of the 3'-endo conformation forms a very strong double helix structure. LNA has the properties of improving the stability of hybridization to DNA, being resistant to enzymatic degradation, and being phosphoramidite produced. PNA is difficult to produce because it contains an amino acid backbone. It can be entirely automated if the phosphoramidite method is used, which decreases the difficulties of preparation. Furthermore, a DNAzyme (LNAzyme) with enzymatic degradation resistance can be generated by exploiting LNA's enzymatic degradation resistance and substituting several bases of DNAzyme with LNA.

LNA can create a stable hybridization with DNA and can invade a stable DNA double helix, similar to PNA. Zorro-LNA [74], which achieved double duplex invasion by creating a probe with a very distinctive structure, is the most characteristic technique of antigene effect by LNA. Zorro-LNA invades like a DNA double helix when the probe has already hybridized to the target DNA. The force needed to push out the probe is weakened in the structure in which the invasion is pried open and hybridized, allowing a stable invasion structure to emerge.

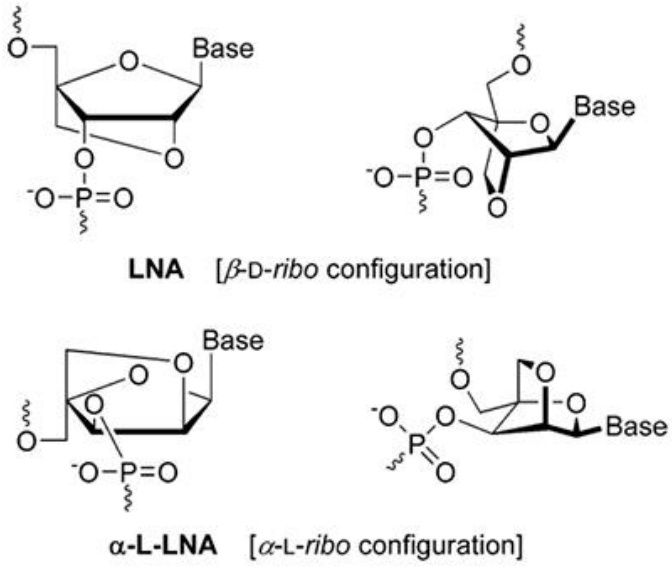

Figure 1.21 Chemical structure of LNA and α-L-LNA

1.9 3-cyanovinuylcarbazole (^{CNV}K)

^{CNV}K is a reversible photoresponsive artificial nucleic acid that specifically photo-cross-links and cleaves pyrimidine bases upon UV irradiation [76]. It has a carbazole skeleton, and from the 3-position of carbazole, a vinyl group with a cyano group extends. Furthermore, the nitrogen at position 9 forms a nucleoside by covalently bonding with deoxyribose. Because carbazole contains two benzene rings, it features hydrophobic flatness and a simple molecular electronic transition. UV irradiation causes electrons to move to the vinyl group on the cyano group's side, which is an appealing substituent. The electrons going to the vinyl group form a covalent link with the pyrimidine base's double bond between C5 and C6 ([2+2] photocyclization process). Furthermore, the ^{CNV}K-photo-cross-linked vinyl group reacts with the pyrimidine base on the 3' side to 1 base. It has the advantage of reacting at an ultra-high speed compared to other photo-cross-linking devices because the cross-linking only takes 1 second to react. Furthermore, when treated with light at 312 nm under heating circumstances, covalent bonds undergo a photocleavage reaction. ^{CNV}K has used a cross-linking procedure to achieve ^{19}F-NMR chemical shift imaging [77] and site-specific deamination to convert cytosine to uracil [78]. Furthermore, ^{CNV}K introduced antigene probe was successful in double duplex invasion via photo-cross-linking [79]. double duplex invasion is normally a thermodynamically unstable equilibrium reaction. When ^{CNV}K is photo-cross-linked in the double duplex invasion state, however, the thermal equilibrium is irreversible and the probe is immobilized. ^{CNV}K is a one-of-a-kind photo-responsive molecule that contributes significantly to both medicinal and DNA nanotechnology applications.

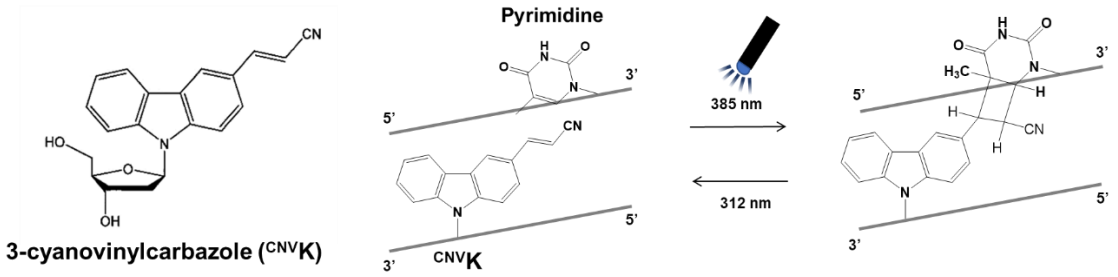

Figure 1.22 Chemical structure of ^{CNV}K and photo reversible reaction of ^{CNV}K

1.9.1 DNA strand displacement reaction

The T_m value is extensively used as a numerical indicator of double-stranded DNA stability. The T_m value is the temperature at which double-stranded DNA dissociates by 50% to become single-stranded DNA due to thermal equilibrium. The stability of the double strand is closely linked to its length as well as its interactions with nearby molecules, such as the number of hydrogen bonds between the AT and GC pairs. Thermodynamic calculation approaches include the GC percent method and the nearest base pairing method [80]. The T_m value is frequently used to determine the length of the primer used in PCR.

A DNA strand (Invader strand) with a steady T_m value displaces a partially complementary DNA strand (Passenger strand) of a double-stranded DNA in the DNA strand displacement reaction [82]. The partially complementary DNA strand (Passenger strand) and the template DNA strand (Template strand) both have a non-complementary sequence (Toehold), and the Invader strand becomes a complementary foothold sequence. When the Invader chain is hydrogen-bonded to the Toehold section, it competes with the Passenger chain for equilibrium. The equilibrium reaction, however, favors the Invader chain and finally expels the Passenger chain because the Invader chain is thermodynamically more stable than the Passenger chain. The direction and speed of the DNA strand substitution process can be freely changed by adjusting the length of the toehold. The DNA strand displacement reaction is intended to be used to create precise and information-processing molecular circuits using physical arithmetic elements [81] and logic gates [82].

We concentrated on the equilibrium of the DNA strand substitution reaction in our lab, and we were able to induce the photocleavage reaction under more relaxed conditions [83]. ^{CNV}K photo-cleavage reaction necessitates irradiation with light at 312 nm while heated, and cytotoxicity has been a concern. When irradiated with light at 366 nm, the cross-linking and cleavage reactions are in equilibrium in ^{CNV}K, but the cross-linking process is overwhelmingly favorable.

The Invader strand has a thermodynamic advantage over the Passenger strand in inducing an equilibrium reaction of 366 nm photoirradiation at the cross-linking location to a >80% cleavage reaction, according to research. By permitting reversible reaction at long wavelengths, it is likely to be applied to novel applications [84].

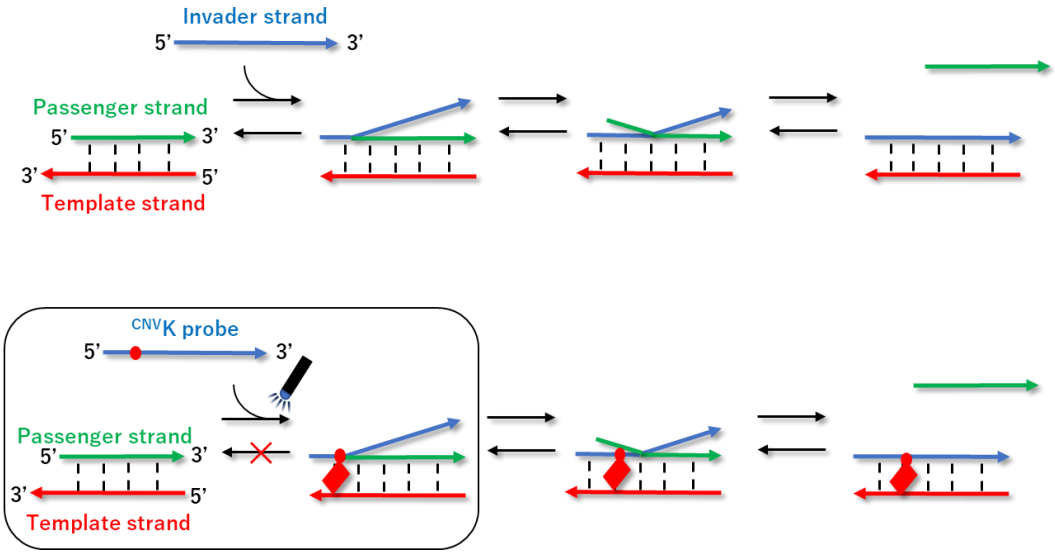

Figure 1.23 DNA strand exchange reaction and thermally irreversible DNA strand exchange reaction using ^{CNV}K probe

1.10. Spatial and temporal control

In order to elucidate advanced biological phenomena caused by the aggregation of a large number of cells, it is necessary to analyze the individuality of each cell in a cell population such as a living tissue. In recent years, the use of photoirradiation to elucidate, regulate, and image biological functions has been actively pursued in biology. Photoirradiation is easy to control in terms of timing, power, and irradiation range.

Optogenetics has been attracting attention as a field of biology that utilizes photoirradiation. Optogenetics is a technology that controls cellular activities by turning light irradiation on and off. By exposing photo activable substances in specific groups of cells or specific neural pathways to photoirradiation, it is now possible to control their expression. For example, by irradiating photo on neurons expressing channelrhodopsin, they have succeeded in actually inducing hand movement. [85]

Nucleic acid drugs that use photoirradiation as an external trigger have many great advantages. In other words, ^{CNV}K has the potential to become a photo-triggered, spatiotemporally controllable nucleic acid drug. By combining the technology of optogenetics, it is expected to have a very wide range of applications, including easy introduction into cells.

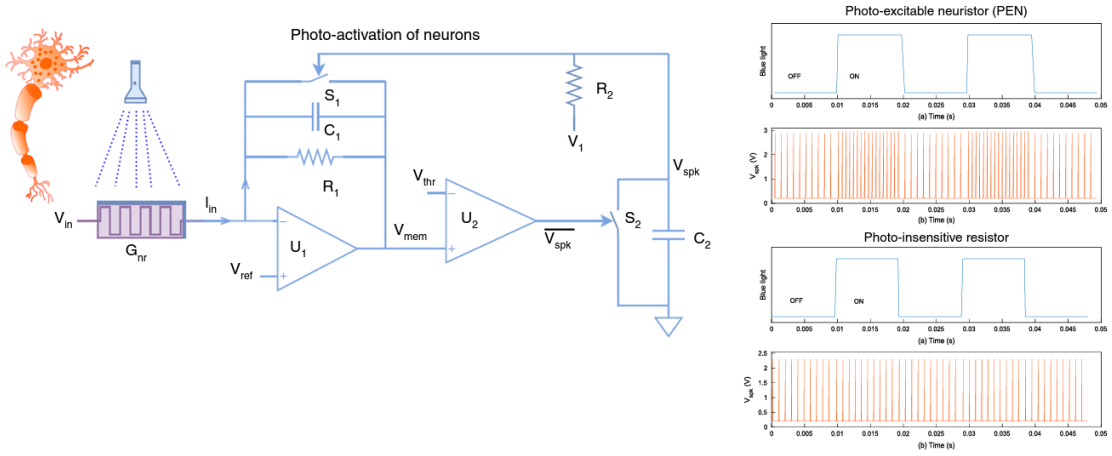

Figure 1.24 Regulation of ion channels by photoirradiation. (*Nature Commun.* **2020**, 11, 3211)

1.11 Objective of this study

Genome editing has gained a great deal of interest in the fields of genetic engineering and gene therapy. Among genome editing, gene disruption is used for various purposes such as recombination and knockout. Currently, CRISPR-Cas9 is attracting attention as a DNA cleavage tool, and RNAi is attracting attention as an RNA cleavage tool. However, enzymatic methods have limitations in terms of reaction conditions such as optimal pH, buffer, and temperature. Nucleic acid cleavage using artificial oligonucleotides has been developed as a non-enzymatic method. The method using artificial oligonucleotides has fewer restrictions on reaction conditions and has higher sequence selectivity. But on the other hand, the cleavage of nucleic acids by artificial oligonucleotides has many problems compared to enzymes, such as low reactivity and difficulty in control. To solve these problems, the aim of this study is to develop a new nucleic acid cleavage tool using ^{CNV}K, which is independent of hydrogen bonding. ^{CNV}K specifically forms covalent bonds with pyrimidine bases upon photo-irradiation. Nucleic acid cleavage tools combined with ^{CNV}K form thermally irreversible structures and are expected to be spatiotemporally controlled.

In Chapter 2, we will control the activity of DNAzyme, which is expected to be a tool for RNA cleavage. The DNAzyme is a nuclease composed of nucleic acids that can specifically cleave target RNA. However, DNAzyme has not been applied to RNAi under in vivo conditions because its activity is always at ON state but it is necessary to control its activity at the desired location and timing. In the control methods reported so far, the switch from the active OFF state to ON state is dependent on hydrogen bonding. Therefore, we devised a thermally irreversible control method of DNAzyme activity by covalent bonding. The photo-cross-linked DNAzyme can completely inhibit the interaction with the target sequence. In addition, the covalent bond is expected to provide resistance to enzymatic degradation.

In Chapter 3, we aim to construct a thermally irreversible structure of DDI probes. The invasion structure of DDI probes is important for DNA cleavage using artificial oligonucleotides. When a DDI probe invades a DNA duplex, it induces a site-specific single-stranded structure. In combination with Ce/EDTA or S1 nuclease, which specifically cleave single-stranded structures, DNA duplex cleavage becomes possible. However, the DDI probes

developed in previous studies are thermoreversible, and it is difficult to maintain the invasion structure. Therefore, we aimed to develop a DDI probe incorporating ^{CNV}K to construct a thermally irreversible invasion structure. However, there is a concern that the DDI probe with ^{CNV}K may cause self-photo-cross-linking between probes. In this study, we investigate a device that suppresses the self-photo-cross-linking of probes. In addition to 5-cyanouracil, which has already been reported, we will examine Spacer and dSpacer.

As DNA increases in size, it forms multiple higher-order structures. This can vary from supercoiled structures in plasmid DNA to histone interactions in genomic DNA. Against this background, previous studies have validated DDI for DNA of several hundred base pairs, and the next step is to study plasmids and genomes. Therefore, in Chapter 4, we will examine DDI photo-cross-linking for 400 mer DNA. In addition, we will optimize the probe using the self-crosslinking inhibitor selected in Chapter 3.

References

[1] C Hélène, J J Toulmé. Specific regulation of gene expression by antisense, sense and antigene nucleic acids. *Biochim Biophys Acta.,* **1990**, 1049(2), 99-125.

[2] Stanley T Crooke, Progress in antisense technology. *Annu Rev Med.,* **2004**, 55, 61-95.

[3] M E Davis, J E Zuckerman, C H J Choi, D Seligson, A Tolcher, C A Alabi, Y Yen, J D Heidel, A Ribas. Evidence of RNAi in humans from systemically administered siRNA via targeted nanoparticles. *Nature*. **2010**, 464(7291), 1067-70.

[4] O C Farokhzad, J Cheng, B A. Teply, I Sherifi, S Jon, P W. Kantoff, J P Richie, R Langer. Targeted nanoparticle-aptamer bioconjugates for cancer chemotherapy *in vivo*. *Proc Natl Acad Sci U S A.*, **2006**, 103(16), 6315-20.

[5] M Jinek, K Chylinski, I Fonfara, M Hauer, J A Doudna, E Charpentier. A programmable dual-RNA-guided DNA endonuclease in adaptive bacterial immunity. *Science*, **2012**, 337(6096), 816-21.

[6] Y G Kim, J Cha. S Chandrasegaran, Hybrid restriction enzymes: zinc finger fusions to Fok I cleavage domain. *Proc Natl Acad Sci U S A*, **1996**, 93(3), 1156–60.

[7] Michelle Christian 1, Tomas Cermak, Erin L Doyle, Clarice Schmidt, Feng Zhang, Aaron Hummel, Adam J Bogdanove, Daniel F Voytas. Targeting DNA double-strand breaks with TAL effector nucleases. *Genetics*, **2010**, 186(2), 757-61.

[8] Ralf Dahm. Friedrich Miescher and the discovery of DNA. *Dev Biol.*, **2005**, 278(2), 274-88.

[9] M E Jones, Albrecht Kossel. A biographical sketch. *Yale J Biol Med.*, **1953**, 26(1), 80-97.

[10] A Bashirullah, R L Cooperstock, H D Lipshitz. Spatial and temporal control of RNA stability. *Proc Natl Acad Sci U S A*, **2001**, 98(13), 7025-8.

[11] Istva'n Hargittai. The tetranucleotide hypothesis: a centennial. *Struct Chem.*, **2009**, 20, 753–6.

[12] D Elson, E Chargaff. On the desoxyribonucleic acid content of sea urchin gametes. *Experientia*, **1952**, 8(4), 143-5.

[13] J. D. Watson, F. H. C. Crick. Molecular Structure of Nucleic Acids: A Structure for Deoxyribose Nucleic Acid. *Nature.* **1953**, 171, 737–8.

[14] A. Ficq, J. Brachet. RNA-Dependent DNA Polymerase: Possible Role in the Amplification of Ribosomal DNA in Xenopus oocytes. *PNAS.*, **1971**, 68 (11), 2774-6.

[15] T.R. Caspersson, E Lein, A R Ringrt. Cytochemical Studies on Some Effects of X-Radiation on Three Ascites Tumors. *Canc. Res.*, **1958**, 18 (7), 857-62,

[16] K T. Kohara, N Iizuka, M Kohara, A Nomoto. Internal ribosome entry site within hepatitis C virus RNA. *J Virol.*, **1992**, 66(3), 1476–83.

[17] F Crick. Central dogma of molecular biology. *Nature*, **1970**, 227(5258), 561-3.

[18] S Osawa, T H Jukes, K Watanabe, A Muto. Recent evidence for evolution of the genetic code. *Microbiol Rev.*, **1992**, 56(1), 229-64.

[19] G J Quigley, A Rich. Structural domains of transfer RNA molecules
Science, **1976**, 194(4267), 796-806.

[20] E Volkin, L Astrachan. Phosphorus incorporation in Escherichia coli ribonucleic acid after infection with bacteriophage T2. *Virology*, **1956**, 2(2), 149-61.

[21] F Jacob, J Monod. Genetic regulatory mechanisms in the synthesis of proteins
J Mol Biol., **1961**, 3, 318-56.

[22] E Volkin, L Astrachan, J L Countryman. Metabolism of RNA phosphorus in Escherichia coli infected with bacteriophage T7. *Virology*, **1958**, 6(2), 545-55.

[23] H M Temin, S Mizutani. RNA-dependent DNA polymerase in virions of Rous sarcoma virus. *Nature*, **1970**, 226(5252), 1211-3.

[24] M R Lerner, J A Boyle, S M Mount, S L Wolin, J A Steitz, Are snRNPs involved in splicing? *Nature*, **1980**, 283(5743), 220-4.

[25] S E Wells, P E Hillner, R D Vale, A B Sachs. Circularization of mRNA by eukaryotic translation initiation factors. *Mol Cell*, **1998**, 2(1), 135-40.

[26] N Uchida, S Hoshino, H Imataka, N Sonenberg, T Katada. A novel role of the mammalian GSPT/eRF3 associating with poly(A)-binding protein in Cap/Poly(A)-dependent translation. *J Biol Chem.*, **2002**, 277(52), 50286-92.

[27] H F Noller, C R Woese. Secondary structure of 16S ribosomal RNA. *Science*, **1981**, 212(4493), 403-11.

[28] S H Kim, F L Suddath, G J Quigley, A M Pherson, J L Sussman, A H Wang, N C Seeman, A Rich. Three-dimensional tertiary structure of yeast phenylalanine transfer RNA. *Science*, **1974**, 185(4149), 435-40.

[29] K B Mullis. The unusual origin of the polymerase chain reaction. *Sci Am.*, **1990**, 262(4), 56-65.

[30] P T Gilham, H G Khorana. Studies on Polynucleotides. I. A New and General Method for the Chemical Synthesis of the C5"-C3" Internucleotidic Linkage. Syntheses of Deoxyribodinucleotides. *J. Am. Chem. Soc.*, **1958**, 80(23), 6212–22.

[31] C B Reese. The chemical synthesis of oligo- and poly-nucleotides by the phosphotriester approach. Tetrahedron, **1978**, 34(21), 3143-79.

[32] T Dörper, E L Winnacker. **1983**, Improvements in the phosphoramidite procedure for the synthesis of oligodeoxyribonucleotides. *Nucleic Acids Res.,* 11(9), 2575-84.

[33] S L Beaucage M H Caruthers. Deoxynucleoside phosphoramidites—A new class of key intermediates for deoxypolynucleotide synthesis. *Tetrahedron Letters*, **1981**, 22(20), 1859-62.

[34] J Kurreck. Antisense technologies. Improvement through novel chemical modifications. *Eur J Biochem.*, **2003**, 270(8), 1628-44.

[35] A Bielinska, R A Shivdasani, L Q Zhang, G J Nabel. Regulation of gene expression with double-stranded phosphorothioate oligonucleotides. *Science*, **1990**, 250(4983), 997-1000.

[36] X Shen, D R Corey, Chemistry. mechanism and clinical status of antisense oligonucleotides and duplex RNAs. *Nucleic Acids Res.*, **2018**, 46(4), 1584-1600.

[37] S T Crooke, J L Witztum, C F Bennett, B F Baker. RNA-Targeted Therapeutics. *Cell Metab.*, **2018**, 27(4), 714-39.

[38] S T Crooke. Molecular Mechanisms of Antisense Oligonucleotides. *Nucleic Acid Ther.*, **2017**, 27(2), 70-77.

[39] R M Orr. Technology evaluation: fomivirsen, Isis Pharmaceuticals Inc/CIBA vision. *Curr Opin Mol Ther.*, **2001**, 3(3), 288-94.

[40] R D Santos, P B Duell, C East, J R Guyton, P M Moriarty, W Chin, R S Mittleman. Long-term efficacy and safety of mipomersen in patients with familial hypercholesterolaemia: 2-year interim results of an open-label extension. *Eur Heart J.*, **2015**, 36(9), 566-75.

[41] A Grishok, A E Pasquinelli, D Conte, N Li, S Parrish, I Ha, D L Baillie, A Fire, G Ruvkun, C C Mello. Genes and mechanisms related to RNA interference regulate expression of the small temporal RNAs that control C. elegans developmental timing. *Cell*, **2001**, 106(1), 23-34.

[42] Femke Simmer, Celine Moorman, Alexander M van der Linden, Ewart Kuijk, Peter V E van den Berghe, Ravi S Kamath, Andrew G Fraser, Julie Ahringer, Ronald H A Plasterk.

Genome-wide RNAi of C. elegans using the hypersensitive rrf-3 strain reveals novel gene functions. *PLoS Biol.*, **2003**, 1(1), 12.

[43] S G Jones. The microRNA Registry. *Nucleic Acids Res.*, **2004**, 32, D109-11.

[44] J A Doudna, T R Cech. The chemical repertoire of natural ribozymes. *Nature*, **2002**, 418, 222–8.

[45] H F Noller, V Hoffarth, L Zimniak. Unusual resistance of peptidyl transferase to protein extraction procedures. *Science*, **1992**, 256(5062), 1416-9.

[46] I Nitta, Y Kamada, H Noda, T Ueda, K Watanabe. Peptide bond formation: retraction. *Science*, **1999**, 283(5410), 2019-20.

[47] H W Pley, K M Flaherty, D B McKay. Three-dimensional structure of a hammerhead ribozyme. *Nature*, **1994**, 372, 68–74.

[48] P B Rupert, R Adrian, 2001, F D'Amaré. Crystal structure of a hairpin ribozyme–inhibitor complex with implications for catalysis. *Nature,* **2001**, 410, 780–6.

[49] M P Robertson, A Ellington. *In vitro* selection of an allosteric ribozyme that transduces analytes to amplicons. *Nature Biotech.*, **1999**, 17, 62–6.

[50] C R Dass, P F M Choong, L M Khachigian. DNAzyme technology and cancer therapy: cleave and let die. *Mol Cancer Ther.*, **2008**, 7(2), 243-51.

[51] K Zagorovsky, W C W Chan. A plasmonic DNAzyme strategy for point-of-care genetic detection of infectious pathogens. *Angew Chem Int Ed Engl.*, **2013**, 52(11), 3168-71.

[52] H Fan, X Zhang, Y Lu. Recent advances in DNAzyme-based gene silencing. *Science China Chemistry*, **2017**, 60, 591–601.

[53] Y Wang, S K Silverman. Deoxyribozymes That Synthesize Branched and Lariat RNA. *J. Am. Chem. Soc.*, **2003**, 125, 6880－81.

[54] K Schlosser, Y Li. Understanding DNA-based catalysis one molecule at a time. *Nature Chemical Biology*, **2007**, 3, 753–4.

[55] W Wang, L P Billen, Y Li. Sequence Diversity, Metal Specificity, and Catalytic Proficiency of Metal-Dependent Phosphorylating DNA Enzymes. *Chem Biol.*, **2002**, 9(4), 507-17.

[56] K E Nelson, P J Bruesehoff, Y Lu. *In vitro* selection of high temperature Zn(2+)-dependent DNAzymes. *J Mol Evol.*, **2005**, 61(2), 216-25.

[57] A A Fokina, M I Meschaninova, T Durfort, A G Venyaminova, J C François. Targeting

insulin-like growth factor I with 10-23 DNAzymes: 2'-O-methyl modifications in the catalytic core enhance mRNA cleavage. *Biochemistry*, **2012**, 20, 51(11), 2181-91.

[58] L M Khachigian. Deoxyribozymes as Catalytic Nanotherapeutic Agents. *Cancer Res.*, **2019**, 79(5), 879-888.

[59] R M Horton, H D Hunt, S N Ho, J K Pullen, L R Pease. Engineering hybrid genes without the use of restriction enzymes: gene splicing by overlap extension. *Gene*, **1989**, 77(1), 61-8.

[60] Y G Kim, J Cha, S Chandrasegaran. Hybrid restriction enzymes: zinc finger fusions to Fok I cleavage domain. *Proc Natl Acad Sci U S A*, **1996**, 93(3), 1156–1160.

[61] T Sakuma, H Ochiai, T Kaneko, T Mashimo, D Tokumasu, Y Sakane, K Suzuki, T Miyamoto, N Sakamoto, S Matsuura, T Yamamoto. Repeating pattern of non-RVD variations in DNA-binding modules enhances TALEN activity. *Scientific Reports*, **2013**, 3, 3379.

[62] M Jinek, K Chylinski, I Fonfara, M Hauer, J A Doudna, E Charpentier. A programmable dual-RNA-guided DNA endonuclease in adaptive bacterial immunity. *Science*, **2012**, 337(6096), 816-21.

[63] K A Molla, Y Yang. CRISPR/Cas-Mediated Base Editing: Technical Considerations and Practical Applications. *Trends Biotechnol.*, **2019**, 37(10), 1121-42.

[64] J P Broughton, X Deng, G Yu, C L Fasching, V Servellita, J Singh, X Miao, J A Streithorst, A Granados, A S Gonzalez, K Zorn, A Gopez, E Hsu, W Gu, S Miller, C Y Pan, H Guevara, D A Wadford, J S Chen, C Y Chiu. CRISPR-Cas12-based detection of SARS-CoV-2. *Nat Biotechnol.*, **2020**, 38(7), 870-4.

[65] Jie Zhao, Bing Li, Jianxiong Ma, Weilin Jin, Xinlong Ma. Photoactivatable RNA N^6-Methyladenosine Editing with CRISPR-Cas13. Small. **2020**, 30, e1907301.

[66] H Yang, D J Patel. Inhibition Mechanism of an Anti-CRISPR Suppressor AcrIIA4 Targeting SpyCas9. *Mol Cell.*, **2017**, 67(1), 117-27.

[67] M Zuckermann, V Hovestadt, C B K Thomsen, M Zapatka, P A Northcott, K Schramm, J Belic, D T W Jones, B Tschida, B Moriarity, D Largaespada, M F Roussel, A Korshunov, G Reifenberger, S M Pfister, P Lichter, D Kawauchi, J Gronych. Somatic CRISPR/Cas9-mediated tumour suppressor disruption enables versatile brain tumour modelling. *Nat Commun.*, **2015**, 6, 7391.

[68] M Egholm, O Buchardt, P E Nielsen, R H Berg. Peptide nucleic acids (PNA). Oligonucleotide analogs with an achiral peptide backbone. *J. Am. Chem. Soc.*, **1992**, 114(5),

1895–7.

[69] M Egholm, P E Nielsen, O Buchardt, R H. Berg. Recognition of guanine and adenine in DNA by cytosine and thymine containing peptide nucleic acids (PNA). *J. Am. Chem. Soc.*, **1992**, 114(24), 9677–78.

[70] M Komiyama, Y Aiba, T Ishizuka, J Sumaoka. Solid-phase synthesis of pseudo-complementary peptide nucleic acids. *Nature Protocols*, **2008**, 3, 646–54.

[71] T Ishizuka, J Yoshida, Y Yamamoto, J Sumaoka, T Tedeschi, R Corradini, S Sforza, M Komiyama. Chiral introduction of positive charges to PNA for double-duplex invasion to versatile sequences. *Nucleic Acids Res.*, **2008**, 36(5), 1464-71.

[72] H Kuhn, V V Demidov, J M Coull, M J Fiandaca. Brian D. Gildea, and Maxim D. Frank-Kamenetskii, Hybridization of DNA and PNA Molecular Beacons to Single-Stranded and Double-Stranded DNA Targets. *J. Am. Chem. Soc.*, **2002**, 124(6), 1097–1103.

[73] D A Braasch, D R Corey. Locked nucleic acid (LNA): fine-tuning the recognition of DNA and RNA. *Chem Biol.*, **2001**, 8(1), 1-7.

[74] E M Zaghloul, A S Madsen, P M D Moreno, I I Oprea, S E Andaloussi, B Bestas, P Gupta, E B Pedersen, K E Lundin, J Wengel, C I Edvard Smith. Optimizing anti-gene oligonucleotide 'Zorro-LNA' for improved strand invasion into duplex DNA. *Nucleic Acids Res.*, **2011**, 39(3), 1142-54.

[75] Y Yoshimura, K Fujimoto. Ultrafast Reversible Photo-Cross-Linking Reaction: Toward in Situ DNA Manipulation. *Org. Lett.*, **2008**, 10(15), 3227–30.

[76] S Nakamura, Y Takashima, K Fujimoto. Multiplexed detection of nucleic acids using 19F NMR chemical shift change based on DNA photo-cross-linking of 3-vinylcarbazole derivatives. *Organic Biomolecular Chemistry*, **2018**, 16, 891–4.

[77] S Sethi, S Nakamura, K Fujimoto. Study of Photochemical Cytosine to Uracil Transition via Ultrafast Photo-Cross-Linking Using Vinylcarbazole Derivatives in Duplex DNA. *Molecules*, **2018**, 23(4), 828-937.

[78] K Fujimoto, H Yang, S Nakamura. Strong inhibitory effects of antisense probes on gene expression through ultrafast RNA photo-crosslinking. *Chemistry-An Asian Journal*, **2019**, 14(11), 1912-6.

[79] S Nakamura, H Kawabata, K Fujimoto. Double duplex invasion of DNA induced by ultrafast photo-cross-linking using 3-cyanovinylcarbazole toward for antigene method.

Chemical Communications, **2017**, 53, 7616-9.

[80] K J Breslauer, R Frank, H Blöcker, L A Marky. Predicting DNA duplex stability from the base sequence. *Proc Natl Acad Sci U S A*, **1986**, 83(11), 3746–50.

[81] David Yu Zhang, Georg Seelig, Dynamic DNA nanotechnology using strand-displacement reactions. *Nature Chemistry*, **2011,** 3, 103–113.

[82] E Skotadis, G Tsekenis, M Chatzipetrou, L Patsiouras, L Madianos, P Bousoulas, I Zergioti, D Tsoukalas. Heavy metal ion detection using DNAzyme-modified platinum nanoparticle networks. *Sensors and Actuators B: Chemical*, **2017**, 239, 962-9.

[83] F C Simmel, B Yurke, H R. Singh. Principles and Applications of Nucleic Acid Strand Displacement Reactions. *Chem. Rev.*, **2019**, 119(10), 6326–69.

[84] S Nakamura, H Kawabata, K Fujimoto. Sequence-specific DNA photo-splitting of 3-cyanovinylcarbazole using DNA strand displacement. *ChemBioChem.*, **2016**, 17(16), 1499-1503.

[85] Rohit Abraham John, Jyotibdha Acharya, Chao Zhu, Abhijith Surendran, Sumon Kumar Bose, Apoorva Chaturvedi, Nidhi Tiwari, Yang Gao, Yongmin He, Keke K. Zhang, Manzhang Xu, Wei Lin Leong, Zheng Liu, Arindam Basu, Nripan Mathews. Optogenetics inspired transition metal dichalcogenide neuristors for in-memory deep recurrent neural networks. *Nature Commun.* **2020**, 11, 3211.

[Chapter 2] Control of DNAzyme activity using photo-cross-linkable artificial nucleic acid

2.1 Introduction

Ribozymes are nucleic acid enzymes composed of RNA and are unique molecules that cleave RNA [1]. It was discovered in the 1980s and is currently being studied all around the world as a key clue to the puzzle of biological evolution. Ribozymes are comprised of two regions: an enzyme core and a substrate core, the latter of which can be altered artificially [2]. In the 1990s, an *in vitro* selection strategy was used to generate a DNA-based nucleic acid enzyme that was more stable than ribozyme and facilitated artificial production [3]. While DNAzyme is likely to be used in DNA nanotechnology and biosensors, it has a number of drawbacks when it comes to gene therapy.

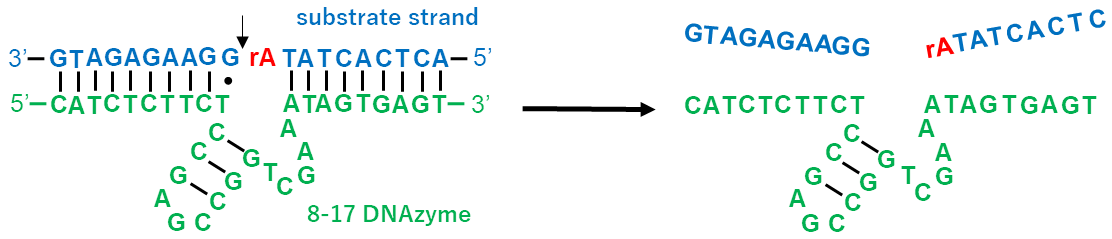

Figure 2.1. Cleavage scheme of 8-17 DNAzyme

In order to use DNAzyme *in vivo*, it is necessary to have precise activity regulation, ease of trigger injection, and no release of distinct molecules. However, it is difficult to entirely control DNAzyme activity *in vivo*. So far, strand displacement reactions [4, 5], metal ions [6, 7], disulfide exchange reactions [8] and have been used to regulate DNAzyme activity. The method of controlling DNAzyme using strand displacement reactions is the simplest, and there are many reports. The OFF state forms a higher-order structure so that the enzyme core cannot be activated. The OFF state has mask strand, which is a complementary sequence to the substrate strand. When the substrate strand hybridizes to the OFF state DNAzyme, the enzyme core forms an ON state. DNAzyme activity controled by disulfide exchange reactions is a method that uses inhibitor strands that form disulfide bonds instead of substrate strands. Inhibitor strands are sequences that are completely complementary to DNAzymes and inhibit substrate strand hybridization. Hypoxic X-irradiation cleavages the disulfide bond and

switches the DNAzyme to the ON state. The DNAzyme activity control method using metal ions switches the structure by complex formation. Normally, it is in the OFF state in a single-stranded ODN, but when a specific metal ion approaches, it forms a complex possessing a secondary structure like a DNAzyme. However, because the cell contains a variety of reducing agents and metal ions, disulfide bonds are cleaved, producing conformational alterations. They are unable to completely inhibit DNAzyme activity because they generate DNAzyme activity leakage. As a photochemical approach for modulating DNAzyme activity [9, 10], it was created using cage nucleosides and azobenzene [11]. The control method using photoresponsive molecules utilizes artificial nucleic acids to form an OFF state secondary structure. Photoirradiation causes the protecting group to come off and isomerization occurs, switching to the ON state. However, introducing just one photoresponsive molecule causes a leak of DNAzyme activity, hence many photoresponsive molecules are required. To solve the problem of DNAzyme activity regulation, designing a method that can form reversible covalent connections and is easy to manage both temporally and spatially is required.

We previously reported a reversible photo-cross-linker termed 3-cyanovinylcarbazole, which can photo-cross-link to a pyrimidine base positioned One base 3' to its counter base via [2+2] cycloaddition by 385 nm or 365 nm irradiation and photo-split by 312 nm irradiation. A T4 loop[12] and passenger strand were extended from the 3' side of the 8-17 DNAzyme to design a sequence that photo-cross-link with substrate strand. When photo-cross-linking happened, it was expected that DNAzyme activity would be inhibited, and with photo-splitted DNAzyme (psDNAzyme) activity would flip from the OFF state to the ON state.

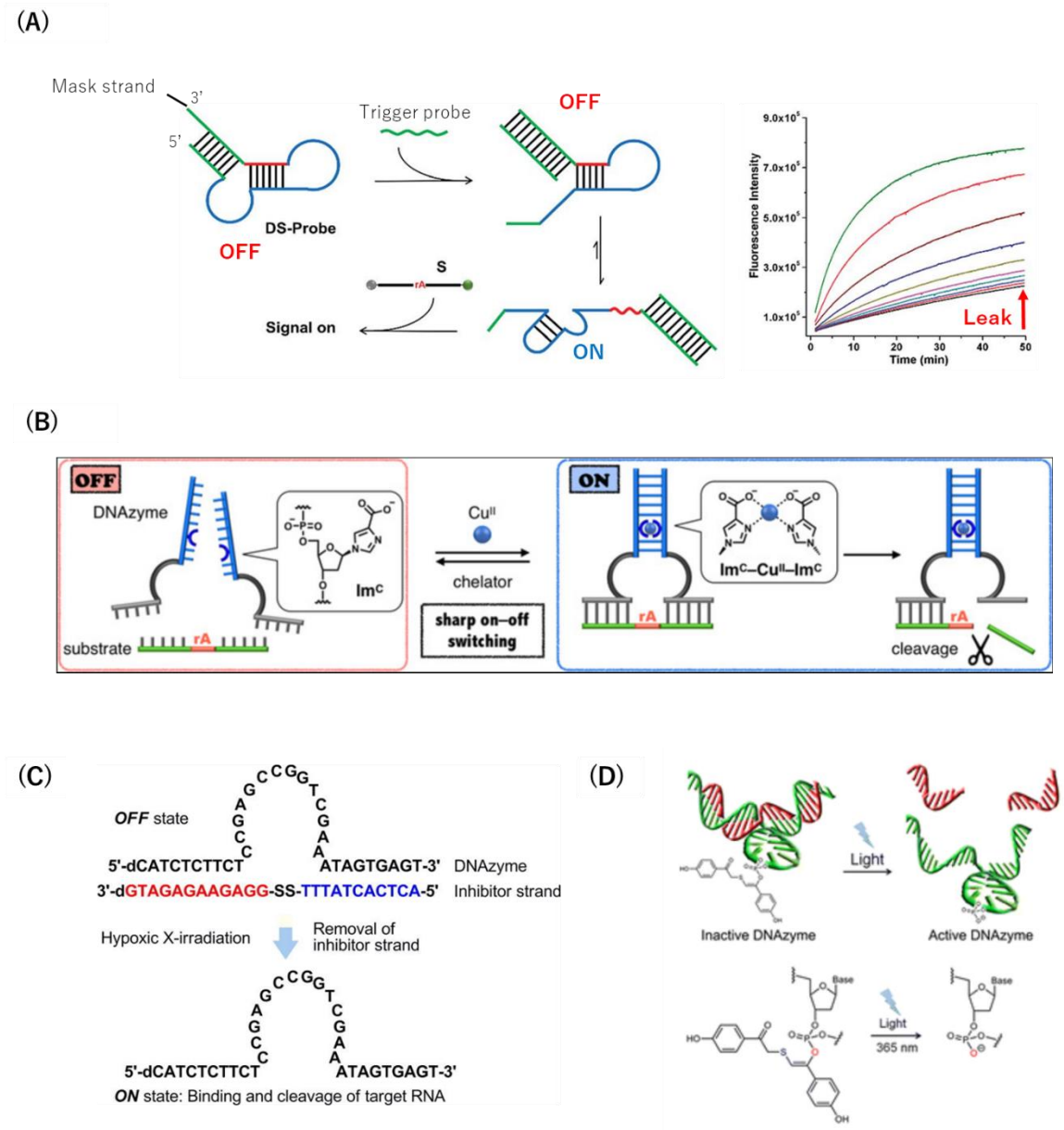

Figure 2.2. DNAzyme activity control method. (A) DNAzyme activity control scheme using DNA strand substitution reaction (*RSC Adv.*, **2018**, 8, 29338). (B) DNAzyme activity control scheme using metal ions (*Angew Chem Int Ed Engl.*, **2020**, 59(48), 21488). (C) DNAzyme activity control scheme using disulfide exchange reaction (*Bioorg Med Chem Lett.*, **2015**, 25(2), 310-2). (D) DNAzyme activity control scheme using photocaged nucleoside. (*ACS Chem. Biol.*, **2016**, 11(2), 444–451.)

2.2 Materials and Methods

2.2.1. Synthesis of ^{CNV}K amidite

Phosphoramidite of ^{CNV}K was synthesized using the method outlined in the literatute (Figure 2.3-2.9).

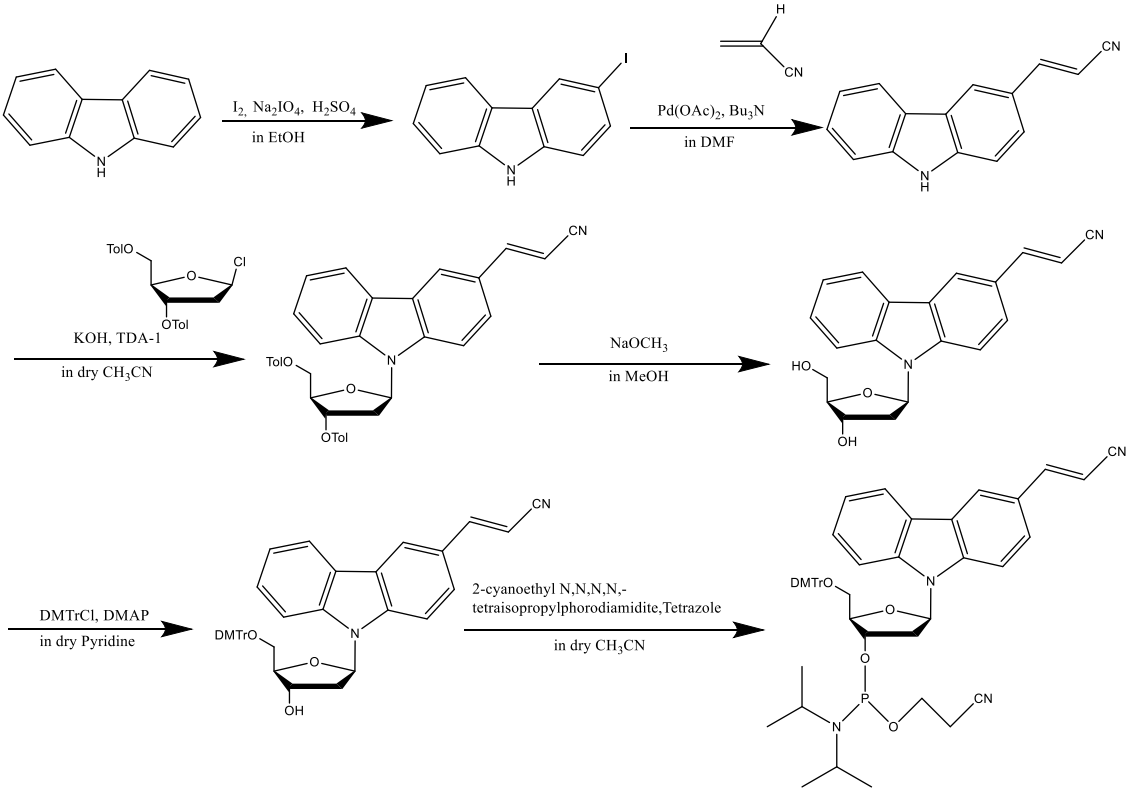

Figure 2.3. Synthesis overview scheme of ^{CNV}K amidite

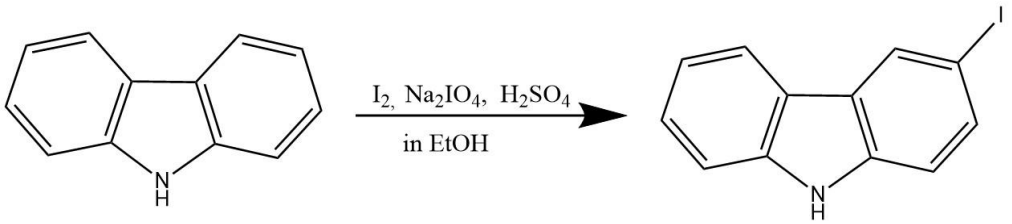

Figure 2.4. Synthesis scheme of 3-Iodocarbazole

Carbazole (8.0 g) was placed in a 1000 ml flask, and H_2SO_4 (2.5 ml) in EtOH (100 ml), NaIO4 (2.58 g), and Iodine (6.16 g) were added in this order and reacted at 65 ℃. for 1 h. The reaction was followed by TLC (Hexane: Ethyl Acetate = 4: 1), and the disappearance of the starting material was confirmed. Neutralized with NaOH (5.70 g) in EtOH and the product was dissolved with $CHCl_3$. Extraction was performed 3 times using distilled water, and the organic phase was dehydrated for 1 h by adding Na_2SO_4. Na_2SO_4 was removed by filtration and 3-Iodocarbazole was recrystallized from $CHCl_3$. The target product was obtained (5.05 g, 35.8%).

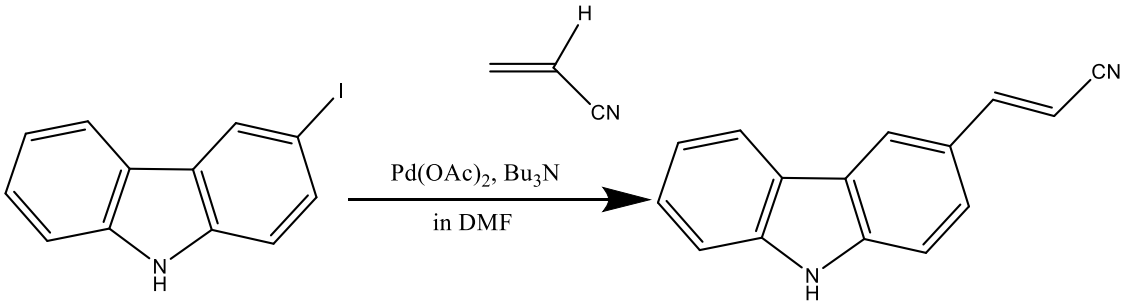

Figure 2.5. Synthesis scheme of 3-cyanovinylcarbazole

In an glass vessel was placed palladium acetate (193 mg, 0.86 mmol), DMF (4.5 mL), 3-Iodocarbazole (2.4 g, 8.23 mmol), tributylamine (2.3 mL), acrylonitrile (1.4 mL, 21.3 mmol). The microwave cavity was sealed and the vessel was placed within. The temperature was scaled from room temperature to the desired temperature of 160 ℃ using 60 W microwave irradiation. The reaction mixture was kept at this temperature for 20 minutes once it was achieved. After allowing the reaction mixture to cool to room temperature, TLC (Hexane/AcOEt, 4:1) was used to check for the presence of starting material. After

evaporating the reaction mixture, the residue was chromatographed on a silica gel with hexane/AcOEt (4:1, v/v) as the eluent, yielding 3-cyanovinylcarbazole (1.47 g, 81.9%).

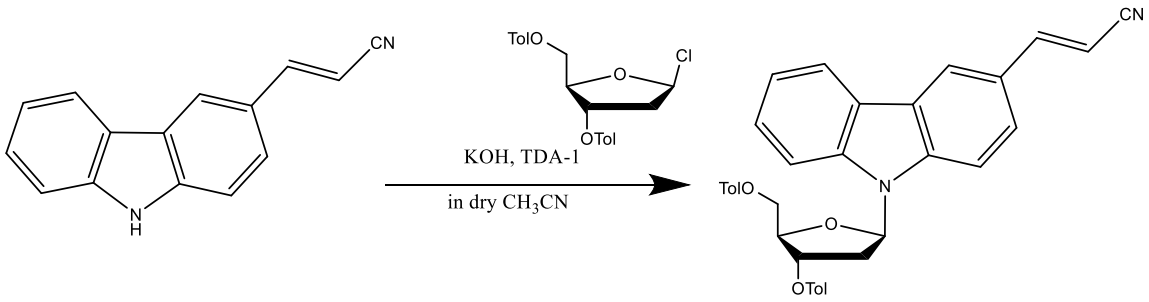

Figure 2.6. Synthesis scheme of 3-cyanovinylcarbazole-1'-β-deoxyriboside-3', 5'-di-(p-toluoyl)ester

3-cyanovinylcarbazole (1.26 g, 13.9 mmol) was added to a solution of potassium hydroxide (1.10 g, 19.9 mmol) and TDA (Tris[2-(2-methoxyethoxy)ethyl] amine) (90.0 mg, 0.28 mmol) in CH_3CN (100 mL) and the reaction mixture was stirred for 30 minutes at room temperature. Toloylchlorosugar (3.00 g, 7.7 mmol) was added to this reaction mixture at room temperature, and the reaction mixture was stirred for 60 minutes at room temperature. TLC (hexane/AcOEt, 4:1) was used to check for the disappeared of starting material in the reaction mixture. The reaction solution was filtered and the solvent was removed by an evaporator as eluent to give 3-cyanovinylcarbazole-1'-β-deoxyriboside-3', 5'-di-(p-toluoyl)ester (3.02 g, 86.0%).

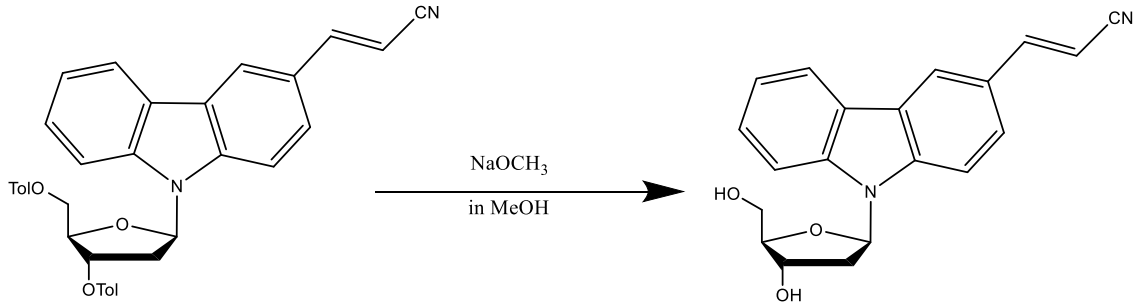

Figure 2.7. Synthesis scheme of 3-cyanovinylcarbazole-1'-β-deoxyriboside

0.5 M methanolic $NaOCH_3$ (0.41 mL, 7.5 mmol) was added to a solution of 3-cyanovinylcarbazole-1'-deoxyriboside-3', 5'-di-(p-toluoyl)ester (3.02 g, 2.0 mmol) in MeOH (85 mL) and the reaction mixture was agitated at room temperature overnight. TLC ($CHCl_3$/MeOH, 9:1) analysis of the reaction mixture revealed the absence of starting material. After evaporating the reaction mixture, the residue was chromatographed on a silica gel using $CHCl_3$/MeOH (9:1, v/v) as eluent to give synthesis of 3-cyanovinylcarbazole-1'-β-deoxyriboside (0.73 g, 78.1%).

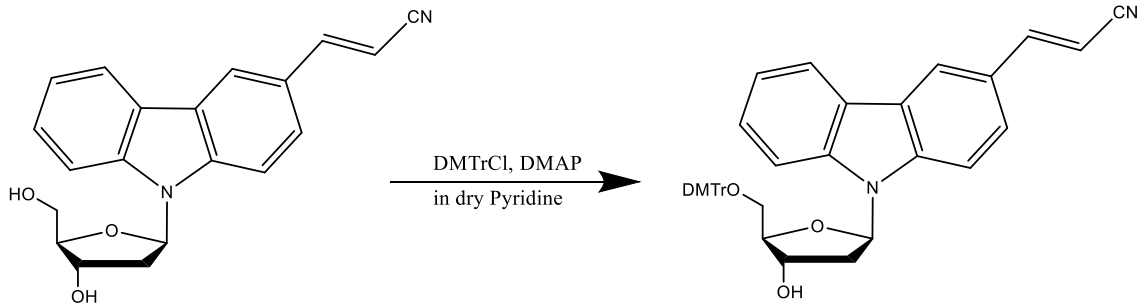

Figure 2.8. Synthesis scheme of 5'-o-(4, 4'-dimethoxytrityl)-3-cyanovinylcarbazole-1'-β-deoxyriboside

A solution of 4,4'-dimethoxytrityl chloride (0.88 g, 2.6 mmol) and 4-(dimethylamino)pyridine (54.2 mg, 0.44 mmol) in pyridine (14 mL) was added to a solution of 3-cyanovinylcarbazole-1'-deoxyriboside (0.73 g, 1.96 mmol) in pyridine (14 mL) and the reaction combination. Following the evaporation of the reaction mixture, the residue was chromatographed on a silica gel using $CHCl_3$/MeOH/Et3N (19:1:0.2, v/v/v) as eluent to give 5'-protected 5'-o-(4, 4'-dimethoxytrityl)-3-cyanovinylcarbazole-1'-β-deoxyriboside (0.72 g, 61.2%).

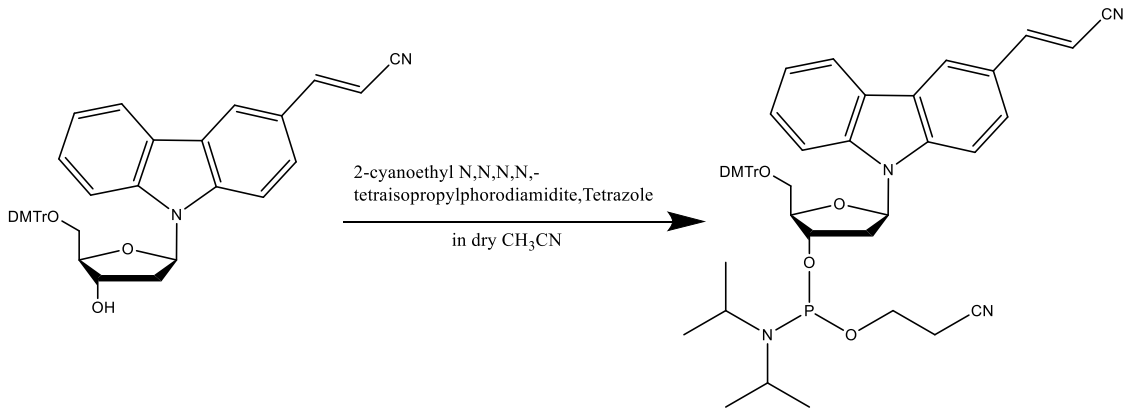

Figure 2.9. Synthesis scheme of 5'-O-(4, 4'-dimethoxytrityl)-3-cyanovinylcarbazole-1'-β-deoxyriboside-3'-O-(cyanothoxy-N, N'-diisopropylamino) phosphoramidite

5'-o-(4, 4'-dimethoxytrityl)-3-cyanovinylcarbazole-1'-β-deoxyriboside (0.72 g, 1.13 mmol), 2-cyanoethyl N,N,N',N'-tetraisopropylphosphorodiamidite (360 mL, 1.1 mmol) in CH_3CN (2.7 mL), and 0.45 M 1H-tetrazole in CH_3CN (1.1 mL) were added, and the reaction After that, AcOEt was used to extract the reaction mixture, which was then washed with a saturated aqueous solution of $NaHCO_3$ and water. The organic layer was recovered, dried over anhydrous sodium sulfate, filtered, and evaporated at reduced pressure to dryness. Then, the crude product in a sealed bottle was dissolved in CH_3CN and coevaporated three times as eluent to give 5'-O-(4, 4'-dimethoxytrityl)-3-cyanovinylcarbazole-1'-β-deoxyriboside-3'-O-(cyanothoxy-N, N'-diisopropylamino) phosphoramidite (0.55 g, 58.4%).

2.2.2. Synthesis and purification of Modified Oligonucleotides

^{CNV}K-introduced oligonucleotides were synthesized using a DNA synthesizer (ABI 3400 DNA Synthesizer, Applied Biosystems, Foster City, CA, USA) according to the phosphoramidite method. The synthesized ODN was reacted with a 28% ammonia solution at room temperature for 1 hour and excised from the CpG support. The protecting group was removed from the collected samples by heating at 65 ℃ for 4 hours. The deprotected ODN was solvent removed with SpeedVac. The target product was purified using a reverse phase column, Inert Sustain TMC18 column, Cosmosil TM5 C18-AR-II column (5 μm, 10 × 150 mm, (Nacalai Tesque, Kyoto, Japan), flow velocity 3.0 mL / min, 60 ℃). Purified samples were freeze dried. The identification of ODN was confirmed by MALDI-TOF-MS. Substrate strand was purchased from Fasmac (Kanagawa, Japan).

Table1. Sequence of DNAzyme and substrate strand

ODN	Sequence (5' to 3')	Cacld. $[M+H]^+$	Found
Pas6	CATCTCTTCTCCGAGCCGGTCGAAATAGTGA GTTTTTACTCA**K**TATAGAAGA	16052.72	16053.09
Pas9	CATCTCTTCTCCGAGCCGGTCGAAATAGTGA GTTTTTACTCACTA**K**AGAAGA	16037.72	16045.89
Pas11	CATCTCTTCTCCGAGCCGGTCGAAATAGTGA GTTTTTACTCACTATA**K**AAGA	16012.71	16013.51
Pas13	CATCTCTTCTCCGAGCCGGTCGAAATAGTGA GTTTTTACTCACTATAGA**K**GA	16028.71	16028.54
Substrate	Cy3-ACTCACTATrAGGAAGGATG	*	*

2.2.3. Denaturing PAGE Analysis

Polyacrylamide gel electrophoresis (PAGE) was performed using 15% polyacrylamide containing 8M urea. Electrophoresis was performed at 150 V for 60 minutes, and the fluorescence image was analyzed with a fluorescent image was analyzed by luminescent image analyzer (LAS3000, Fujifilm, Tokyo, Japan).

2.2.4. DNAzyme cleavage activity evaluation

pclDNAzyme (100 nM), buffer (50 mM Tris-HCl (pH = 7.5) containing 200 mM KCl and 100 μM KCl) and 1000 nM substrate chain were mixed. Mixed solution was incubated in a heat block at 37 ℃ for 15 minutes and illuminate at 37 ° C for 15 minutes at 312 nm using a UV-LED illuminator (Funakoshi, Tokyo, Japan, 15 W) to cleave the photo-cross-linked DNAzyme.

2.2.5. T_m value measurement

Sample solutions were prepared by mixing 10 μM DNAzyme and buffer (50 mM Tris-HCl (pH = 7.5) containing 200 mM KCl and 100 μM KCl). The Melting curve was analyzed at 260 nm, 85 ℃ to 4 ℃ using a uv-vis spectrophotometer (v-630, JASCO Corporation, Japan), and the T_m value was calculated with the differential method. [13].

2.2.6. T5 exsonuclease resistance of pclDNAzyme

^{CNV}K-introduce DNAzyme or pclDNAzyme (200 nM) in NEBuffer 4 (pH=7.9) was incubated

in a heat block at 37 ℃ for 15 minutes and Phosphodiesterase I (SIGMA-ALDRICH, SL, USA, 10 mM) was added.

2.3 Results and discussion

2.3.1. Denatured PAGE purification of photo-cross-linked DNAzyme (pclDNAzyme)

10 μM ^{CNV}K-introduced DNAzyme and buffer (50 mM Tris-HCl (pH = 7.5) containing 200 mM KCl and 100 μM KCl) were mixed. The mixed sample solution was annealed from 90 ℃ to 4 ℃. The mixed sample solution was illuminated with a UV-LED illuminator (OMRON, Tokyo, Japan, 1600 mW) at 385 nm for 5 minutes. Electrophoresis (150 V, 100 min) using 20% denaturing gel was performed to extract photo-cross-linked DNAzyme (pclDNAzyme) and soaked overnight at 37 ℃ with 5 × TB buffer.

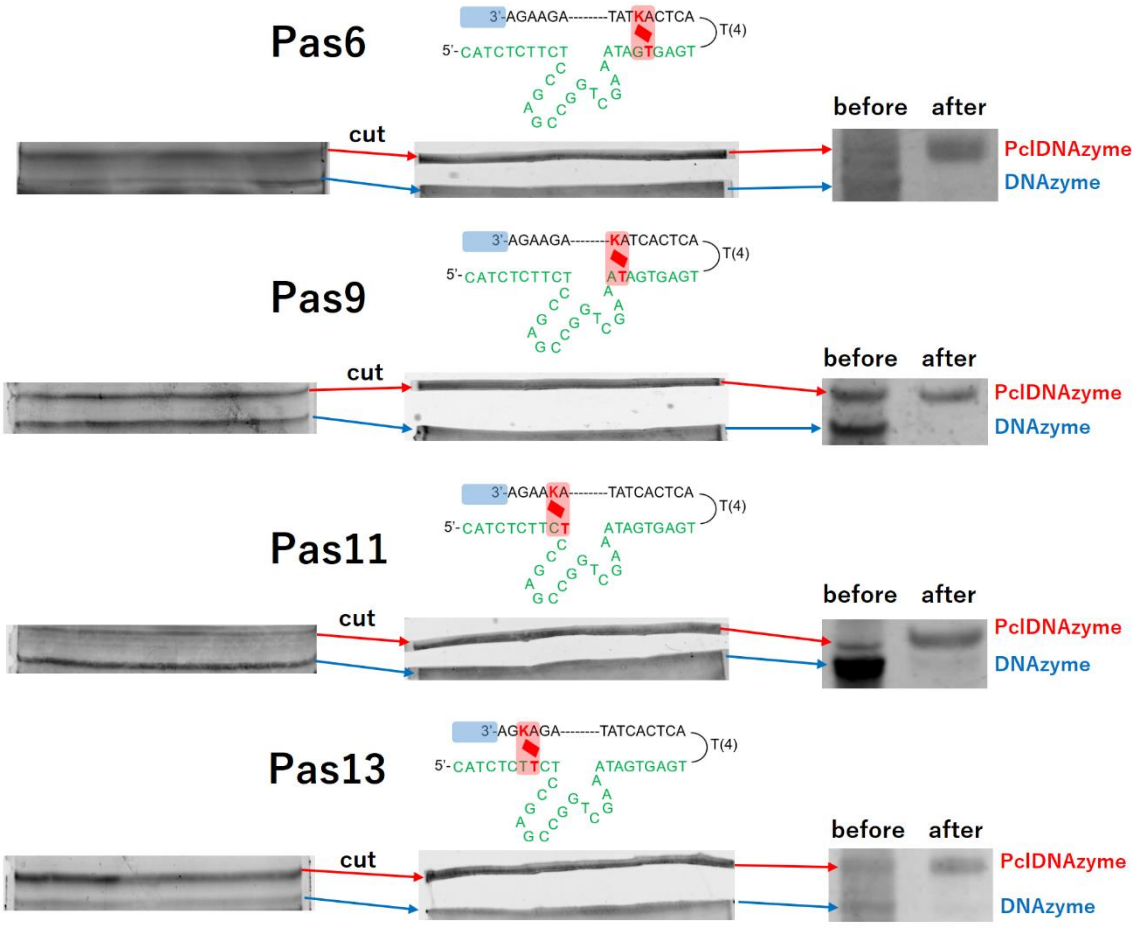

Figure 2.10. Purification of photo-cross-linked DNAzyme by denaturing. Each ^{CNV}K-introduced DNAzyme solution in buffer (10 × buffer (50 mM Tris-HCl (pH = 7.5) containing 200 mM KCl and 100 M ZnCl) was annealed in a heat block at 90 ℃ to 4 ℃. A UV-LED lamp was used to photoirradiate the solution at 385 nm for 5 minutes. The pclDNAzyme was purified using a 20% denaturing PAGE electrophoresis, and the band corresponding to the pclDNAzyme was excised and eluted from the gel into 5xTB buffer overnight.

2.3.2 Complete inhibition of DNAzyme activity by photo-cross-linking

Pas13 was used to verify the activity-suppressing efficacy of pclDNAzyme. Non-photo-cross-linked DNAzyme and pclDNAzyme were combined with substrate strands and reacted at 37 ℃. To see convasion, reaction solution was sampled at 0, 15, 30, 60, 120, and 180 minutes and electrophoresed on a 15% polyacrylamide denatured gel. Quantified by Cy3 fluorescence modified at the 5' position of the substrate strand. The non-photo-cross-linked DNAzyme (ON state) cleavage rate was calculated to be 84.2% at 60 minutes and 85.6% at 180 minutes. On the other hand, the photo-cross-linked DNAzyme maintained a cleavage rate of 0% from 0 min to 180 min. Which proves that photo-cross-linking has the effect of entirely turning off the activity. A DNA strand substitution reaction extrudes passenger strand in the non-photo-cross-linked DNA enzyme (ON state) into the substrate strand. RNA is cleaved when invasion of the substrate strand proceeded to the active site. The pclDNAzyme (OFF state) can prevent the invasion of the substrate strand by the covalent bond of ^{CNV}K. As a result, the pclDNAzyme is thought to have created a thermo irreversible structure that may entirely restrict activity.

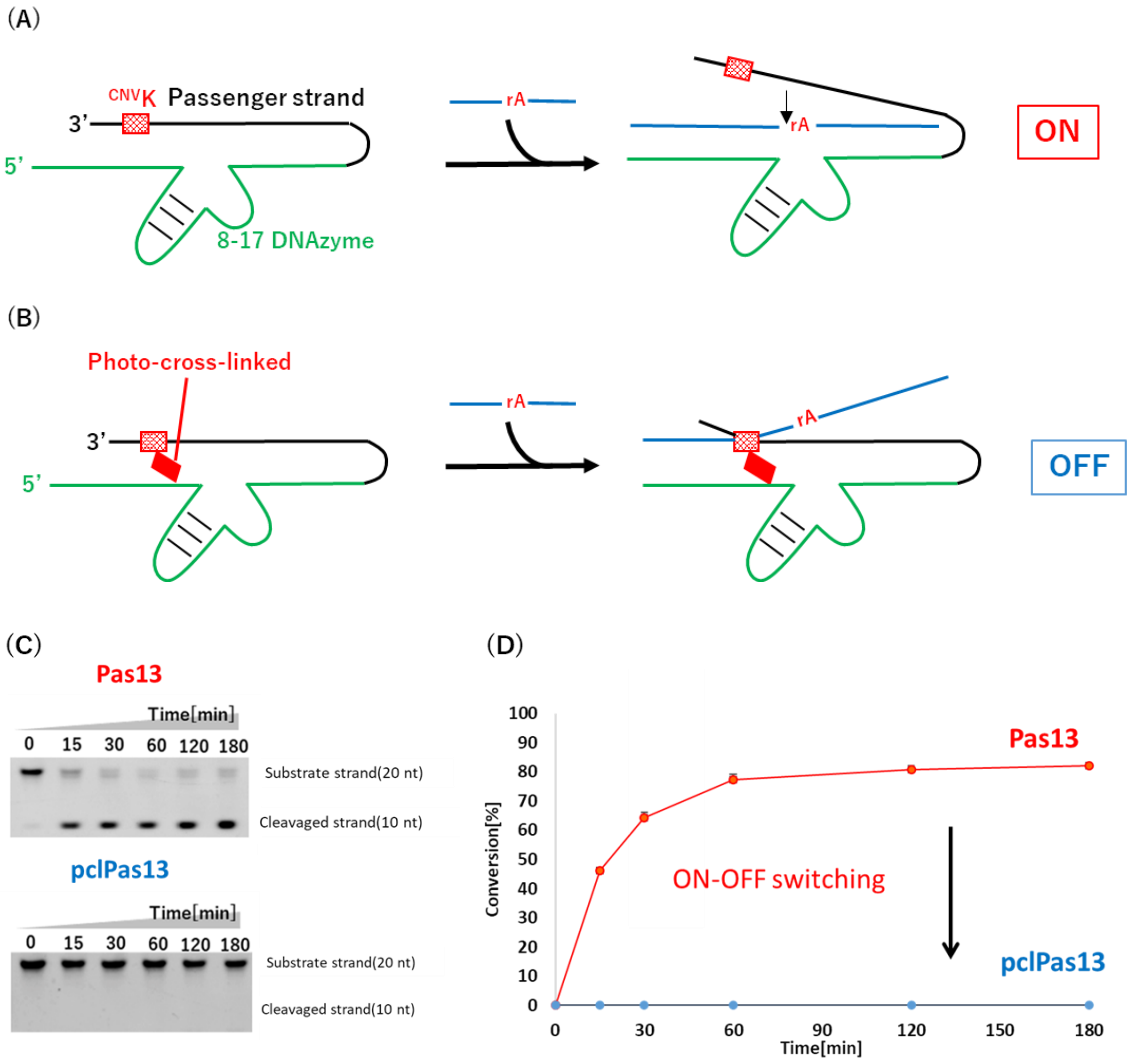

Figure 2.11. (A) (B) Substrate strand cleavage schemes for pclDNAzyme and non-photo-cross-linked DNAzyme. (C) Denatured PAGE analysis after substrate strand cleavage. (D) Time course of cleavage ratio of substrate strand. The 100 nM DNAzyme strand and 1000 nM target strand in 50 mM Tris-HCl (pH = 7.5) containing 200 mM KCl and 100 μM $ZnCl_2$ was incubated at 37 ℃.

2.3.3 Switching from photo-cross-linked DNAzyme to psDNAzyme

The pclDNAzyme was then photoirradiated at 312 nm to create the psDNAzyme (ON state). Because the covalent bond is photo-split, the psDNAzyme changes from OFF to ON. The pclDNAzyme (100 nM) was combined with the buffer (50 mM Tris-HCl, pH 7.5, 200 mM KCl, and 100 mM $ZnCl_2$) and incubated for 15 minutes. Then, a 1000 nM substrate strand was added to the mixture, followed by 15 minutes of photoirradiation at 312 nm. The time-dependent reaction was set for 0, 15, 30, 60, 120, and 180 minutes at the same time that the photoirradiation started. The pclDNAzyme was photoirradiated at 312 nm to produce a psDNAzyme (ON state) with a cleavage ratio of 38.1% at 180 minutes (k_{cat} = 2.5 min^{-1}) and a first reacton rate of 1.0×10^{-3} min^{-1}. The concentration of substrate in this investigation was ten times that of DNAzyme. The cleavage ratio of psDNAzyme was greater than 10%, indicating that psDNAzyme catalyzed substrate strand cleavage. The DNAzyme activity switches from OFF to ON when ^{CNV}K is photosplit by 312 nm irradiation, according to these results.

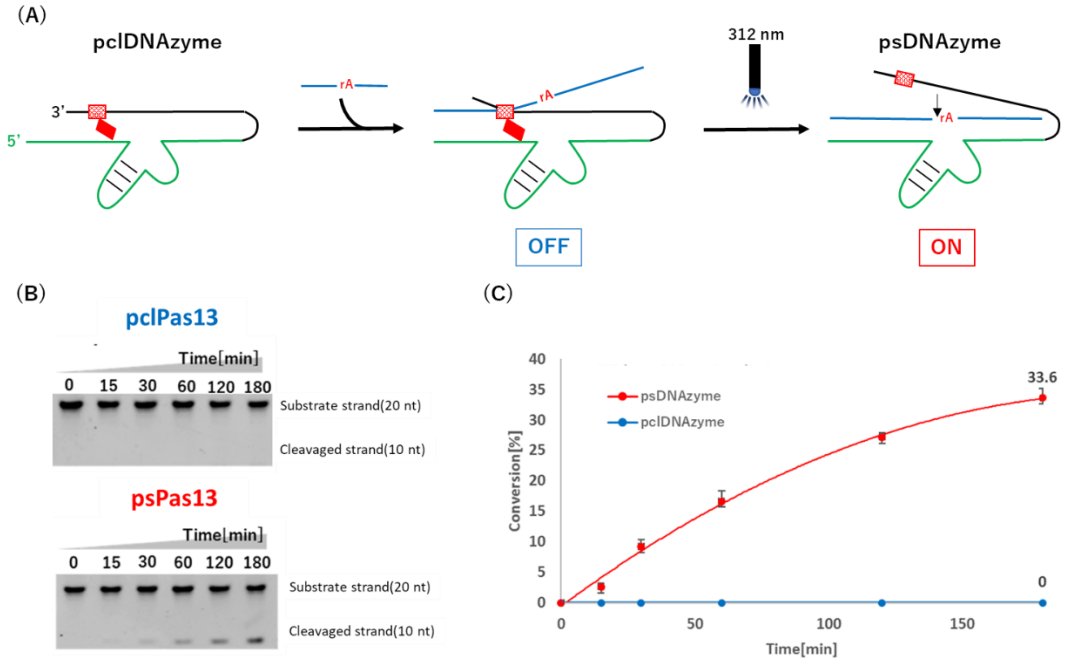

Figure 2.12. (A) Scheme of regulation of DNAzyme activity (B) Denatured PAGE analysis after substrate strand cleavage. (C) Time course of cleavage ratio of substrate strand. The 100 nM DNAzyme strand and 1000 nM target strand in 50 mM Tris-HCl(pH 7.5) containing 200 mM KCl and 100 μM $ZnCl_2$ was incubated at 37 °C. 312 nm-irradiation was performed at 37 °C for 15 min.

2.3.4 Effect of cleavage activity by ^{CNV}K introduction position

It was discovered that pclPas13 succeeded in completely inhibiting its activity and in returning to the ON state by switching to the psDNAzyme. Next, we examined how the activity inhibition efficiency and reactivation efficiency are affected by changing the introduction position of ^{CNV}K. The prepared sequences are the sequences in which the 6th (Pas6), 9th (Pas9), and 11th (Pas11) nucleobases from the 5' side of the Passenger strand are substituted with ^{CNV}K, respectively.

A band identical to the cleaved band was found in the case of pclPas6 and pclPas9, confirming DNAzyme activity leakage. The new band was not observed in the case of pclPas13, as it was in the case of pclPas11. pclPas6, pclPas9, pclPas11, and pclPas13 had cleavage ratios of 37.3 percent, 10.3%, 0%, and 0%, respectively. The cleavage ratios of psDNAzyme were then assessed (ON state). psPas6, psPas9, and psPas11 had cleavage ratios of 60.2%, 59.7%, and 38.1%, respectively. Despite the fact that pclPas9 inhibited DNAzyme activity more than pclPas6, it was not able to entirely stop it. By forming a covalent bond, pclPas11 and pclPas13 were able to prevent DNA strand displacement at the active site completely. According to these findings, a control leak develops when the photo-cross-linking position is 5' away from the active site, and the activity is entirely inhibited when it is 3' away [14]. In addition, the inserted position of caged nucleoside to DNAzyme is a significant element in photochemical activation of DNAzyme activity via photoirradiation. When designing a single photocaged nucleoside to sufficiently reduce DNAzyme activity, careful sequence optimization is essential to avoid metal ion coordination; otherwise, several caged nucleosides are required. However, due to toehold-mediated strand displacement, ^{CNV}K allows very simple designs. It is considered that the change in the cleavage activity of the ON state depending on the photo-cross-linking position of ^{CNV}K is due to the photocleavage rate of pclDNAzyme. The photocleavage rates were determined to be 60.2%, 62.0%, 58.4%, and 50.2% for Pas6, Pas9, Pas11 and Pas13, respectively. It is suggested that the cleavage activity of the ON state decreased due to insufficient photosplit rate and photooxidation by photoirradiation at 312 nm.

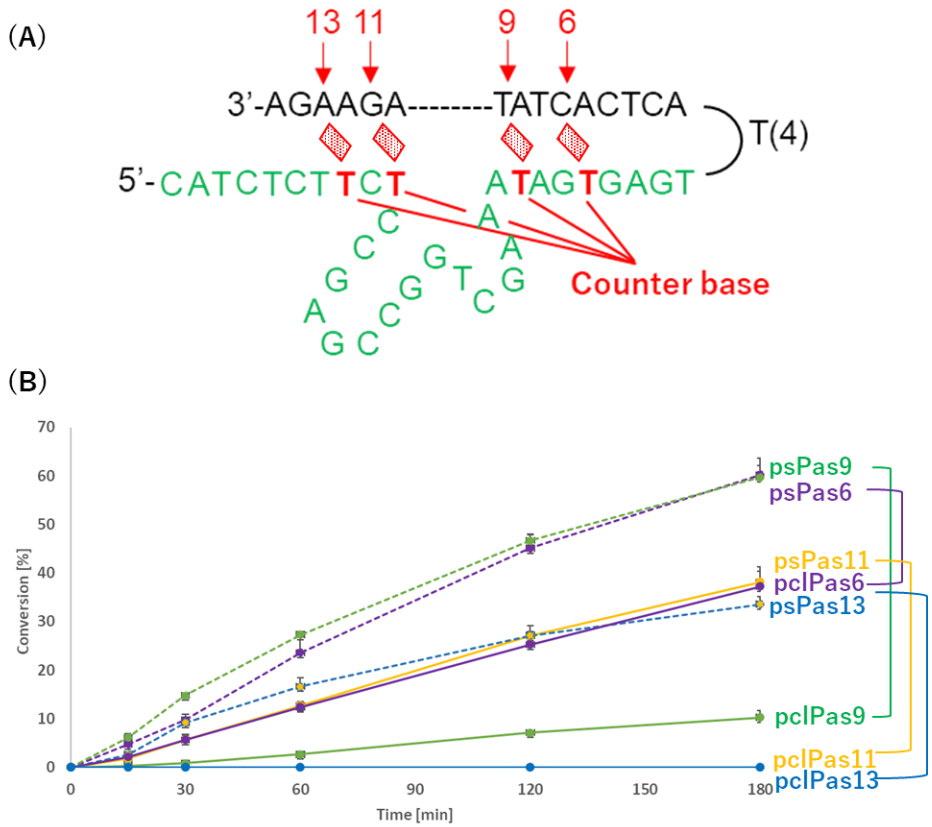

Figure 2.13. (A) ^{CNV}K introduction position and secondary structure. (B) The 100 nM DNAzyme strand and 1000 nM target strand in 50 mM Tris-HCl (pH 7.5) containing 200 mM KCl and 100 μM $ZnCl_2$ was incubated at 37 ℃. 312 nm photoirradiation was performed at 37 ℃ for 15 min.

Table 2.2 Cleavage rate and ON/OFF ratio of each DNAzyme

Entry	Activity* [%] (OFF state)	Activity* [%] (ON state)	ON/OFF ratio	Photosplit rate [%]
pclPas13	< 1	33.6 ± 1.5	100 >	50.2
pclPas11	< 1	38.1 ± 3.1	100 >	58.2
pclPas9	10.3 ± 1.4	59.7 ± 2.4	5.76	62.0
pclPas6	37.3 ± 3.0	60.2 ± 3.4	1.61	62.0

*Activity is cleavage ratio of substrate strand at 37 ℃ for 180 min.

2.3.5 Effect of toehold (TH) length on cleavage activity

It was clarified that the inhibition efficiency and the cleavage activity of psDNAzyme changed depending on the position of ^{CNV}K. The change in activity at the ^{CNV}K position is thought to be due to the stability of hybridization between the DNAzyme and the substrate strand. It is considered that the substrate strand always repeats the DNA strand substitution reaction up to the photo-cross-linking position so that pclPas6 and pclPas9 cause an activity leak. That is, the speed of switching the cleavage activity is affected by the distance to the photo-cross-linking position and the length of TH. Therefore, a sequence (Pas13-TH2) in which TH of Pas13 was shortened from 4 bases to 2 bases was prepared. The experimental conditions are the same as above. The cleavage rate of psPas13-TH2 was 30.0% at 180 min. The cleavage rate of psPas13 was 33.6%, and the cleavage rate decreased while the ^{CNV}K position was exactly the same. It is considered that this is because the equilibrium state between the substrate strand and the photo-cross-linking position is weakened as the length of TH is shortened[15].

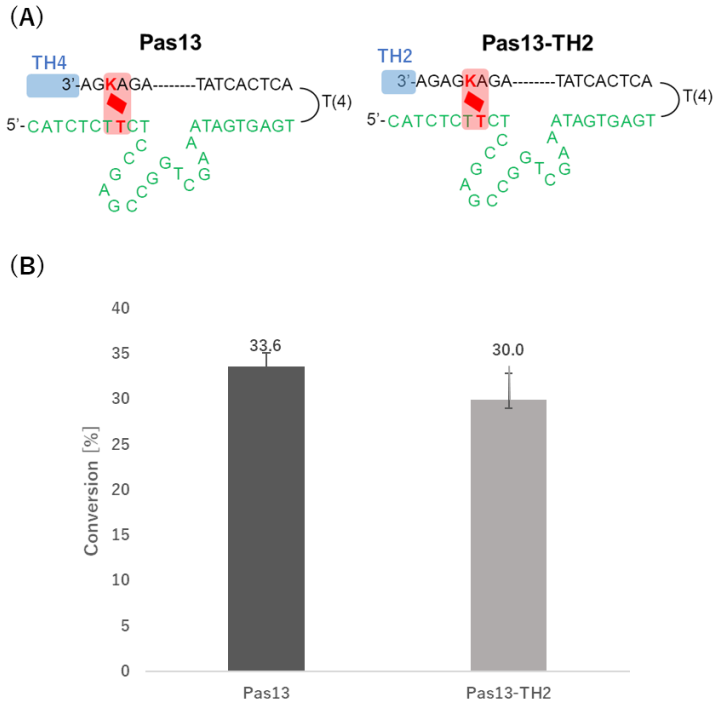

Figure 2.14. (A) Secondary structure of pclPas13 and pclPas13-TH2. (B) The 100 nM DNAzyme strand and 1000 nM target strand in 50 mM Tris-HCl (pH 7.5) containing 200 mM KCl and 100 μM $ZnCl_2$ was incubated at 37 ℃ for 180 min. 312 nm photoirradiation was

performed at 37 ℃ for 15 min.

2.3.6 Relationship between psDNAzyme cleavage activity and T_m value

The photo-cross-linking position and the length of TH were discovered to alter the cleavage activity. The T_m value of each non-photo-cross-linked DNAzyme was measured in order to get data supporting these phenomena. Pas6, Pas9, Pas11, Pas13, Pas13-TH=2, and WT-TH4 had T_m values of 40.6 ℃, 45.1 ℃, 56.4 ℃, 51.2 ℃, 51.6 ℃, and 57.4 ℃, respectively. The T_m value was discovered to be lower because the ^{CNV}K position was on the 5' side of the passenger strand[14]. ^{CNV}K causes steric hindrance and instability of Passenger strands when compared to natural nucleobases. The Passenger strand on the 5' side is thought to be more vulnerable to steric hindrance, and Pas6 and Pas9 have exceptionally low T_m value. Without applying this rule, only Pas11 had a high T_m value. The active site corresponds to the region of thymine, which is the photo-cross-linking position of Pas11, and a sterically free space is generated[15, 16]. The Passenger strand is thought to have become rather stable because the equilibrium state was maintained and the ^{CNV}K was buried in the active site pocket. The near T_m value to the DNAzyme of WT-TH4 without ^{CNV}K further implies that steric hindrance has a significant effect.

The T_m value was in the order of Pas11> Pas13-TH=2 ≧ Pas13> Pas9> Pas6, and the cleavage rate of psDNAzyme was in the order of Pas6> Pas9> Pas11> Pas13> Pas13-TH = 2. It is suggested that the higher the T_m value, the higher the stability of the Passenger strand, and the slower the progress of the DNA strand displacement reaction.

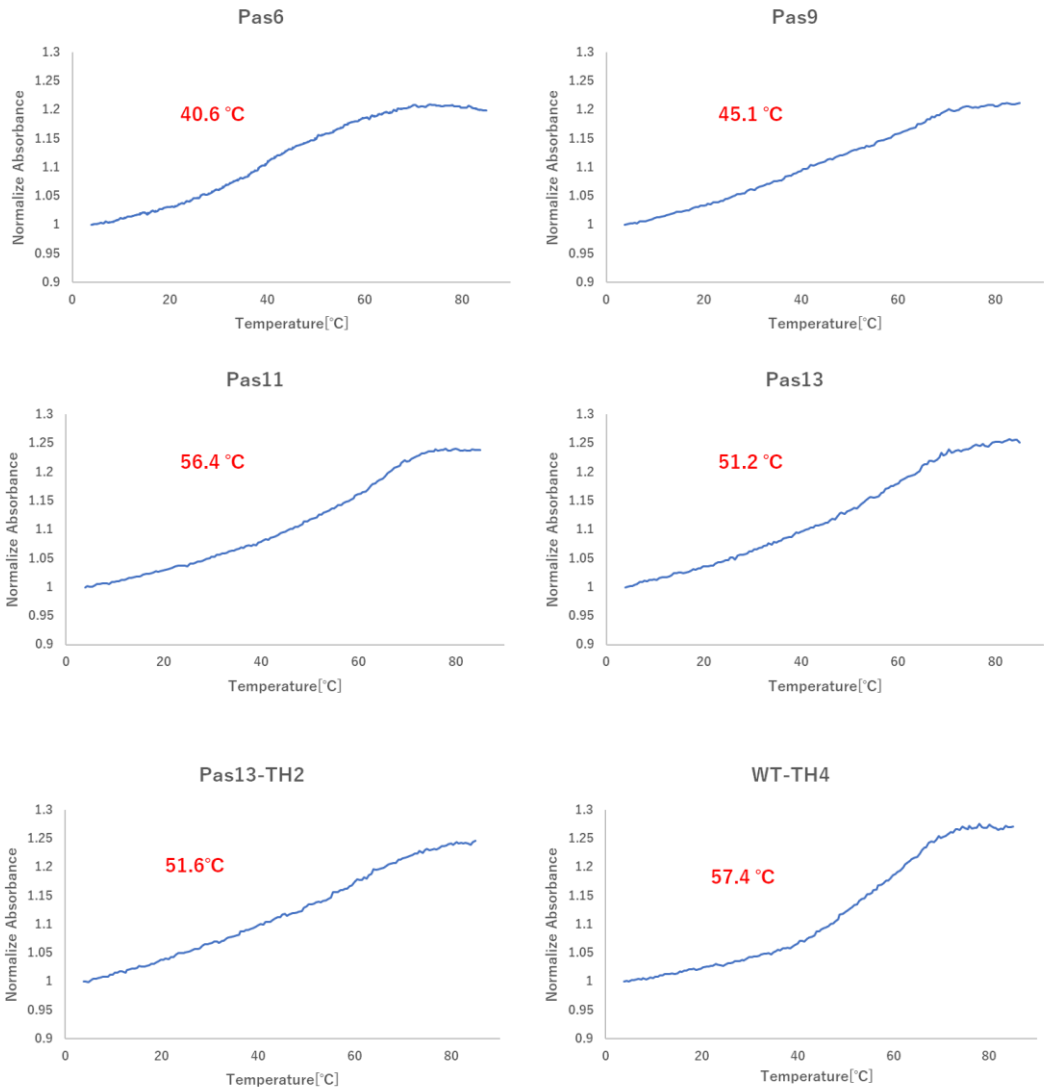

Figure 2.15. Melting curve of each DNAzyme. Sample solutions were prepared by mixing 10 μM DNAzyme and buffer (50 mM Tris-HCl (pH = 7.5) containing 200 mM KCl and 100 μM $ZnCl_2$). The Melting curve was analyzed at 260 nm, 85 ℃ to 4 ℃ using uv-vis spectrophotometer.

2.3.7 Enzymatic degradation resistance of photo-cross-linked DNAzyme

Foreign nucleic acids are always cleaved by nucleases under *in vivo* circumstances[17]. As a result, a number of methods for enhancing nuclease resistance have been devised. The most significant aspect for cellular application is high resistance to DNAzyme nucleases. Phosphorothioate is the most common technique[18]. Phosphorothiolate substitutes sulfur for portion of the phosphoric acid, making it simpler to avoid nuclease recognition. Reverse

thymidine and LNA are two more chemical changes that are well-known[19, 20]. Nuclease resistance is conferred by chemical changes such as ^{CNV}K. We show that photo-cross-linked triple-stranded DNA is resistant to T5 exonuclease enzymatic breakdown[21].

T5 exonuclease treatment was used on the photo-cross-linked DNAzyme in this investigation to imitate its stability under *in vivo* settings. T5 exonuclease and pclDNAzyme or non-photo-cross-linked DNAzyme were incubated at 25 ℃ and evaluated on a 15% AA denatured PAGE. T5 exonuclease completely destroyed the non-photo-cross-linked DNAzyme after 30 minutes. However, a new band for pclDNAzyme was confirmed at 30 minutes. The T5 exonuclease degrades from the 5' side end, implying that the degradation stops at the photo-cross-linking site. In fact, the non-photo-cross-linked DNAzyme degrades with time, from 5 to 10 minutes, and the band vanishes entirely. However, it was discovered that pclDNAzyme did not experience band shift from 5 to 30 minutes and kept the backbone intact. As a result, even after T5 exonuclease treatment, pclDNAzyme retained 75% backbone. The ability of pclDNAzyme to withstand nuclease degradation is a very useful trait for *in vivo* applications.

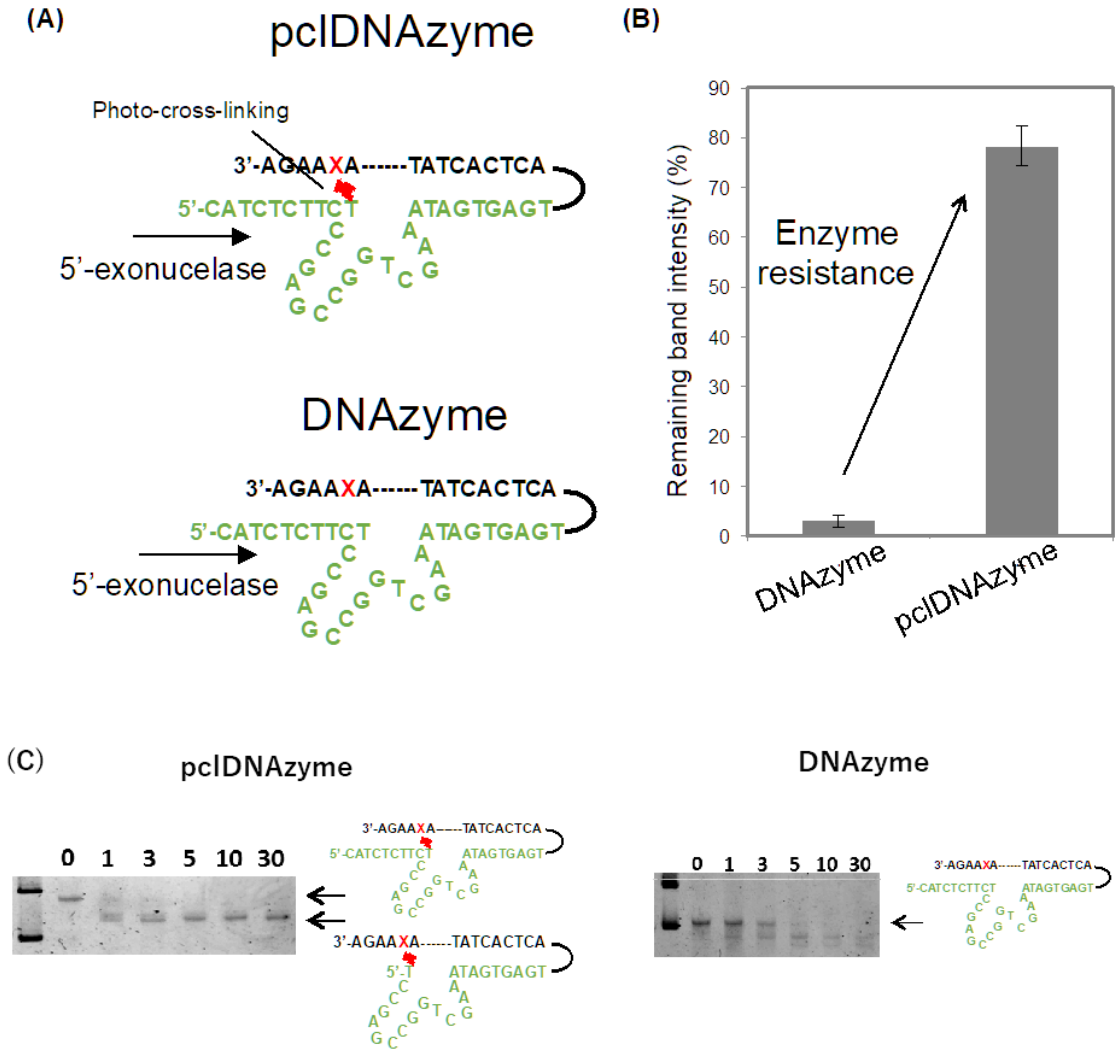

Figure 2.16. (A) T5 exonuclease treatment of DNAzyme and pclDNA. (B) Enzyme resistance of pclDNAzyme. 200 nM DNAzyme in NEBuffer 4 (pH=7.9) and T5 exsonuclease (NEB) were incubated at 37 °C in a heat block for 30min. (C) Time course of cleavage ratio of DNAzyme and pclDNAzyme.

2.3.8 Sequence selectivity of psDNAzyme

Inhibition of mRNA transcription is influenced by sequence specificity. If the psDNAzyme causes the random RNA to cleave, there is a risk of unexpected side effects due to the off-target effect [22]. 8-17 DNAzyme is a sequence-specific nucleic acid enzyme with a high activity. The non-substrate strand (5'-Cy3-GTAGGAAGGrATATCACTCA-3') was used to test the ability of sequence-specific cleavage with psDNAzyme. The reaction conditions are identical to those used previously. 15% AA denaturing PAGE analysis confirmed that The psDNAzyme did not cleave any non-substrate strands. This finding implies that an off-target effect from the introduction of passenger strands and ^{CNV}K is improbable.

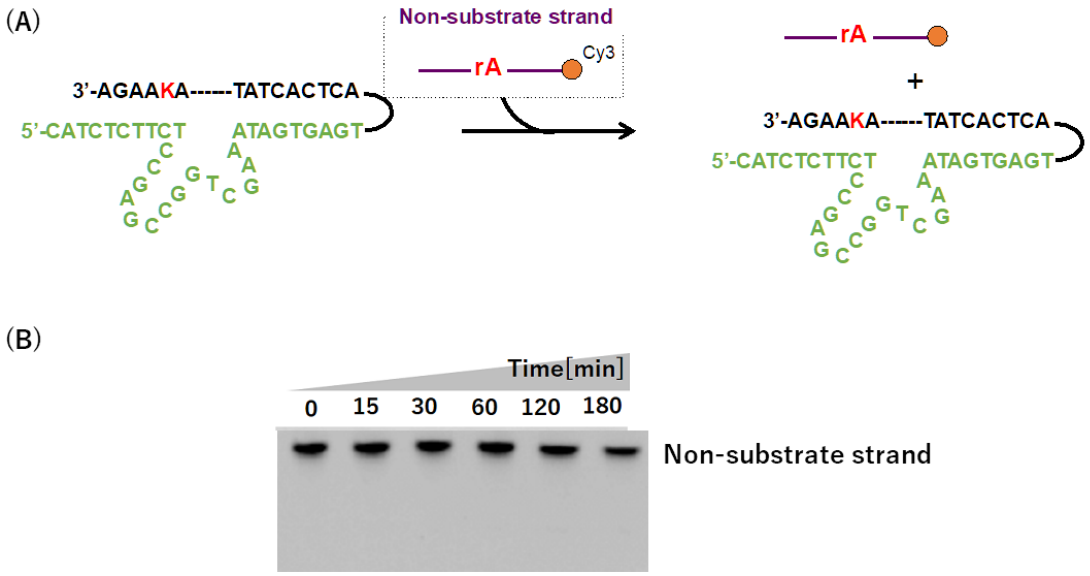

Figure 2.17. (A) Non-substrate strand cleavage scheme by DNAzyme. (B) 100 nM DNAzyme and 1000 nM non-substrate strand in buffer (50 mM Tris-HCl (pH = 7.5) containing 200 mM KCl and 100 μM $ZnCl_2$) was incubated at 37°C. Sample solutions mixed by modifier (saturation urea in formamide).

Conclusion

In this chapter, reversible ultrafast DNA photo-cross-linking of ^{CNV}K was used to demonstrate complete inhibition of DNAzyme activity. Photo-cross-linking completely inhibited DNAzyme activity because the substrate strand cannot invade the photo-cross-linked DNAzyme due to the covalent bond of ^{CNV}K. It was also shown that the DNAzyme activity switches to the "ON state" when the covalent bond of ^{CNV}K is photo-splitted by photoirradiation at 312 nm. It is suggested that pclDNAzyme may not only completely inhibits the activity but also inhibit the degradation of exonuclease. It was demonstrated that T5 exonuclease treatment inhibited enzymatic degradation at the photo-cross-linked position and maintained the backbone. From the above results, the activity of DNAzyme can be regulated accurately and spatiotemporally by photoirradiation. It has become possible to completely inhibits DNAzyme activity, which was difficult in previous studies, and it is expected to be used *in vivo* for its enzyme eresistance.

References

[1] A Wochner, J Attwater, A Coulson, P Holliger. Ribozyme-catalyzed transcription of an active ribozyme. *Science*, **2011**, 332(6026), 209-12.

[2] G William, T ScottJohn, A K Finch. The crystal structure of an AII-RNAhammerhead ribozyme: A proposed mechanism for RNA catalytic cleavage. *Nucleic Acids Symp Ser.*, **1995**, (34), 214-6.

[3] S F Torabi, P Wu, C E. McGhee, L Chen, K Hwang, N Zheng, J Cheng, Y Lu. *In vitro* selection of a sodium-specific DNAzyme and its application in intracellular sensing *PNAS.*, **2015**, 112(19), 5903-8.

[4] Y Chen, M Wang, C Mao. An autonomous DNA nanomotor powered by a DNA enzyme. *Angew Chem Int Ed Engl.*, **2004**, 43(27), 3554-7.

[5] F Yang, Y Liu, B Wang, C Zhou, Q Zhang. Constructing Controllable Logic Circuits Based on DNAzyme Activity. *Molecules*, **2019**, 24(22), 4134.

[6] X H Zhao, R M Kong, X B Zhang, H M Meng, W N Liu, W Tan, G L Shen, R Q Yu. Graphene-DNAzyme based biosensor for amplified fluorescence "turn-on" detection of Pb2+ with a high selectivity. *Anal Chem.*, **2011**, 83(13), 5062-6.

[7] T Nakama, Y Takezawa, D Sasaki, M Shionoya, Allosteric Regulation of DNAzyme Activities through Intrastrand Transformation Induced by Cu(II)-Mediated Artificial Base Pairing. *J. Am. Chem. Soc.*, **2020**, 142 (22), 10153–62.

[8] K Tanabe, K Okada, M Sugiura, T Ito, S Nishimoto, Hypoxic X-irradiation as an external stimulus for conformational change of oligodeoxynucleotides that possess disulfide bond and regulation of DNAzyme function. *Bioorg Med Chem Lett.*, **2015**, 25(2), 310-2.

[9] H Lusic, D D Young, M O Lively, A Deiters. Photochemical DNA activation. *Org Lett.* **2007**, 9(10), 903-6.

[10] K Hwang, P Wu, T Kim, L Lei, S Tian, Y Wang, Y Lu, Photocaged DNAzymes as a general method for sensing metal ions in living cells. *Angew Chem Int Ed Engl.*, 2**014**, 53(50), 13798-802.

[11] M Zhou, X Liang, T Mochizuki, H Asanuma, A light-driven DNA nanomachine for the efficient photoswitching of RNA digestion. *Angew Chem Int Ed Engl.*, **2010**, 49(12), 2167-70.

[12] C E Castro, F Kilchherr, D N Kim, E L Shiao. T Wauer, P Wortmann, M Bathe, H Dietz,

A primer to scaffolded DNA origami. *Nat Methods.*, **2011**, 8(3), 221-9.

[13] J M Sanchez-Ruiz. Theoretical analysis of Lumry-Eyring models in differential scanning calorimetry. *Biophys J.*, **1992**, 61(4), 921-35.

[14] S Nakamura, H Kawabata, K Fujimoto. Sequence-specific DNA photo-splitting of 3-cyanovinylcarbazole using DNA strand displacement. *Chem. Lett.*, 45(8), **2016**, 887-889.

[15] M C Plaza, A Peracchi. Insights into DNA catalysis from structural and functional studies of the 8-17 DNAzyme. *Org Biomol Chem.*, **2020**, 18(9), 1697-1709.

[16] H Liu, X Yu, Y Chen, J Zhang, B Wu, L Zheng, P Haruehanroengra, R Wang, S Li, Jinzhong Lin, Jixi Li, Jia Sheng, Zhen Huang, Jinbiao Ma, Jianhua Gan. Crystal structure of an RNA-cleaving DNAzyme. *Nat Commun.*, **2017**, 8(1), 2006.

[17] H O Smith, K W Wilcox. A restriction enzyme from Hemophilus influenzae: I. Purification and general properties. *J Mol Biol.*, **1970**, 51(2), 379-91.

[18] J P Sheehan, H C Lan. Phosphorothioate oligonucleotides inhibit the intrinsic tenase complex. *Blood*, **1998**, 92(5), 1617-25.

[19] B Vester, L B Lundberg, M D Sørensen, B R Babu, S Douthwaite, J Wengel. LNAzymes: incorporation of LNA-type monomers into DNAzymes markedly increases RNA cleavage. *J Am Chem Soc.*, **2002**, 124(46), 13682-3.

[20] M Chakravarthy, M T Aung-Htut, B T Le, R N Veedu. Novel Chemically-modified DNAzyme targeting Integrin alpha-4 RNA transcript as a potential molecule to reduce inflammation in multiple sclerosis. *Sci Rep.*, **2017**, 7(1), 1613.

[21] K Fujimoto, H Yoshinaga, Y Yoshio, T Sakamoto. Quick and Reversible Photocrosslinking Reaction of 3-Cyanovinylcarbazole Nucleoside in DNA Triplex. *Organic & Biomolecular Chemistry*, **2013**, 11, 5065-5068.

[22] A L Jackson, S R Bartz, J Schelter, S V Kobayashi, J Burchard, M Mao, B Li, G Cavet, P S Linsley. Expression profiling reveals off-target gene regulation by RNAi. *Nat Biotechnol.*, **2003**, (6), 635-7.

[Chapter 3] Development of duplex invasion antigene method via photo-cross-linking reaction

3.1 Introduction

Nucleic acid drugs are expected as a treatment method for intractable diseases such as cancer [1] and muscular dystrophy [2]. Gene therapy is classified into mRNA-targeted methods (RNAi [3], antisense method [4]) and DNA-targeted methods (artificial restriction enzymes [5], antigene method [6]). DNA is the most upstream of the central dogma, and methods targeting genomic DNA provide the underlying disease treatment. Currently, the most famous method of knocking out genomic DNA is CRISPR-Cas9 [7]. CRISPR-Cas9 introduces the encoding gene into a plasmid vector and specifically cleaves genomic DNA [8, 9]. In the CRISPR system, not only genomic DNA cleavage but also proteins capable of base editing [10] and RNA cleavage [11] have been discovered. On the other hand, nucleic acid drugs using RNAi and antisense methods have begun to be used mainly in the United States and Europe in the development of drug delivery systems (DDS) [12]. However, DNA-targeted antigenes have not yet been approved as nucleic acid drugs. Antigene methods are classified into triplex-forming oligodeoxynucleotide (TFO) [13, 14] and strand invasions. TFO is a Hoogsteen base pair formation method that requires biasing of purine and pyrimidine bases, resulting in a limited target sequence. Duplex Strand invasion (DSI) hybridizes to the target DNA with Watson click base pairs, so there are no restrictions on the target sequence. However, mRNA is single-stranded, and fully complementary-stranded ODNs can be easily hybridized. DSI needs to approach the stable double helix structure of DNA, and antigene probes must form thermodynamically unfavorable hybridization. That is, it is more difficult than hybridizing mRNA with Watson-Crick base pairs.

Double duplex invasion (DDI) with PNA and LNA has been developed as a means to solve DSI. Instead of the deoxyribose skeleton, PNA has a base attached to the amino acid skeleton and does not have phosphoric acid, which enables more electrostatically stable hybridization than DNA. In addition, LNA has an N-type nucleoside as a skeleton, which forms a more stable hybridization with DNA by cross-linking the 2' position and the 4'position of the ribose ring. In addition, our laboratory is developing DDI using ^{CNV}K. ^{CNV}K-introduced probe can be photo-cross-linked the moment it hybridizes to the target DNA and covalently binds to form a thermally irreversible structure. Both methods enable DSI by forming a more stable structure than wild-type DNA. However, DDI has major challenges. DDI is a technique that targets the target DNA double chain and uses two complementary probes. That is, DDI

inhibits the invasion of target DNA by hybridization between probes.

Self-complementation of DDI is the largest factor that reduces DSI efficiency, and both methods solve this problem by chemical modification. PNA reports that pseudocomplementary PNA (pcPNA) [15, 16] enhances steric hindrance between probes and reduces T_m values. In addition, 2,6-diaminopurine (D) and d 2-thiouracil (sU) have succeeded in improving stability with DNA not only by steric hindrance but also by hydrophobic interaction. As for PNA, Chiral PNA which is an improved version of pcPNA, has also been developed. Chiral PNA [17] charges the probe with a positive charge by modifying lysine on the side chain of the amino acid skeleton. The probes repel each other by positive charge and form a more stable structure with the target DNA by electrostatic interaction.

Several techniques have been reported to inhibit the interaction of DDI probes in LNA [18]. The first is a method of modifying Pyrene to the 2' position and inhibiting the interaction between probes due to steric hindrance [19]. Pyrene enhances the interaction between the bases of the target DNA by π-π stacking and improves the invasion efficiency. The second is Zorro-LNA [20, 21], which is a method in which DDI probes are pre-complemented and two probes invade like one probe. When invaded, the Zorro-LNA probe can greatly expand the target DNA and form a stable structure.

^{CNV}K needs to inhibit not only hybridization but also self-photo-cross-linking between probes. 5-cyanouracil (^{CN}U) has been reported as a self-cross-linking inhibitor. LUMO levels of uracil base analogs are associated with suppression of photo-cross-linking of ^{CNV}K and uracil analogs [22]. By substituting ^{CN}U at the photo-cross-linking position of the DDI probe, self-photo-cross-linking of the DDI probe can be suppressed. However, ^{CN}U has also been found to be slightly complementary, and more optimized probes need to be designed to improve DDI efficiency. As a new self-cross-linking inhibitor, d-Spacer (dS) having no base and Spacer (S) having no sugar and base will be used for verification.

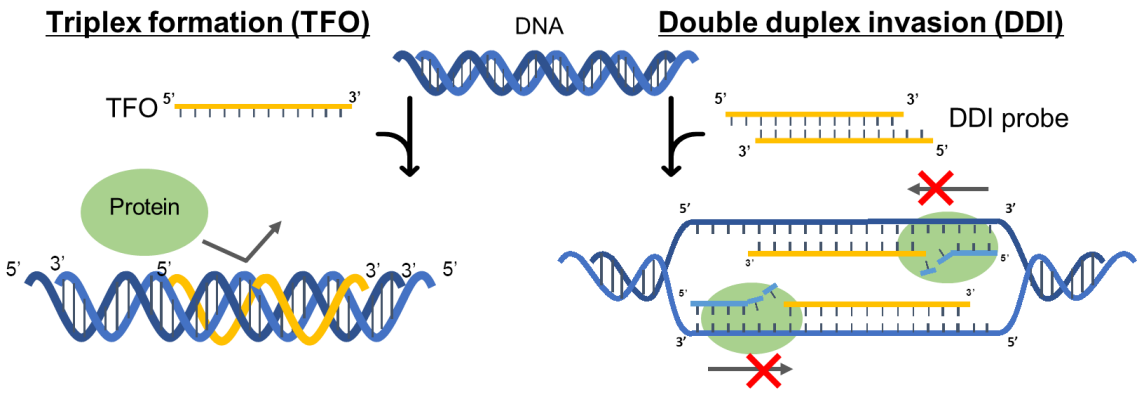

Figure 3.1. Scheme of pre-mRNA transcription inhibition by TFO and DDI.

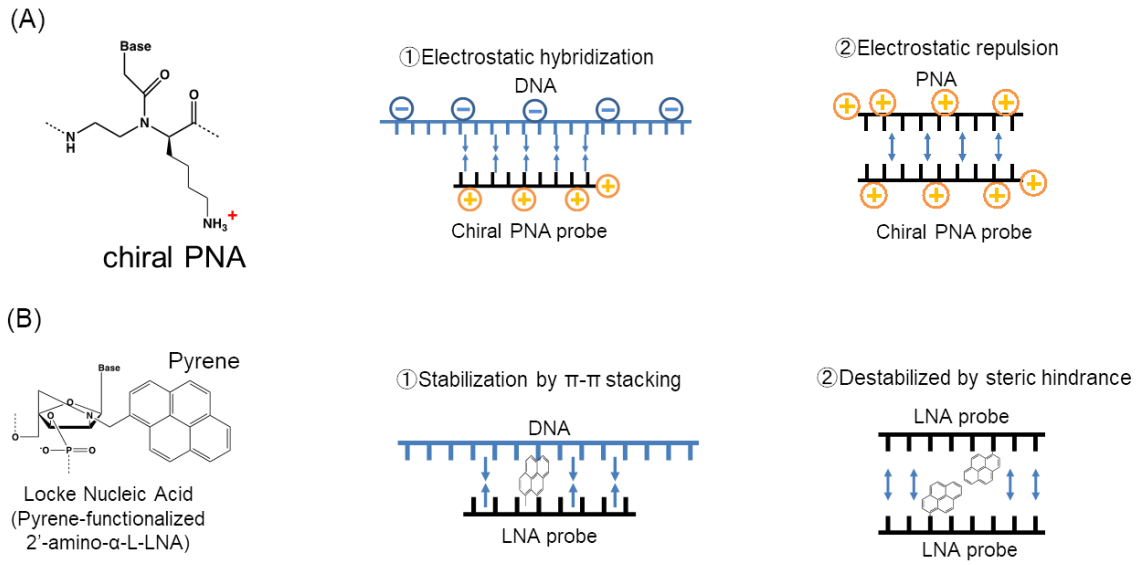

Figure 3.2. (A) Hybridization mode with Chiral PNA probe template and self-complementary repulsion between probes (*Necleic Acids Res.*, **2008**, 36, 1464). (B) Hybridization mode with Pyrene-modified probe template and self-complementary repulsion between probes (*Org.Ciomol. Chem.*, **2010**, 8, 2028).

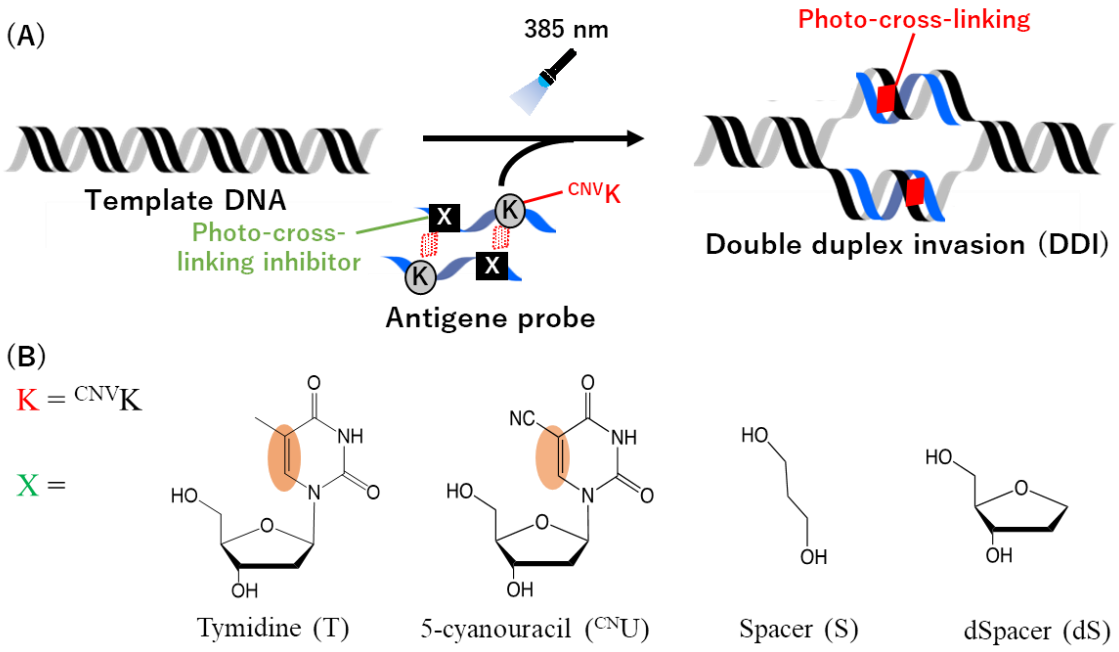

Figure 3.3. (A) DDI scheme using ^{CNV}K and self-photo-cross-linking inhibitor. (B) Self-crosslinking Inhibitor (T, ^{CN}U, dSpacer, Spacer) examined in this study.

3.2 Materials and Methods

3.2.1. Synthesis of ^{TF}T amidite

Phosphoramidite of Trifluorothymidine (^{TF}T) was synthesized using the method outlined in the literatute (Figure 4.2-4.11).

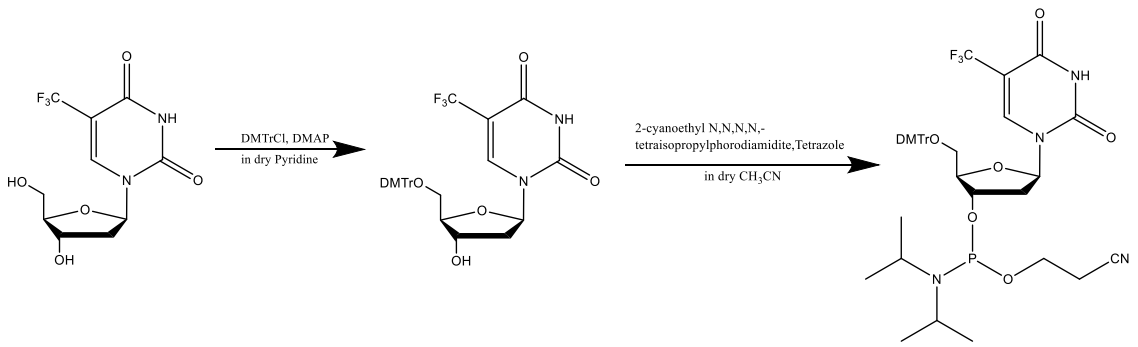

Figure 3.1. Synthesis overview scheme of ^{TF}T amidite

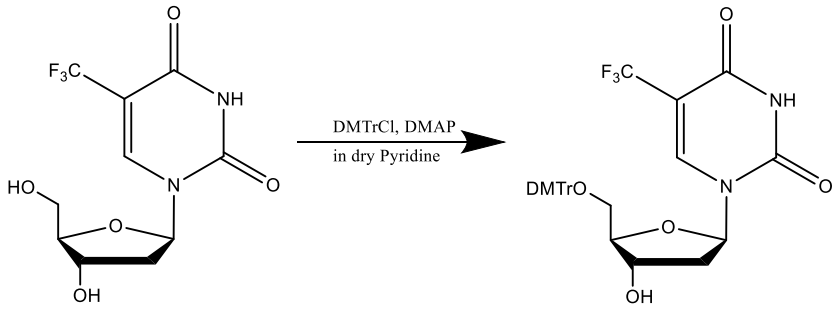

Figure 3.2. Synthesis scheme of 5'-o-(4, 4'-dimethoxytrityl)-3-trifluorothymidine-1'- β -deoxyriboside

A solution of 4,4'-dimethoxytrityl chloride (0.67 g, 1.6 mmol) and 4-(dimethylamino)pyridine (16.0 mg, 0.12 mmol) in pyridine (15 mL) was added to a solution of 5-trifluorothymidine-1'-deoxyriboside (0.40 g, 1.4 mmol) in pyridine (15 mL) and the reaction combination Following the evaporation of the reaction mixture, the residue was chromatographed on a silica gel using $CHCl_3$/MeOH/Et3N (19:1:0.2, v/v/v) as eluent to give 5'-protected 5'-o-(4, 4'-dimethoxytrityl)-3-trifluorothymidine-1'- β -deoxyriboside (0.71 g, 86.9%).

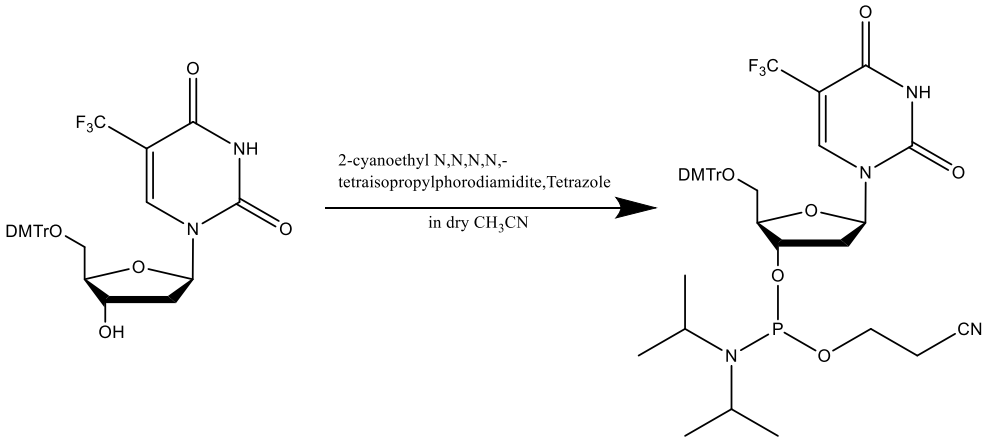

Figure 3.3. Synthesis scheme of 5'-O-(4, 4'-dimethoxytrityl)-5-trifluorothymidine-1'-β-deoxyriboside-3'-O-(cyanothoxy-N, N'-diisopropylamino) phosphoramidite

5'-o-(4, 4'-dimethoxytrityl)-5-trifluorothymidine-1'-β-deoxyriboside (0.71 g, 1.2 mmol), 2-cyanoethyl N,N,N',N'-tetraisopropylphosphorodiamidite (441 μL, 1.4 mmol) in CH_3CN (1.2 mL), and 0.45 M 1H-tetrazole in CH_3CN (2.8 mL) were added, and the reaction After that, AcOEt was used to extract the reaction mixture, which was then washed with a saturated aqueous solution of $NaHCO_3$ and water. The organic layer was recovered, dried over anhydrous sodium sulfate, filtered, and evaporated at reduced pressure to dryness. Then, the crude product in a sealed bottle was dissolved in CH_3CN and coevaporated three times as eluent to give 5'-O-(4, 4'-dimethoxytrityl)-5-trifluorothymidine-1'-β-deoxyriboside-3'-O-(cyanothoxy-N, N'-diisopropylamino) phosphoramidite (0.75 g, 78.4%).

3.2.2. Oligonucleotide synthesis

Oligonucleotides were synthesized by DNA synthesizer (NTS M-2-MIX_NPS) on a 1.0 μmol scale using High Load-CPG (Glen Research) attached each nucleotide. Synthesized oligonucleotides were cleaved from CPG with 28 % ammonia solution followed by deprotection of bases by incubation at 65 ℃ for 4 h. After removal of ammonia solution by speedvanc for 2h, the dry pellets were resuspended in distilled water and purified by HPLC. Purified products were characterized by MALDI-TOF MS.

Table 3.1 The sequence of ODNs

Entry	Sequence 5' to 3'	Calcd. for $[M+H]^+$	Found
Probe 1(T)	C**T**CTCGGCAGA^{CNV}**K**TCATTGGTC	6481.28	6481.14
Probe 2(T)	A**T**CTGCCGAGA^{CNV}**K**AGAGGATTA	6587.38	6587.05
Probe 1(^{CN}U)	C^{CN}**U**CTCGGCAGA^{CNV}**K**TCATTGGTC	6492.26	6491.12
Probe 2(^{CN}U)	A^{CN}**U**CTGCCGAGA^{CNV}**K**AGAGGATTA	6598.36	6597.20
Probe 1(S)	C**S**CTCGGCAGA^{CNV}**K**TCATTGGTC	6315.14	6315.58
Probe 2(S)	A**S**CTGCCGAGA^{CNV}**K**AGAGGATTA	6421.24	6321.53
Probe 1(dS)	C**dS**CTCGGCAGA^{CNV}**K**TCATTGGTC	6357.18	6357.79
Probe 2(dS)	A**dS**CTGCCGAGA^{CNV}**K**AGAGGATTA	6463.28	6463.90

S = Spacer, dS = dSpacer

3.2.3. Evaluation of DDI efficiency depending on various kinds of probes (DDI assay)

Each DDI probes containing ^{CNV}K as photo-cross-linker, and ^{CN}U, Spacer or dSpacer as photo-cross-linking inhibitor was synthesized. Each 100 nM template strand in 10 mM Tris HCl buffer (pH 7.4) were incubated at 37 ℃ for 10 min followed by addition of 10 μM each probe solutions that were incubated at 37 ℃ in the same buffer. After the incubation of the mixture at 37 ℃ for 1 h, it was photoirradiated at 385 nm for 15 min using Omunicure (12400 mW/cm2). Sample solutions were analyzed by denaturing PAGE using 15 % polyacrylamide gel. Cy3 images were obtained by LAS-3000 and band intensity was determined by ImageJ software. DDI efficiency was calculated by the average ratio of shifted band and template band.

3.3.4. Evaluation of the thermodynamics parameters depending on kinds of photo-cross-linking-inhibitor

9 mer template strand containing ^{CNV}K and complementary strand containing ^{CN}U, Spacer and dSpacer were synthesized. For measurement of T_m value, 7.5, 10 and 15 μM each template and complementary strand in 10 mM sodium phosphate solution (pH 7.4, 100 mM NaCl) were prepared. The absorbance of the mixture at 260 nm was measured using UV-vis spectrophotometer (JASCO, V-630bio) ranging from 4 ℃ to 85 ℃ and from 85 ℃ to 4 ℃. T_m

values were determined from obtained data by calculating inflection points of approximate curves.

3.3.5. T_m value measurement

Sample solutions were prepared by mixing 3, 4, 6.25, 7 μM ODN and buffer (10 mM Tris-HCl (pH = 7.5) containing 1 M NaCl). The Melting curve was analyzed at 260 nm, 85 °C to 4 °C using uv-vis spectrophotometer (v-630, JASCO Corporation, Japan), and the T_m value was calculated by the differential method. The thermodynamic parameters were calculated using the following formula.

$$\Delta H = 1.987 \times 10\text{-}3 \,/\, \mathrm{Tilt}$$
$$\Delta S = \Delta H \times 103 \cdot \mathrm{Intercept}$$
$$\Delta G = \Delta H - T_m \cdot \Delta S \times 10^{-3}$$

3.3 Results and discussion

3.3.1 Examination of inhibitors for improving self-photo-cross-linking inhibition

Because Spacer (S) and dSpacer (dS) do not have a double bond between C5C6 of the pyrimidine targeted by ^{CNV}K, it is expected that if photo-cross-linking between probes can be entirely repressed, more efficient DDI will be achievable. Four types of 5 μM Probe1 and Probe2 in 10 mM Tris-HCl (pH 7.4) buffer were incubated for 15 min. The mixed solution was irradiated with light at 385 nm for 5 seconds, analyzed on a 15% acrylamide-modified PAGE, and stained with SYBR gold. In all samples, a probe-derived band was seen before photoirradiation, and a new probe-derived band from the photo-cross-linking probe appeared after photoirradiation. However, there were differences in the photo-cross-linking rates. The residual amount of the probe was quantified by Image J before and after photoirradiation, and the photo-cross-linking rate was calculated. The photo-cross-linking rates for T, ^{CN}U, dS, and S were determined to be 87%, 19%, 17%, and 11%, respectively. ^{CNV}K and thymine have the highest self-cross-linking rate due to their ultrafast photo-cross-linking properties. Moreover, ^{CN}U was able to suppress the cross-linking efficiency compared to T (thymine). In addition, ^{CN}U was able to suppress the photo-cross-linking efficiency compared to T. On the other hand, because dS and S do not have a base, they succeeded in suppressing self-photo-cross-linking

more than ^{CN}U. As a factor of slight photo-cross-linking, it is possible that the probe can move freely because it does not have a base and can photo-cross-link with a pyrimidine other than the target.

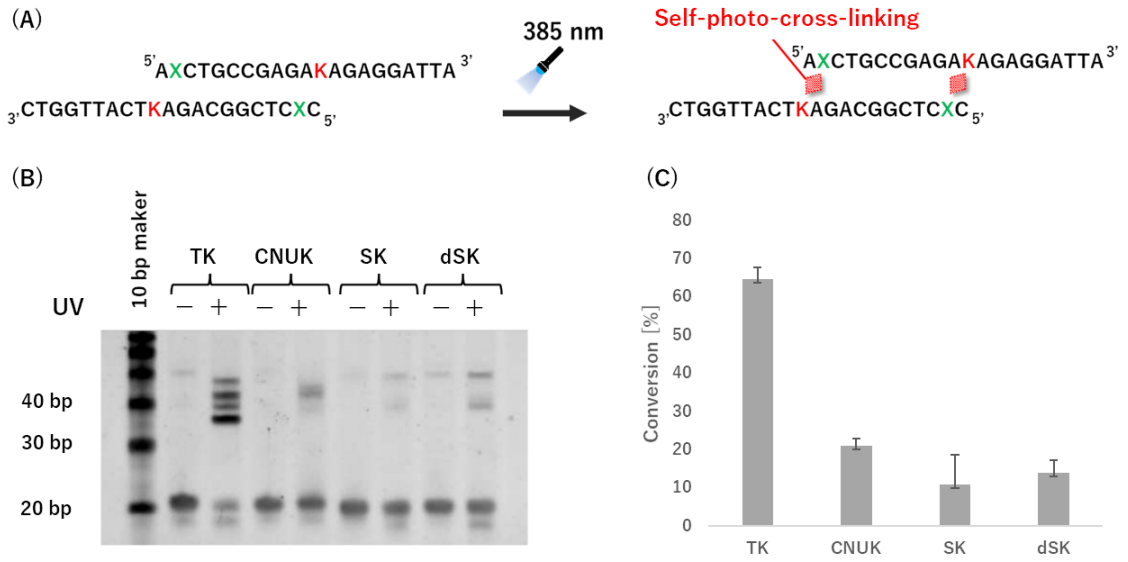

Figure 3.4. (A) Self-photo-cross-link inhibition scheme between antigene. (B) Denaturing PAGE analysis of self-photo-cross-linking. The antigene probe 5 μM in 50 mM Tris-HCl (pH 7.5) was incubated at 37 °C, 1 h, and 385 nm photoirradiation was performed at 37 °C for 15 min. (C) SYBR Gold images were obtained by LAS-3000 and band intensity was determined by ImageJ software. Self-photo-cross-linked efficiency was calculated by the average ratio of shifted band.

3.3.2 DDI photo-cross-linking

Next, DDI photo-cross-linking efficiency was verified using probes containing T, ^{CN}U, S, and dS. 100 nM Temp1 and Temp2 in 10 mM Tris HCl buffer (pH 7.4) were incubated at 37 °C for 10 min followed by addition of 10 μM each probe solutions kept at 37 °C in the same buffer. The mixed solution was photoirradiated at 385 nm for 15 min and analyzed on a 15% polyacrylamide gel. In the gel analysis, Cy3 fluorescence modified to 5' of the template was observed with LAS-3000, and the band intensity was quantified with Image J. Two bands derived from Temp1 and Temp2 were confirmed in pre-photoirradiation lane. A new band derived from the photo-cross-linked template was generated in post-photoirradiation lane. The band intensity of the obtained Cy3 fluorescence image was acquired by Image J, and the

cross-linking rate was determined from the ratio of the post-shift band to the pre-shift band. The average photo-cross-linking rate obtained from the bands corresponding to the two probe-template pairs was calculated as the DDI efficiency. The photo-cross-linking rates of the probes combining the inhibitor and ^{CNV}K were calculated to be ^{CN}U/K 26.1%, T/K 19.3%, S/K 4.1%, and dS/K 3.5% (probe containing ^{CN}U and ^{CNV}K = ^{CN}U/K, similar notation for other types). The DDI photo-cross-linking rate did not correlate with the probe's self-photo-cross-linking inhibition efficiency.

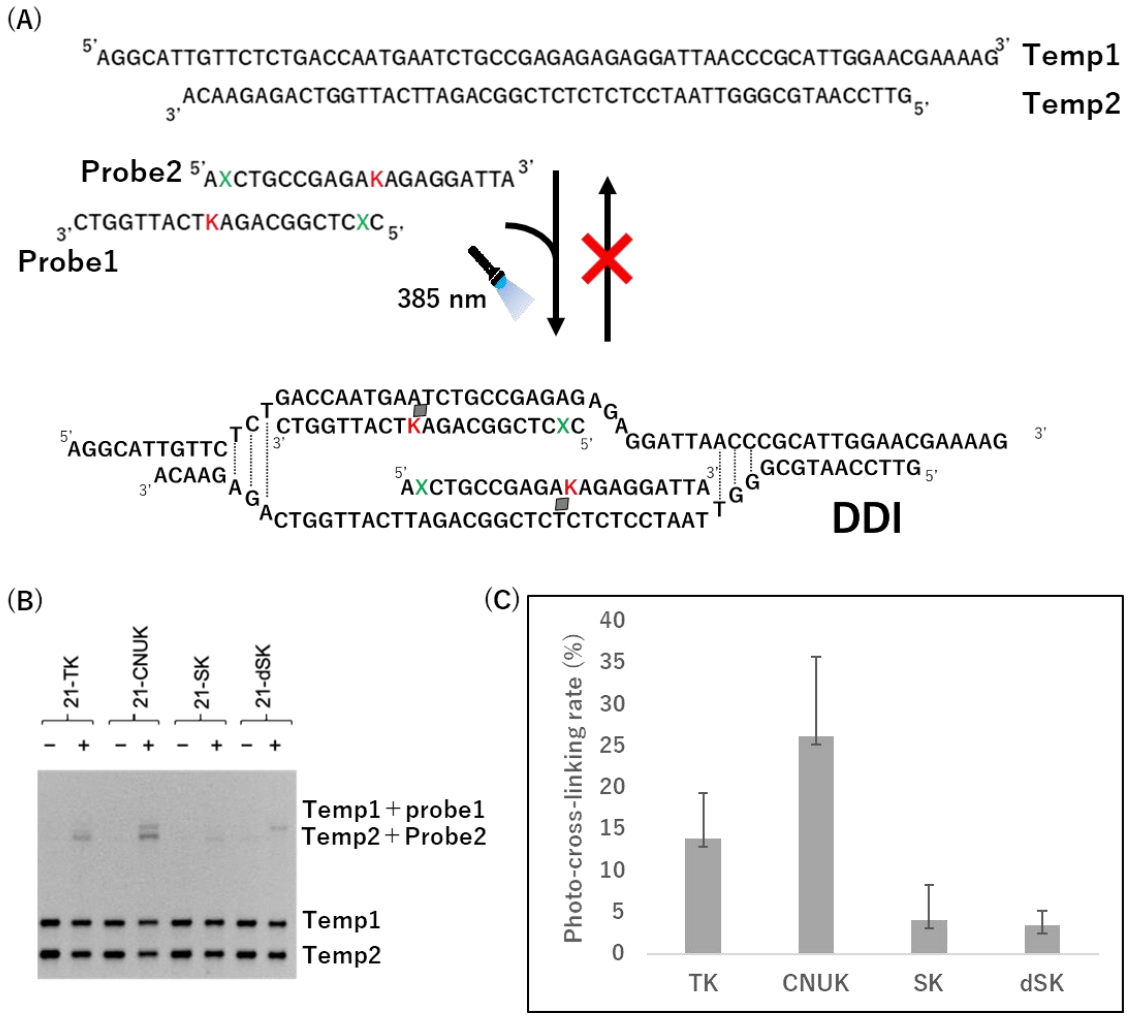

Figure 3.5. (A) DDI photo-cross-linking scheme for Template DNA with ^{CNV}K-introduced antigene probe (B) Each 100 nM template strand in 10 mM Tris HCl buffer (pH 7.4) were incubated at 37 ℃ for 10 min followed by addition of 10 μM each probes solution incubated at 37 ℃ in the same buffer. After the incubation of the mixture at 37 ℃ for 1 h, it was

photoirradiated at 385 nm for 15 min. Sample solutions were analyzed by denaturing PAGE using 15 % polyacrylamide gel. (C) Cy3 images were obtained by LAS-3000 and band intensity was determined by ImageJ software. DDI efficiency was calculated by the average ratio of shifted band and template band.

3.3.3 Thermodynamic parameters between probes

Although we succeeded in improving the self-photo-cross-linking inhibition of the probe, we thought that there were several factors before DDI photo-cross-linking that no correlation was obtained in the evaluation of DDI efficiency. For PNA and LNA, DDI efficiency was improved by lowering the T_m value between Probes and increasing the T_m value of Probe/Template. In other words, to evaluate DDI efficiency in detail, it is necessary to measure the Tm value between Probe/Template. As a result, the thermal stability of T, ^{CN}U, S, and dS ODN DNA (5'-ACGGGXGCA-3') and its complementary strands was tested. We created a 9-mer template strand using ^{CNV}K and a complementary strand with ^{CN}U, S, and dS. For the T_m value measurement, 7.5, 10 and 15 M of each template and complementary strand were produced in a 10 mM sodium phosphate solution (pH 7.4, 100 mM NaCl). A UV-vis spectrophotometer (JASCO, V-630bio) was used to measure the absorbance of the combination at 260 nm at temperatures ranging from 4 ℃ to 85 ℃ and from 85 ℃ to 4 ℃. T_m values were calculated from the collected data by calculating estimated curve inflection points. The thermal dynamic parameter of duplex consisting of ODN(^{CNV}K)-9 and ODN(X)-9 containing T, ^{CN}U, S, or dS was evaluated. The duplex (^{CNV}K/T) (37.3 ℃) has the highest T_m value, followed by duplex (^{CNV}K/^{CN}U) 33.5±0.1 ℃ duplex (^{CNV}K/S) (25.2±0.9 ℃), and duplex (^{CNV}K/dS) (24.9±1.1 ℃). ^{CN}U was thought to create a hydrogen bond with A as the counter base, similar to T, however the T_m value was approximately 3 ℃ lower. Furthermore, because S and dS lack a base part for building hydrogen bonds, T_m is substantially lower than T, resulting in a smaller enthalpy loss for S and dS than T and ^{CN}U. T and ^{CN}U have nearly identical enthalpy losses and can form hydrogen bonds, however, the CN group at ^{CN}U's 5-position is an electron aspirator, which influences hydrogen bond formation or is a structural component. On the other hand, S through ODN(^{CN}U/K) hybridization was smaller than S through ODN(S/K) or ODN(dS/K), implying that ^{CN}U's comparatively flexible structure inhibits entropic loss through hybridization [24].

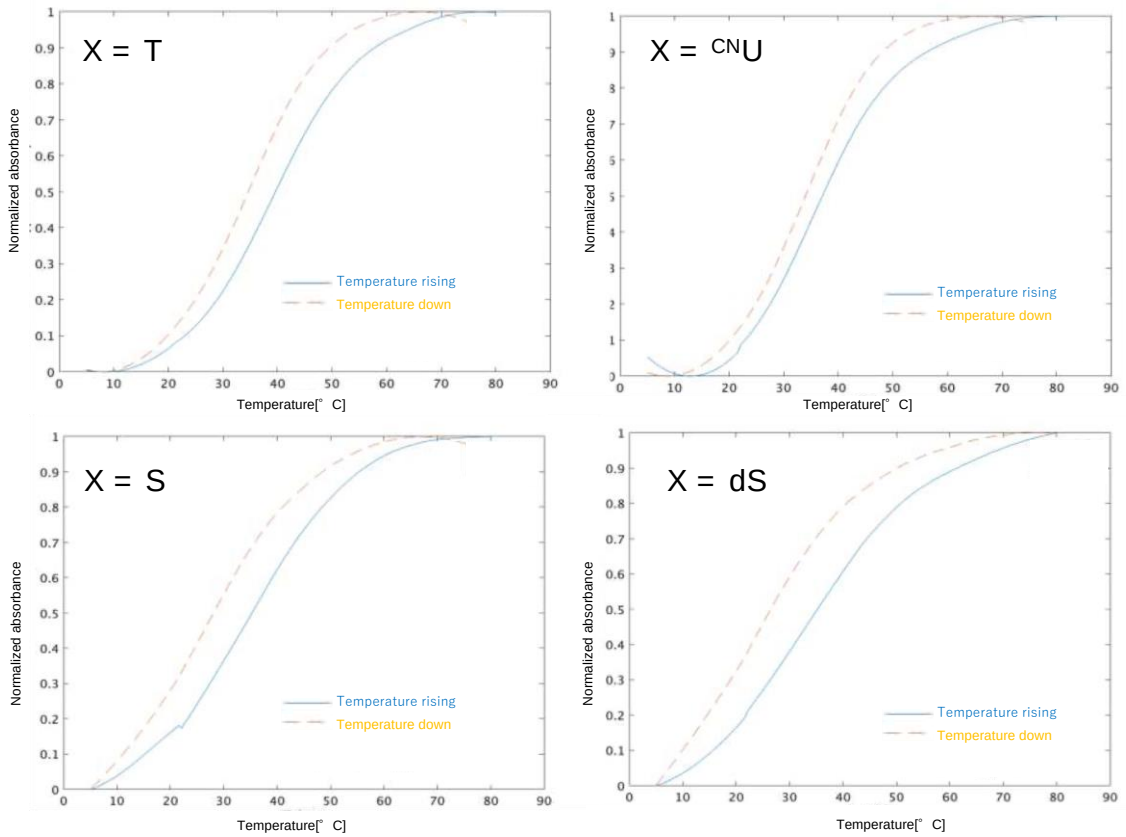

Figure 3.6. Melting temperature of duplex ODN consisting of ODN(^{CNV}K)(5'-TGCA^{CNV}KCCGT-3') and ODN(X)(5'-ACGGGXGCA-3'; X = T, ^{CN}U, S, dS).

Table 3.2. T_m value and thermodynamic parameters of Antigene probe

Entry	ΔG [kcal/mol]	ΔH [kcal/mol]	ΔS [kcal/mol・K]	T_m [°C]
T	-7.65	-40.5	-105.8	37.3
^{CN}U	-8.01	-36.8	-93.9	33.5
S	-7.77	-34.5	-89.6	25.2
dS	-7.67	-25.4	-59.5	24.9

DDI efficiency is considered to consist of the balance between the T_m value of Probe/Probe and the T_m value of Probe/Template. In other words, when dS or S is used, the T_m value of Probe/Probe and self-photo-cross-linking can be inhibited, but the Tm value of

Probe/Template is reduced. On the other hand, T and ^{CN}U are inferior to dS and S in self-photo-cross-link inhibition, but the T_m value of Probe/Template increases and so does the DDI efficiency. In Figure 3.7, plotting with T_m value on the horizontal axis and DDI efficiency on the vertical axis suggests that ^{CN}U is the most desirable inhibitor.

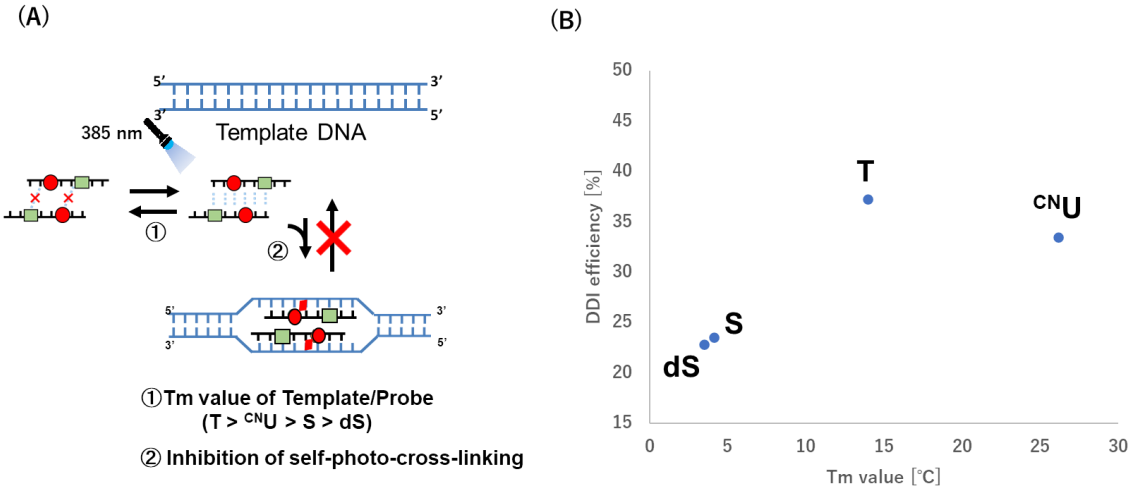

Figure 3.7. (A) Two equilibrium reactions related to DDI efficiency. (B) A graph showing the superiority of photo-cross-linking inhibitors when the vertical axis is the DDI efficiency and the horizontal axis is the T_m value.

3.3.4 DDI efficiency by increasing T_m value of Probe/Template

It was discovered that not only the inhibition of self-cross-linking between Probes but also the T_m values of template and probe are important factors for the efficiency of ^{CNV}K introduced DDI. Therefore, in order to increase the T_m value of template-probe, DDI photo-cross-linking was verified using 18 mer, 21 mer, 24 mer, and 27 mer probes. 100 nM Temp1 and Temp2 in 10 mM Tris HCl buffer (pH 7.4) were incubated at 37 ℃ for 10 min followed by addition of 10 μM each probe solutions kept at 37 ℃ in the same buffer. The mixed solution was photoirradiated at 385 nm for 15 min and analyzed on a 15% polyacrylamide gel. As a result of quantifying the Cy3 band and calculating the DDI efficiency, it was determined to be 14.3%, 36.2%, 46.3% and 51.4%, respectively from the shortest probe to the longest. Photo-cross-linking rate of 18 mer was lower than 15%, and the photo-cross-linking rate improved by about 10% from 21 mer to 24 mer. It is considered that as the length of the probe becomes longer, the single-stranded sequence becomes longer, and it becomes easier to hybridize with the target DNA.

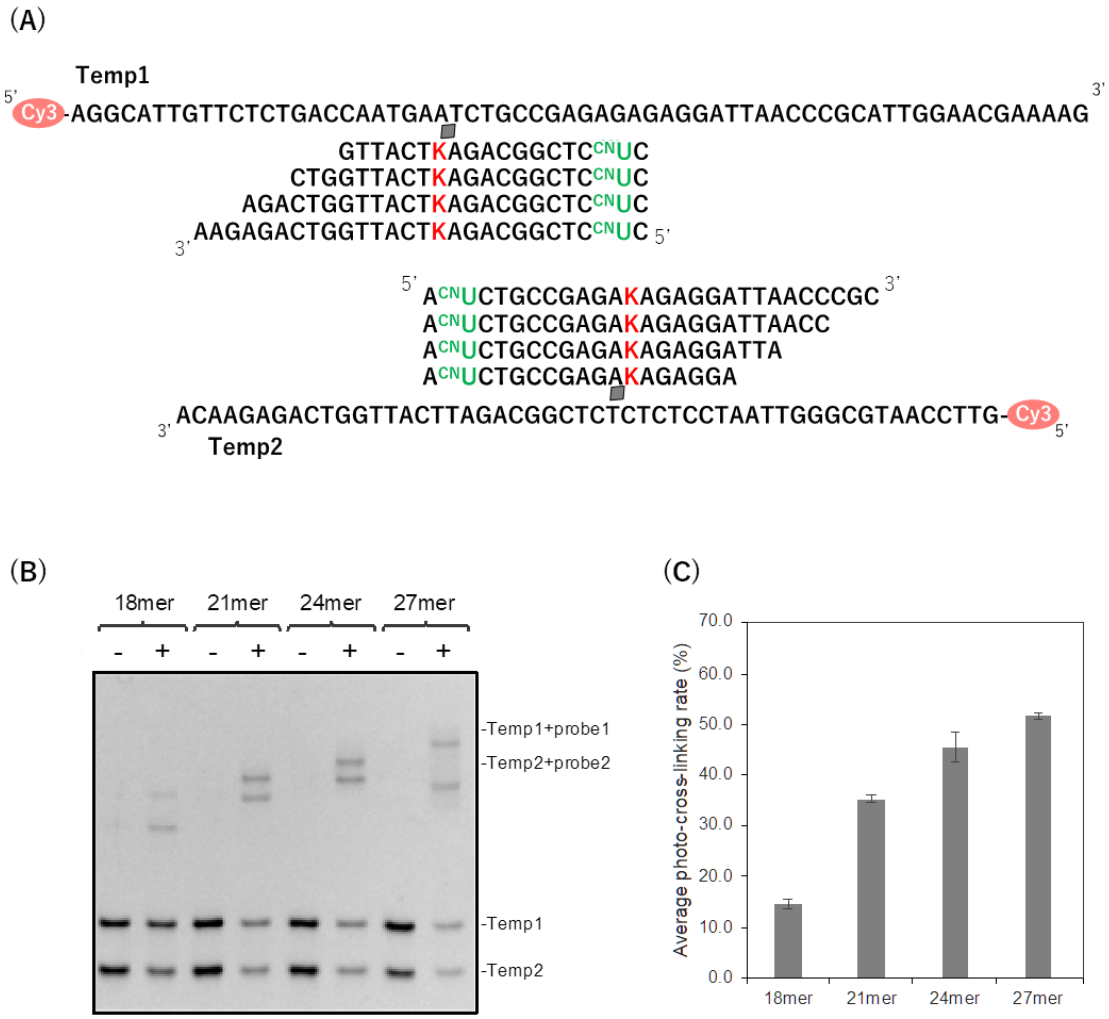

Figure 3.8. (A) DDI with antigene probes of each length (15mer, 18 mer, 21 mer, 24 mer, 27 mer). (B) Each 100 nM template strand in 10 mM Tris HCl buffer (pH 7.4) were incubated at 37 ℃ for 10 min followed by addition of 10 μM each probes solution incubated at 37 ℃ in the same buffer. After the incubation of the mixture at 37 ℃ for 1 h, it was photoirradiated at 385 nm for 15 min. Sample solutions were analyzed by denaturing PAGE using 15 % polyacrylamide gel. (C) Cy3 images were obtained by LAS-3000 and band intensity was determined by ImageJ software. DDI efficiency was calculated by the average ratio of shifted band and template band.

3.3.5 DDI efficiency with probes with all thymines replaced by ^{CN}U

As another improvement related to DDI efficiency, all thymines were replaced by ^{CN}U with the aim of improving the efficiency of inhibiting self-photo-cross-linking between probes. 18 mer, 21 mer, 24 mer, and 27 mer probes were prepared and their DDIs were verified. 100 nM Temp1 and Temp2 in 10 mM Tris HCl buffer (pH 7.4) were incabated at 37 ℃ for 10 min followed by addition of 10 μM each probes solution kept at 37 ℃ in the same buffer. The mixed solution was photoirradiated at 385 nm for 15 min and analyzed on a 15% polyacrylamide gel. It was calculated as 9.7%, 28.2%, 38.9%, and 38.1% from the combination of shortest probes to the longest, respectively. Replacing all T in the probe by ^{CN}U reduced DDI efficiency. It is considered that the introduction of multiple ^{CN}Us changed the structure of the DNA probe and reduced the stability of the double strand, leading to a decrease in DDI efficiency.

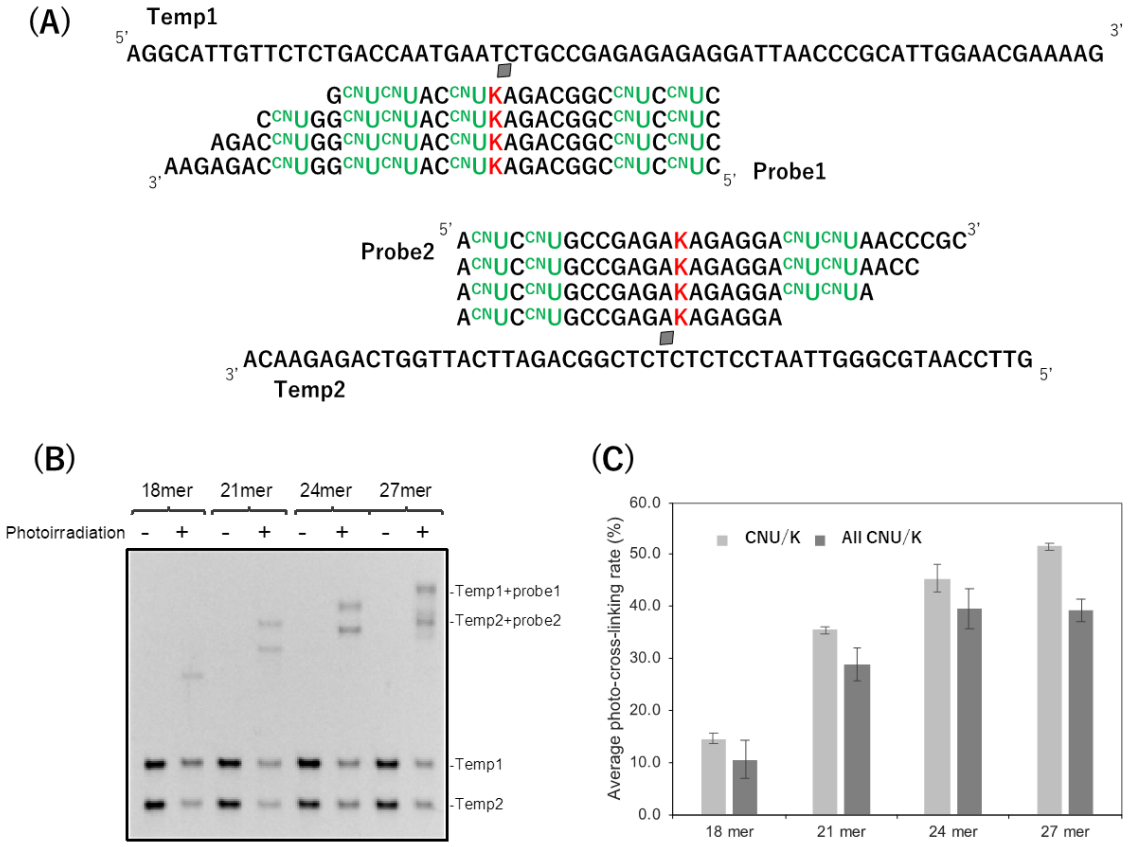

Figure 3.9. (A) DDI probe with all thymine replaced with ^{CN}U (18 mer, 21 mer, 24 mer, 27 mer). (B) Each 100 nM template strand in 10 mM Tris HCl buffer (pH 7.4) were incubated at 37 ℃ for 10 min followed by addition of 10 μM each probes solution incubated at 37 ℃ in

the same buffer. After the incubation of the mixture at 37 ℃ for 1 h, it was photoirradiated at 385 nm for 15 min. Sample solutions were analyzed by denaturing PAGE using 15 % polyacrylamide gel. (C) Cy3 images were obtained by LAS-3000 and band intensity was determined by ImageJ software. DDI efficiency was calculated by the average ratio of shifted band and template band.

Conclusion

In this study, two new inhibitors (dSpacer, Spacer) were prepared to improve the DDI efficiency using ^{CNV}K. It was shown that these two inhibitors have a higher inhibitory effect than ^{CN}U. However, in terms of DDI efficiency, ^{CN}U had the highest photo-cross-linking rate, and dSpacer and Spacer were lower than thymine. From the T_m value and thermodynamic parameter measurement, it was found that the DDI efficiency of the ^{CNV}K-introduced probe depends not only on the self-photo-crosslink inhibition efficiency but also on the balance of probe/template stability. Therefore, we succeeded in improving the DDI efficiency by extending the length of the probe. However, replacing all thymines by ^{CN}U has been shown to reduce DDI efficiency.

References

[1] Peter A.Jones, S B.Baylin. The Epigenomics of Cancer. *Cell*. **2007**, 28(4):683-92.

[2] J R Mendell, L R R Klapac, Z Sahenk, K Roush, L Bird, L P Lowes, L Alfano, A M Gomez, S Lewis, J Kota, V Malik, K Shontz, C M Walker, K M Flanigan, M Corridore, J R Kean, H D Allen, C Shilling, K R Melia, P Sazani, J B Saoud, E M Kaye, Eteplirsen Study Group. Eteplirsen for the treatment of Duchenne muscular dystrophy. *Ann Neurol.*, **2013**, 74(5), 637-47.

[3] S M Hammond, S Boettcher, A A Caudy, R Kobayashi, G J Hannon. A link between genetic and biochemical analyses of RNAi. *Science.*, **2001**, 10, 293(5532), 1146-50.

[4] N Iwamoto, D C Butler, N Svrzikapa, S Mohapatra, I Zlatev, D W Sah, Meena, S M Standley, G Lu, L H Apponi, M F Kamenetsky, J J Zhang, C Vargeese, G L Verdine. Control of phosphorothioate stereochemistry substantially increases the efficacy of antisense oligonucleotides. *Nat Biotechnol.*, **2017**, 35(9), 845-51.

[5] T Gaj, C A Gersbach, C F Barbas 3rd. ZFN, TALEN, and CRISPR/Cas-based methods for genome engineering. *Trends Biotechnol.*, **2013**, 31(7), 397-405.

[6] G Cutrona, E M Carpaneto, M Ulivi, S Roncella, O Landt, M Ferrarini, L C Boffa. Effects in live cells of a c-myc anti-gene PNA linked to a nuclear localization signal. *Nat Biotechnol.*, **2000**, 18(3), 300-3.

[7] L Cong, F Zhang. Genome engineering using CRISPR-Cas9 system. *Methods Mol Biol.*, **2015**, 1239, 197-217.

[8] D Mashiko, S A Young, M Muto, H Kato, K Nozawa, M Ogawa, T Noda, Y J Kim, Y Satouh, Y Fujihara, M Ikawa. Feasibility for a large scale mouse mutagenesis by injecting CRISPR/Cas plasmid into zygotes. *Dev Growth Differ.*, **2014**, 56(1), 122-9.

[9] D Mashiko, Y Fujihara, Y Satouh, H Miyata, A Isotani, M Ikawa. Generation of mutant mice by pronuclear injection of circular plasmid expressing Cas9 and single guided RNA. *Sci Rep.*, 2013 27(3), 3355.

[10] C Kuscu, M Parlak, T Tufan, J Yang, K Szlachta, X Wei, R Mammadov, M Adli. CRISPR-STOP: gene silencing through base-editing-induced nonsense mutations. *Nat Methods*, **2017**, 14(7), 710-2.

[11] O O Abudayyeh, J S Gootenberg, P Essletzbichler, S Han, J Joung, J J Belanto, V Verdine, D B T Cox, M J Kellner, A Regev, E S Lander, D F Voytas, A Y Ting, F Zhang. RNA targeting

with CRISPR-Cas13. *Nature*, **2017**, 550(7675), 280-284.

[12] K Hanai, F Takeshita, K Honma, S Nagahara, M Maeda, Y Minakuchi, A Sano, T Ochiya. Atelocollagen-Mediated Systemic DDS for Nucleic Acid Medicines. *Ann N Y Acad Sci.*, **2006**, 1082, 9-17.

[13] F A Rogers, K M Vasquez, M Egholm, P M Glazer. Site-directed recombination via bifunctional PNA-DNA conjugates. *Proc Natl Acad Sci U S A*, **2002**, 99(26), 16695-700.

[14] U Christensen, N Jacobsen, V K Rajwanshi, J Wengel, T Koch. Stopped-flow kinetics of locked nucleic acid (LNA)-oligonucleotide duplex formation: studies of LNA-DNA and DNA-DNA interactions. *Biochem J.*, **2001**, 354(3), 481-4.

[15] T Sugiyama, G Hasegawa, C Niikura, K Kuwata, Y Imamura, Y Demizu, M Kurihara, A Kittaka. PNA monomers fully compatible with standard Fmoc-based solid-phase synthesis of pseudocomplementary PNA. *Bioorg Med Chem Lett.*, **2017**, 27(15), 3337-41.

[16] P Lonkar, K H Kim, J Y Kuan, J Y Chin, F A Rogers, M P Knauert, R Kole, P E Nielsen, P M Glazer. Targeted correction of a thalassemia-associated beta-globin mutation induced by pseudo-complementary peptide nucleic acids. *Nucleic Acids Res.*, **2009**, 37(11), 3635-44.

[17] S Sforza, R Corradini, S Ghirardi, A Dossena, R Marchelli. DNA Binding of A D-Lysine-Based Chiral PNA: Direction Control and Mismatch Recognition. *Euro Jour of Org Chem.*, **2000**, 16, 2905-13.

[18] P M D Moreno, S Geny, Y V Pabon, H Bergquist, E M Zaghloul, C S Rocha, I I Oprea, B Bestas, S E Andaloussi, P T Jørgensen, E B Pedersen, K E Lundin, R Zain, J Wengel, C I E Smith. Development of bis-locked nucleic acid (bisLNA) oligonucleotides for efficient invasion of supercoiled duplex DNA. *Nucleic Acids Res.*, **2013**, 41(5), 3257-73.

[19] P J. Hrdlicka, B R Babu, M D. Sørensen, N Harrit, J Wengel. Multilabeled Pyrene-Functionalized 2'-Amino-LNA Probes for Nucleic Acid Detection in Homogeneous Fluorescence Assays. *J. Am. Chem. Soc.*, 2005, 127(38), 13293–9.

[20] R Ge, J E Heinonen, M G Svahn, A J Mohamed, K E Lundin, C E Smith. Zorro locked nucleic acid induces sequence-specific gene silencing. *FASEB J.* **2007**, 21(8), 1902-14.

[21] R Ge, M G Svahn, O E Simonson, A J Mohamed, K E Lundin, C E Smith. Sequence-specific inhibition of RNA polymerase III-dependent transcription using Zorro locked nucleic acid (LNA). *J Gene Med.*, **2008**, 10(1), 101-9.

[22] S Nakamura, H Kawabata, H Muramatsu, Kenzo Fujimoto. Effect of 5-substitution of

uracil base in DNA photo-cross-linking using 3-cyanovinylcarbazole *Chem. Lett.*, **2016**, 45(8), 887-9.

[23] J S Lucia Jr, D Hicks. The thermodynamics of DNA structural motifs. *Annu Rev Biophys Biomol Struct.*, **2004**, 33, 415-40.

[24] G Bonnet, S Tyagi, A Libchaber, F R Kramer. Thermodynamic basis of the enhanced specificity of structured DNA probes. *Proc Natl Acad Sci U S A.* **1999**, 96(11), 6171-6.

[Chapter 4] Double duplex invasion to 400 mer double strand oligodeoxynucleotide using ultrafast DNA photo-cross-linking

4.1 Introduction

Double duplex invasion (DDI) is an antigene method that recognizes target DNA with Watson-Crick base pairs [1, 2], and is known to have high sequence selectivity and few restrictions on the target sequence. Several gene expression regulations have already been reported for antigene under *in vivo* conditions. PNA has succeeded in inhibiting the gene expression of the oncogene gene c-myc in mice [3, 4]. LNA succeeded in suppressing the NF1 gene, which is the cause of neurofibromatosis [5, 6]. In these previous studies, several steps had been taken to conduct experiments toward the antigene of genomic DNA [7, 8]. First, the DDI is validated with a 200-400 mer model sequence, and then the DDI to the plasmid is validated. After that, DDI is verified against the plasmid to verify the mRNA expression *in vivo*. The longer the target DNA double strand, the more difficult it is to invade the DDI probe. This is because DNA forms very complex secondary and tertiary structures. The plasmid is a double helix of DNA that further forms a helical structure to form supercoiled DNA (scDNA) [9, 10]. scDNA requires invasion for the added stability of double helix and tertiary structure. In addition, genomic DNA existing in the living body has DNA wrapped around histones. Again, it must be invasioned for stability with histones in addition to the DNA double helix [11, 12, 13]. DDI for probes with large DNA sizes may require probe design with higher invasion efficiency. Therefore, in this Chapter, as the next step, we will verify the photo-cross-linked DDI for 400 bp. A sequence obtained by extending the model sequence used in Chapter 3 to a length of 400 bp was prepared. Aiming at editing genomic DNA, we will also optimize the probe by targeting more stable DNA.

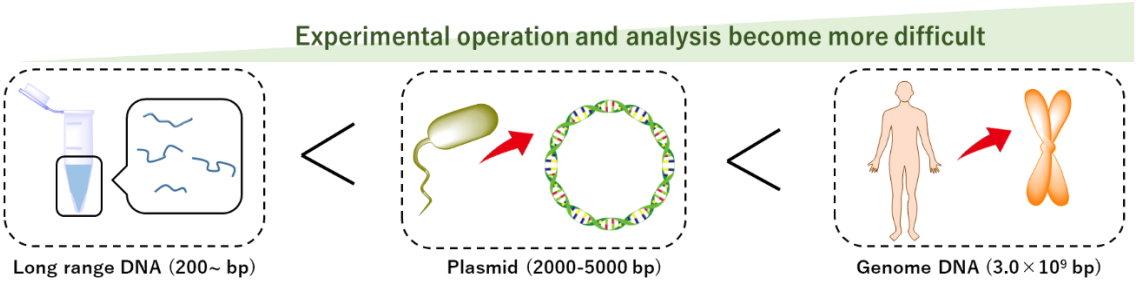

Figure 4.1. The effect of DNA size on DDI efficiency

4.2 Materials and Methods

4.2.1. Oligodeoxynucleotide synthesis

Oligodeoxynucleotides were synthesized by DNA synthesizer (NTS M-2-MIX_NPS) on a 1.0 μmol scale High Load-CPG (Glen Research). Synthesized oligonucleotides were cleaved from CPG with 28 % ammonia solution followed by deprotection of bases by incubation at 65 ℃ for 4 h. The CF_3 group of ^{TF}T changes to a ^{CN}U group in the process of deprotection. ammonia solution removed by freeze drying overnight. Oligodeoxynucleotide purified by reverse phase HPLC (PU-980, HG-980-31, DG-980-50, UV-970system (Jasco, Japan) equipped with Cosmosil® 5C18-AR-II column (5 μm, 10 I.D.x150 mm, Nacalai Tesque, Japan)) with a gradient of 2-40% acetonitrile and flow rate of 1 ml/min. Target DNA was purchased from Integrated DNA Technologies Co., Ltd.

Table 4.1 Sequence of DDI probe

Entry	Sequence 5' to 3'	Calcd. for $[M+H]^+$	Found
1-11bp-5nt	GTTCCAAKGCGGGTTAATCCUC	6805.47	6806.87
2-11bp-5nt	AGAGAGAKGATTAACCCGCAUT	6871.54	6872.21
1-21CNUK	CUCTCGGCAGAKTCATTGGTC	6492.26	6491.12
2-21CNUK	AUCTGCCGAGAKAGAGGATTA	6598.36	6597.20
1-11bp-5nt-Cy3	Cy3GTTCCAAKGCGGGTTAATCCUC	7313.06	7312.25
2-11bp-5nt-Cy3	Cy3AGAGAGAKGATTAACCCGCAUT	7375.45	7375.89

K=^{CNV}K, U=^{CN}U

Target DNA (Template sequence of Chapter 3)

5'-ACGACGGCGGCCCTACGATACCTTACTAGGGTCTCAGCTAATTTCACACAGA
TATGTTCCTTACCCCGTTTACCACGCAGGAGAGTTAAACGAAAGCAGCCTACGT
ATTTTTCGAGCTCTTTCAGCACTCTACTTGACGGACTTTGGAATCCTAGTTGGC
AGTATGGAGGCATTGTTCTCTGACCAATGAATCTGCCGAGAGAGAGGATTAACC
CGCATTGGAACGAAAAGTTTGTTTTTTATGAGCCAGCCTTCGGTTGTCGATATG
AGGATCTCGCGATTGAAAAGTTCATGTCTCCGTCTAATCACGATGTGAGTGGTG
GGGGGTACTTCATACAAGATGCTGGATCCTTAATGAGTGGGGCTAGAGTAGCA
GGCAAATACCCTAGAGCCTATTAA-3' (400 mer)

Figure 4.2. One-sided sequence of target DNA used in this chapter

4.2.2. Photo-cross-linking between DDI probe and target DNA and its evaluation

25 nM target DNA in 10 mM Tris HCl buffer (pH 7.4) was incubated at 37 ℃ for 15 min followed by addition of 2.5 μM each probes solution incubated at 37 ℃ in the same buffer. After the incubation of the mixture at 37 ℃ for 1 h, it was photoirradiated at 385 nm for 1 min using Omunicure (12400 mW/cm2). The sample solution was mixed with a denaturant (sat. Urea in formamide) and incubated at 90 ℃ for 5 min. Sample solutions were analyzed by denaturing PAGE using 8 % polyacrylamide gel. Cy3 and SYBR Gold images were obtained by LAS-3000 and band intensity was determined by ImageJ software.

4.3 Results and discussion

4.3.1 DDI photo-cross-linking to 400 mer DNA

The long model sequence was designed by extending the model sequence used in Chapter 3 from both ends to 400 bp. To confirm the sequence generality, a new 11bp-5nt sequence was prepared. we designed a sequence in which the number of complementary bases between the probes was 11 and the sticky end was 5 nt [16, 17, 18]. The complementary region of 21-CNUK was designated as Target site A, and the complementary region of 11b-5nt was designated as Target site B. 25 nM target DNA in 10 mM Tris HCl buffer (pH 7.4) were incubated at 37 ℃ for 15 min followed by addition of 2.5 μM each probes solution incubated at 37 ℃ in the same buffer. After the incubation of the mixture at 37 ℃ for 1 h, it was photoirradiated at 385 nm for 1 min. Sample solutions were evaluated by 300 V, 60 min electrophoresis on an 8% AA-denatured gel, images of SYBR Gold-stained were analyzed.
From the analysis results, a DDI photo-cross-linking rate of 22.7% was shown, which was correlated with the results of Chapter 3. The result of DDI photo-cross-linking was analyzed using the same method, the yield of 11bp-5nt was calculated to be 74.6%.

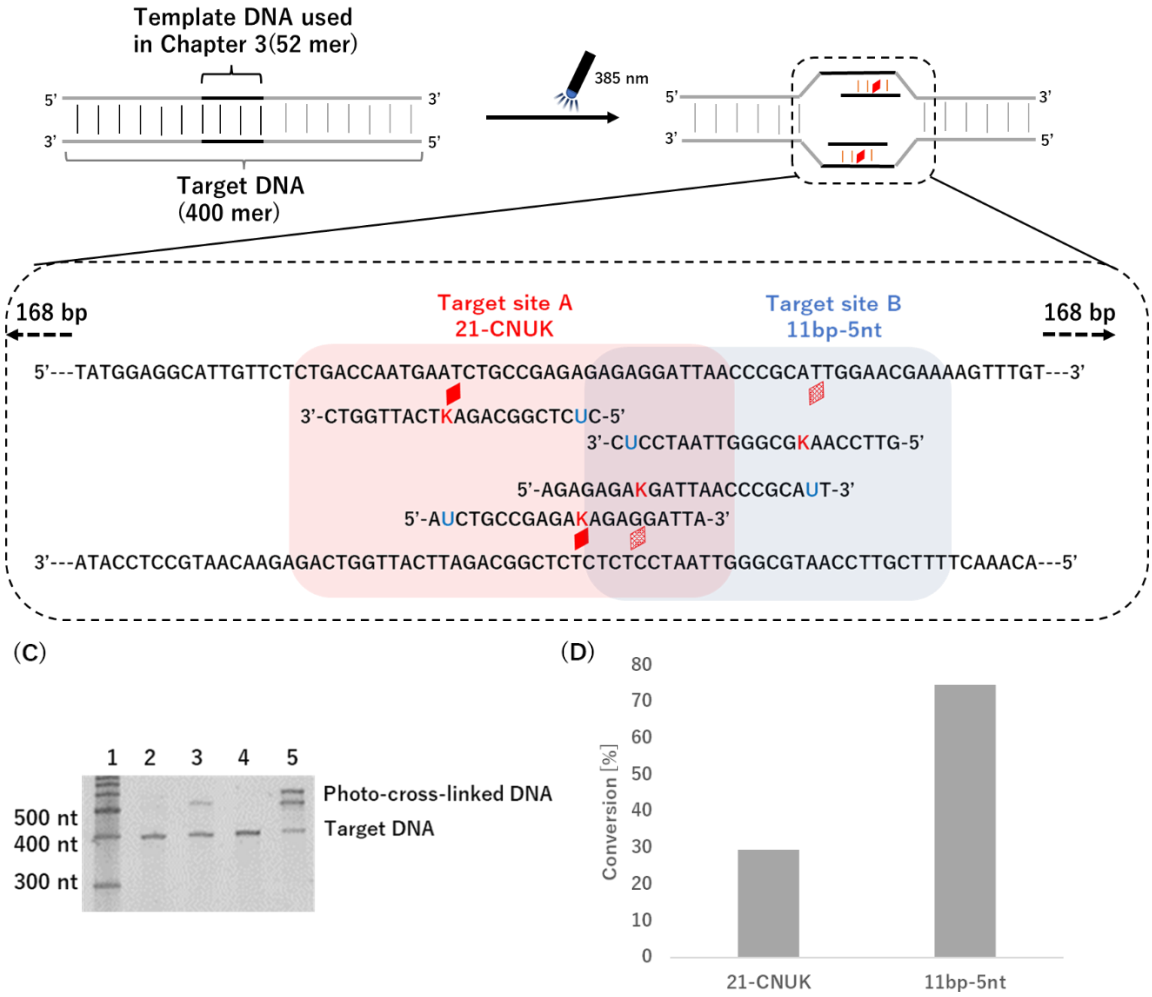

Figure 4.3. (C) DDI photo-cross-linking to 400 mer DNA with 21-CNUK and 11bp-5nt. 25 nM target DNA in 10 mM Tris HCl buffer (pH 7.4) were incubated at 37 ℃ for 15 min followed by addition of 2.5 μM each probes solution incubated at 37 ℃ in the same buffer. After the incubation of the mixture at 37 ℃ for 1 h, it was photoirradiated at 385 nm for 1 min. SYBR Gold images were obtained by LAS-3000 and band intensity was determined by ImageJ software. (D) DDI efficiency was calculated by the template band and remaining template band.

It was considered that when only the probe was photo-irradiated up to 1 min, the self-photo-cross-linked DNA of Probe was the cause of suppressing DDI. In 21-CNUK, not only the photo-cross-linking between probes but also the photo-cross-linking reaction of the monomer probe proceeded, and the PAGE analysis showed a downward shift. In particular, there was a major? change between 1 and 10 seconds. 11bp-5nt was able to significantly suppress self-

photo-cross-linking between probes and self-photo-cross-linking of monomer probes. There are two possible reasons for the suppression of self-photo-cross-linking between the probes. The first is the difference in the nucleotide sequence around ^{CNV}K, where three bases on both sides of ^{CNV}K are flanked by "AGA" in 21-CNUK. The homology of the surrounding bases may have caused an off-target effect, resulting in photo-cross-linking with other pyrimidine bases. The second is the suppression of self-photo-cross-linking of probe monomers: 21CNUK has 8 bases of self-complementary length between probes, while 21-11bp-5nt has 11 bases. It is suggested that if the probes can easily form double strands with each other, the self-photo-cross-linking between single strands can be suppressed.

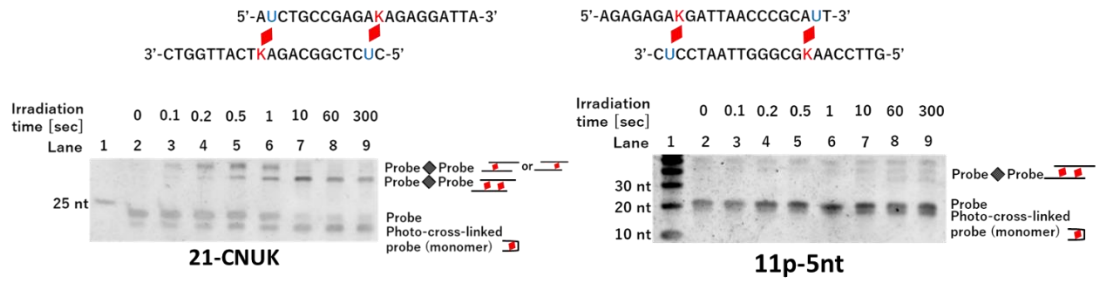

Figure 4.4. (A) Self-photo-cross-linking evaluation of 21-CNUK (0 to 300 sec). (B) Self-photo-cross-linking evaluation of 11bp-5nt (0 to 300 sec).

4.3.2 Identification of band shift by photo-cross-linked DNA

In 11bp-5nt, the bands that seemed to be two photo-cross-linked DNA were shifted by light irradiation. Therefore, Cy3-modified probes were prepared, and each photo-cross-linked DNA was tracked in four different patterns. 25 nM target DNA in 10 mM Tris HCl buffer (pH 7.4) were incubated at 37 ℃ for 15 min followed by addition of 2.5 μM each probes solution incubated at 37 ℃ in the same buffer. After the incubation of the mixture at 37 ℃ for 1 h, it was photoirradiated at 385 nm for 1 min. Sample solution was evaluated by 300 V, 60 min, 50 ℃ electrophoresis on an 8% AA-denatured gel, images of SYBR Gold-stained were analyzed. It was confirmed that the band shifted up was a photo-cross-linked DNA of 1-11bp-5nt with the target DNA, and the band shifted down was a photo-cross-linked DNA of 2-11bp-5nt with the target DNA. From the results so far, it is known that the band shift differs

depending on the length of the probe and the position of the photo-cross-linked DNA. It is suggested that the structure of the photo-cross-linked DNA is different, which makes a difference in electrophoresis.

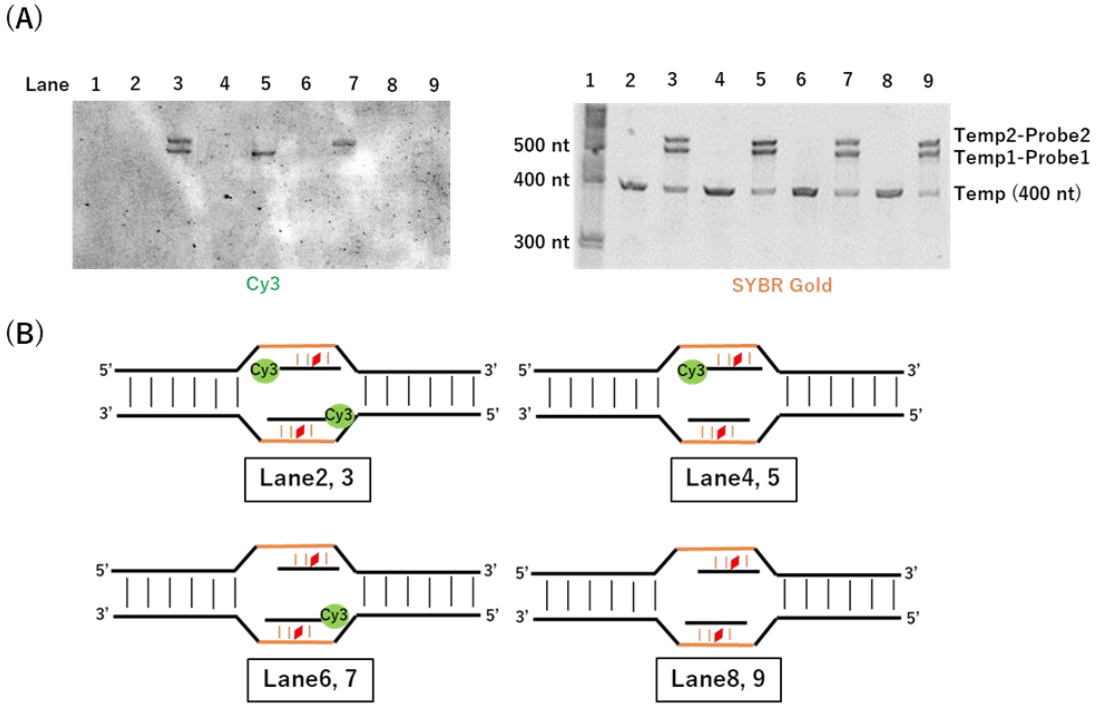

Figure 4.4. (A) DDI photo-cross-linking reaction using Cy3-modified probe. 25 nM target DNA in 10 mM Tris HCl buffer (pH 7.4) were incubated at 37 ℃ for 15 min followed by addition of 2.5 μM each probes solution incubated at 37 ℃ in the same buffer. After the incubation of the mixture at 37 ℃ for 1 h, it was photoirradiated at 385 nm for 1 min (left: Cy3 image, right: SYBR Gold image). (B) DDI optical crosslinking structure of each lane.

4.3.3 Examination of reaction conditions for photo-cross-linking

(1) Photoirradiation time

^{CNV}K is an ultrafast photo-cross-linker, and it is known that the reaction proceeds in a few seconds at 385 nm. Therefore, the photoirradiation time was verified at 0, 0.1, 0.2, 0.5, 1, 10, 60, 300 seconds. 25 nM target DNA in 10 mM Tris HCl buffer (pH 7.4) were incubated at 37 ℃ for 15 min followed by addition of 2.5 μM each probes solution incubated at 37 ℃ in

the same buffer. After the incubation of the mixture at 37 ℃ for 1 h, it was photoirradiated at 385 nm for X sec. Sample solution was evaluated by 300 V, 60 min, 50 ℃ electrophoresis on an 8% AA-denatured gel, images of SYBR Gold-stained were analyzed. The photo-cross-linking rate was calculated to be 79.3% in 1 second and 78.8% in 300 seconds. The reaction became rate-determining in 1 second, and it became clear that the DDI photo-cross-linking structure was formed by the ultrafast photo-cross-linking reaction.

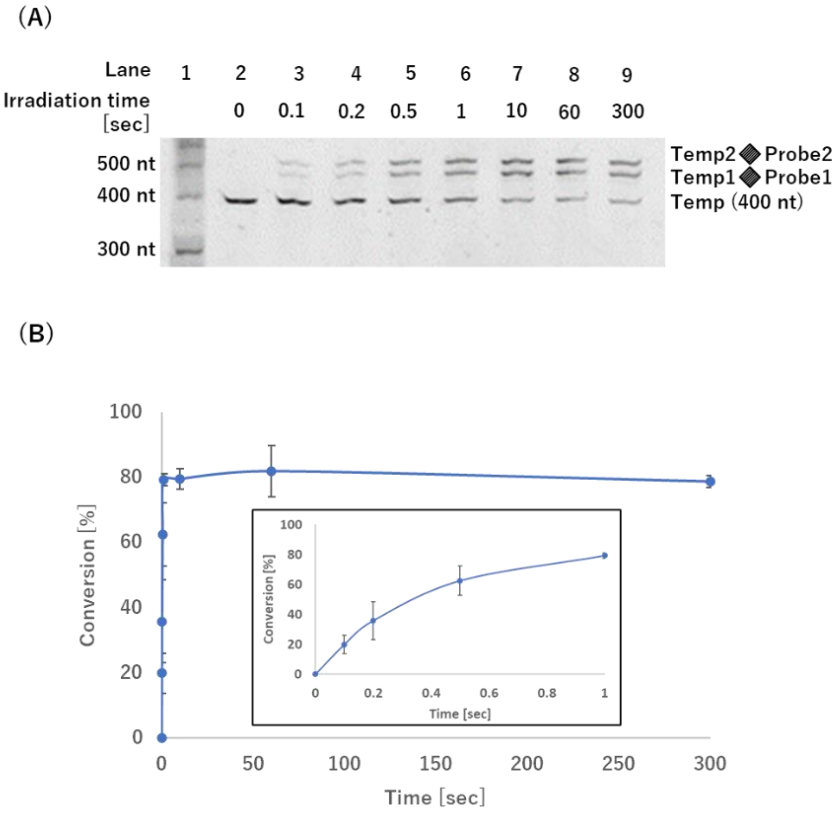

Figure 4.5. (A) Time course of photoirradiation time using 11bp-5nt and target DNA. (0 to 300 sec). (B) DDI efficiency was calculated by the template band and remaining template band.

(2) Incubation time

For the DDI photo-cross-linking reaction, the intermediate in which the DDI probe invades the target DNA is important. Incubation time was verified at 0, 1, 5, 15, 60 min to clarify the best timing. 25 nM target DNA in 10 mM Tris HCl buffer (pH 7.4) were incubated at 37 ℃ for 15 min followed by addition of 2.5 μM each probes solution incubated at 37 ℃ in the same

buffer. After the incubation of the mixture at 37 ℃ for X min, it was photoirradiated at 385 nm for 1 min. Sample solution was evaluated by 300 V, 60 min electrophoresis on an 8% AA-denatured gel, images of SYBR Gold-stained were analyzed. The photo-cross-linking rates of 0, 1, 5, 15, and 60 min incubation were 2.1%, 5.1%, 37.4%, 70.8%, and 77.4%, respectively. The photo-cross-linking efficiency increased significantly from 5 min to 15 min, with 60 min showing the highest conversion.

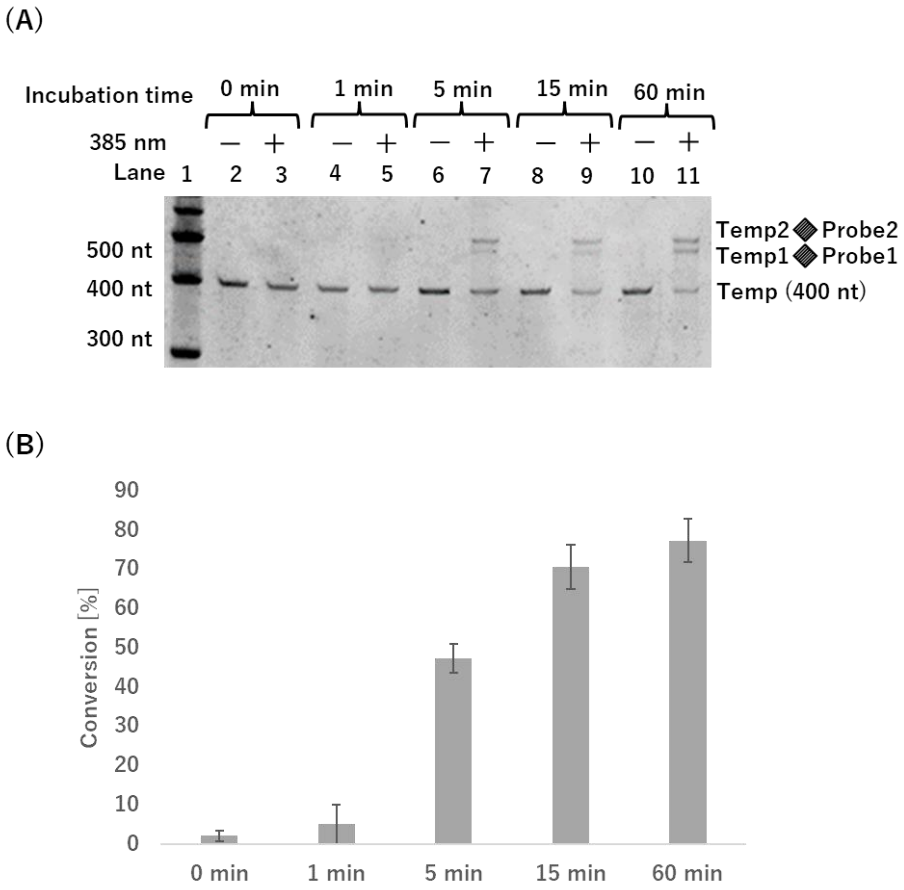

Figure 4.5. (A) Time course of incubation time using 11bp-5nt and target DNA. (0 to 60 min). (B) DDI efficiency was calculated by the template band and remaining template band.

(3) Equivalent

The reaction efficiency of DDI changes depending on the equivalent number of target DNA and probe. Therefore, the DDI photo-cross-linking was verified by changing the concentration of the probe using 1, 2, 5, 10, and 100 equivalents, respectively. 25 nM target DNA in 10 mM Tris HCl buffer (pH 7.4) were incubated at 37 ℃ for 15 min followed by

addition of X μM each probes solution incubated at 37 ℃ in the same buffer. After the incubation of the mixture at 37 ℃ for 1 h, it was photoirradiated at 385 nm for 1 min. Sample solution was evaluated by 300 V, 60 min electrophoresis on an 8% AA-denatured gel, images of SYBR Gold-stained were analyzed. The photo-cross-linking rate of 10 equivalents was 34.1% and of 100 equivalents was 78.7%. Since DNA-based DDI probes are a thermodynamically unfavorable reaction, 100 equal volumes of probes are required to improve invasion efficiency.

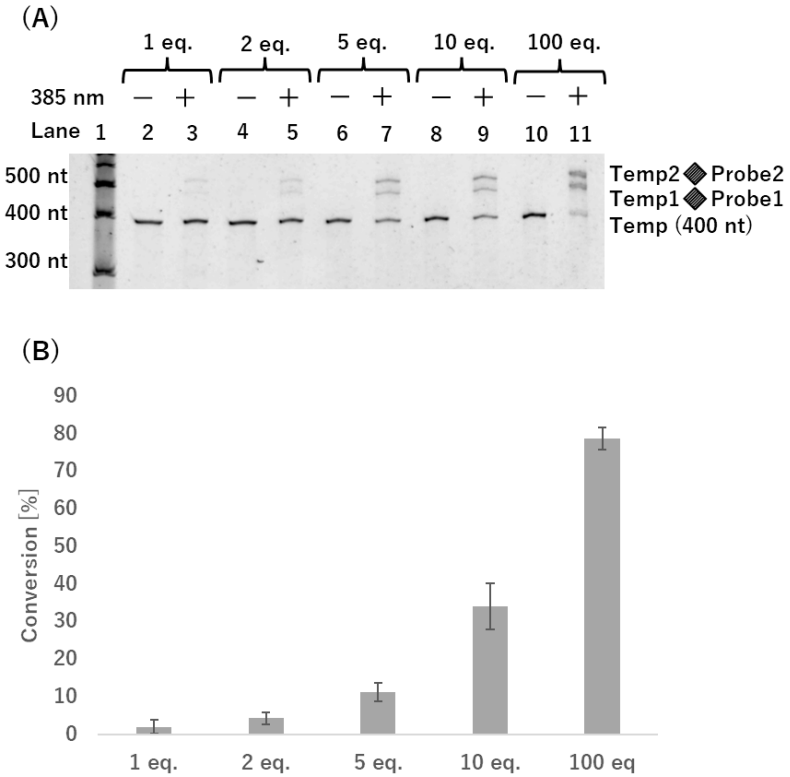

Figure 4.5. (A) DDI photo-cross-linking efficiency at equal doses of each probe. (1 to 100 eq.). (B) DDI efficiency was calculated by the template band and remaining template band.

So far, no previous study of DDI with probes composed of DNA has been reported. Even with Zorro-LNA, which is a combination of DNA and LNA, the reaction towards invasion takes a long time, up to 144 h. Since hydrogen bonds are reversible, despite their ability to carse hybridization. By changing the irradiation time, incubation time and molar ratio, the non-progressive reaction proceeds at an ultrafast rate. However, Photo-cross-linking induces the

formation of thermally irreversible bonds. These results suggest that the rate of photo-cross-linking play a significant role in DNA strand displacement [19, 20].

4.4 Conclusion

In this chapter, DDI photo-cross-linking was evaluated using the 400 mer duplex DNA as target DNA. First, photo-cross-linking was evaluated using 21-CNUK used in Chapter 3. Designing a more efficient probe, 11bp-5nt significantly reduced self-photo-cross-linking. When 11bp-5nt was used as the DDI probe, a photo-cross-linking rate of up to 78% was confirmed with the target DNA. The optimum reaction conditions for the photoirradiation time, incubation time, and equivalent were 1 min, 1 h, and 100 eq, respectively.

4.5 References

[1] P Wittung, P Nielsen, B Nordén. Direct Observation of Strand Invasion by Peptide Nucleic Acid (PNA) into Double-Stranded DNA. *J. Am. Chem. Soc.*, **1996**, 118, 30, 7049–54.

[2] S P Sau, T S Kumar, P J Hrdlicka. Invader LNA: efficient targeting of short double stranded DNA. *Org Biomol Chem.*, **2010**, 8(9), 2028-36.

[3] L C Boffa, G Cutrona, M Cilli, S Matis, G Damonte, M R Mariani, E Millo, M Moroni, S Roncella, F Fedeli. M Ferrarini. Inhibition of Burkitt's lymphoma cells growth in SCID mice by a PNA specific for a regulatory sequence of the translocated *c-myc*. *Cancer Gene Ther.*, **2007**, 14(2), 220-6.

[4] Peter E Nielsen. Gene targeting and expression modulation by peptide nucleic acids (PNA). *Curr Pharm Des.*, **2010**, 16(28), 3118-23.

[5] J Q Ling, A Hou, A R Hoffman. Long-range DNA interactions are specifically altered by locked nucleic acid-targeting of a CTCF binding site. *Biochim Biophys Acta.*, **2011**, 1809(1), 24-33.

[6] M S Stark, V F Bonazzi, G M Boyle, J M Palmer, Judith Symmons, C M Lanagan, C W Schmidt, A C Herington, R Ballotti, P M Pollock, N K Hayward. miR-514a regulates the tumour suppressor NF1 and modulates BRAFi sensitivity in melanoma. Oncotarget. **2015**, 6(19), 17753-63.

[7] S Rapireddy, G He, S Roy, B A Armitage, D H Ly. Strand invasion of mixed-sequence B-DNA by acridine-linked, gamma-peptide nucleic acid (gamma-PNA). *J Am Chem Soc.* **2007**, 129 (50), 15596-600.

[8] G He, S Rapireddy, R Bahal, B Sahu, D H Ly. Strand Invasion of Extended, Mixed-Sequence B-DNA by γ PNAs. *J Am Chem Soc.*, **2009**, 131(34), 12088-90.

[9] S Ando, D Putnam, D W Pack, R Langer. PLGA microspheres containing plasmid DNA: Preservation of supercoiled DNA via cryopreparation and carbohydrate stabilization. *J Pharm Sci.*, **1999**, 88(1), 126-30.

[10] T C Boles, J H White, N R Cozzarelli. Structure of plectonemically supercoiled DNA. J Mol Biol., **1990**, 213(4), 931-51.

[11] A Saha, J Wittmeyer, B R Cairns. D Miller, M Brinkworth, D Iles. Paternal DNA packaging in spermatozoa: more than the sum of its parts? DNA, histones, protamines and epigenetics. *Reproduction*, **2010**, 139(2), 287-301.

[12] S B Rothbart, B D Strahl. Interpreting the language of histone and DNA modifications. *Biochim Biophys Acta.*, **2014**, 1839(8), 627-43.

[13] Howard Cedar, Yehudit Bergman. Linking DNA methylation and histone modification: patterns and paradigms. *Nat Rev Genet.*, **2009**, 10(5), 295-304.

[14] C W Dieffenbach, T M Lowe, G S Dveksler. General concepts for PCR primer design. *PCR Methods Appl.*, **1993**, 3(3), 30-7.

[15] K Ishii, M Fukui. Optimization of annealing temperature to reduce bias caused by a primer mismatch in multitemplate PCR. *Appl Environ Microbiol.*, **2001**, 67(8), 3753-5.

[16] X Yang, Y Tang, S M Traynor, F Li. Regulation of DNA Strand Displacement Using an Allosteric DNA Toehold. *J. Am. Chem. Soc.*, **2016**, 138(42), 14076–82.

[17] D Y Zhang, E Winfree. Control of DNA Strand Displacement Kinetics Using Toehold Exchange. *J. Am. Chem. Soc.*, **2009**, 131(47), 17303–14.

[18] S Nakamura, H Kawabata, K Fujimoto. Sequence-specific DNA photo-splitting of 3-cyanovinylcarbazole using DNA strand displacement. *Chem Lett.*, **2016**, 45(8), 887-9.

[19] Kenzo Fujimoto; Hung Yang, Shigetaka Nakamura. Strong inhibitory effects of antisense probes on gene expression through ultrafast RNA photo-crosslinking. *Chemistry An Asian Journal*, **2019**, 14 (11), 1912-16.

[20] Kenzo Fujimoto, Nanami Watanabe. Fluorescence In Situ Hybridization of 16S rRNA in Escherichia coli Using Multiple Photo-Cross-Linkable Probes. *ChemistrySelect*, **2020**, 5(46), 14670-6.

[Chapter 5] General conclusion

Artificial enzymes that cut and edit DNA and RNA, such as CRISPR-Cas9, have attracted a great deal of attention. However, due to off-target effects and limitations of the reaction conditions, there are issues with operability. Therefore, we have developed the following method. Artificial ODNs have been developed as a non-enzymatic nucleic acid editing technique. Artificial ODNs have high sequence selectivity and few restrictions on reaction conditions. They are less stable than enzymes because their reaction and regulatory efficiencies depend on hydrogen bonding. In this study, we developed a spatiotemporally controllable nucleic acid cleavage tool that does not depend on hydrogen bonding. The thermally irreversible structure using ^{CNV}K enables reactivity and precise control, which has been a challenge for artificial ODNs. The results of this research are summarized below for each chapter.

[Chapter 2]

In Chapter 2, we attempted to control the activity of DNAzyme triggered by photo with the aim of developing nucleic acid drugs *in vivo*. By introducing ^{CNV}K into a part of DNAzyme, we succeeded in completely inhibiting the invasion of the substrate strand by covalent bond. The covalent bond was also resistant to exonuclease degradation and maintained a 75% backbone. ^{CNV}K is a photoreversible artificial nucleic acid, and when photolyzed by photoirradiation at 312 nm, it showed 38.0% cleavage activity at 15 min, 10 equal doses. This result has made it possible to control the expression level of mRNA spatiotemporally using ^{CNV}K as a trigger.

[Chapter 3]

Chapter 2 succeeded in inhibiting the translation of mRNA into protein using DNAzyme and ^{CNV}K. In Chapter 3, we aimed to develop an antigene method that inhibits transcription into mRNA by changing the target to DNA. For the purpose of improving the DDI efficiency, the self-photo-cross-link inhibition efficiency (T, ^{CN}U, dS, S) of the antigene probe was compared. The self-photo-cross-link inhibition efficiency increased in the order of S, dS, ^{CN}U, and T, demonstrating the effectiveness of base-free dS and S. Next, when the DDI photo-cross-linking efficiency was compared, it increased in the order of ^{CN}U, T, S, dS. Because no correlation could be confirmed with the self-crosslink inhibition efficiency, the stability of

probe and target DNA related to DDI efficiency was measured. The T_m value measurement showed that the stability was higher in the order of T, ^{CN}U, dS, S. We found that ^{CN}U, which has both high self-photo-cross-link inhibition and high T_m value, has the highest DDI efficiency, and that the balance of the two factors changes the DDI efficiency. Based on these results, we found further improvements in the antigene probe. In the future, it will be necessary to develop a stable artificial nucleic acid that forms hydrogen bonds with the target base and does not have double bonds at the photo-cross-linking position. It is suggested that the absence of double bonds involved in the photoreaction will result in higher efficiency of self-photo-cross-linking inhibition.

[Chapter 4]

Chaper 4 demonstrated the DDI photo-cross-linking to 400 mer sequences for long-range DNA. With the 11bp-5nt DDI probe, a band derived from the photo-cross-linking of the DDI probe with target DNA. First, photo-cross-linking was assessed using 21-CNUK, which was previously discussed in Chapter 3. 11bp-5nt reduced self-photo-cross-linking by designing a more efficient probe. Moreover, The optimum reaction conditions for the photoirradiation time, incubation time, and equivalent were 1 min, 1 h, and 100 eq, respectively. In the future, we would like to design a probe with a different ^{CNV}K position, and verify DDI photo-cross-linking to plasmids and genomic DNA.

The future prospect of this research is to study nucleic acid cleavage and regulation under *in vivo* conditions. For this purpose, it is necessary to conduct research using photo-cross-linking devices with longer wavelengths than ^{CNV}K. In our laboratory, we have already developed an artificial nucleic acid called pyranocarbazole [1], which is photo-responsive at 450 nm. Artificial nucleic acids that recognize counter bases have also been developed to eliminate the off-target effect derived from ^{CNV}K [2]. There are a number of other proposed improvements for in vivo applications, such as using phosphorothioate ODNs to make the probes resistant to enzymatic degradation.

In the future, in order to verify the results of this research *in vivo*, we will target mRNA existing in cells. For example, we want to knock out c-Jun, the pathogenic gene for squamous cell carcinoma, in living cells [3]. In addition, aiming for more accurate control, it is necessary

to use an artificial nucleic acid that exhibits a photoreversible reaction at a longer wavelength than ^{CNV}K.

Moreover, it will be necessary to develop a stable artificial nucleic acid that forms hydrogen bonds with the target base and does not have double bonds at the photo-cross-linking position. It is suggested that the absence of double bonds involved in the photoreaction will result in higher efficiency of self-photo-cross-linking inhibition.

If DDI photo-cross-linking to genomic DNA becomes possible, site-specific cleavage will be possible. As an alternative technology to CRISPR, we are expecting genetic recombination and knockout of target genes. For example, N-myc, the causative gene of rhabdomyosarcoma, can be knocked down or knocked out by DDI photo-cross-linking, which could lead to a radical therapy [4]. In addition, the characteristics of ^{CNV}K will enable various applications such as C to U editing.

References

[1] K Fujimoto, K Ishida, L Xue, S Nakamura. *Photochemical & Photobiological Sciences*, **2020**, 19, 776–82. Effect of linker length on photo-cross-linking position mediated by click chemistry via [2+2]photocycloaddition.

[2] K Fujimoto, S Sasago, J Mihara, S Nakamura. *Org. Lett.*, **2018**, 20, 10, 2802–5. DNA Photo-cross-linking Using Pyranocarbazole and Visible Light.

[3] H Cai, F S Santiago, L Prado-Lourenco, B Wang, M Patrikakis, M P Davenport, G J Maghzal, R Stocker, C R Parish, B H Chong, G J Lieschke, T Wong, C N Chesterman, D J Francis, F J Moloney, R S C Barnetson, G M Halliday, L M Khachigian. *Sci Transl Med*. **2012**, 4(139):139ra82. DNAzyme targeting c-jun suppresses skin cancer growth.

[4] R Tonelli, A McIntyre, C Camerin, Z S Walters, K D Leo, J Selfe, S Purgato, E Missiaglia, A Tortori, J Renshaw, A Astolfi, K R Taylor, S Serravalle, R Bishop, C Nanni, L J Valentijn, A Faccini, I Leuschner, S Formica, J S Reis-Filho, V Ambrosini, K Thway, M Franzoni, B Summersgill, R Marchelli, P Hrelia, G Cantelli-Forti, S Fanti, R Corradini, A Pession, J Shipley. *Clin Cancer Res*. **2012**, 18(3), 796-807.

Achievement

Journal Articles

1. Yasuha Watanabe, Kenzo Fujimoto*
   Complete Photochemical Regulation of 8-17 DNAzyme Activity using Reversible DNA Photo-cross-linking
   ChemBioChem, **2020**, 21, 22, 3244-3248.
2. Kenzo Fujimoto*, Ayumu Hirano, Yasuha Watanabe, Ami Shimabara, Shigetaka Nakamura
   The inhibition effect of photo-cross-linking between probes in photo-induced double duplex invasion DNA.
   Chembiochem. **2021**, 22(24), 3402-3405.

International conferences

1. Yasuha Watanabe, Hung Yang, Shigetaka Nakamura, Kenzo Fujimoto
Photochemical Inhibition of GFP Protein Expression by Ultrafast RNA Photo-cross-linking in GFP-HeLa Cell.
The Commemorative International Symposium of the Japan Society of Nucleic Acids Chemistry, July 2019 in Hyogo

Domestic conferences

1. Yasuha Watanabe, Kenzo Fujimoto.
   OFF-ON switching of DNAzyme activity using reversible photo-cross-linking.
   13th Bio-related Chemistry Symposium, September 2019 in Miyagi. (Poster)
2. Yasuha Watanabe, Shigetaka Nakamura, Kenzo Fujimoto.
   Photo-switching of DNAzyme activity using photoreversible DNA photo-cross-linking.
   Hokuriku Chemical Society of Japan, November 2019 in Ishikawa. (Poster)
3. Yasuha Watanabe, Shigetaka Nakamura, Kenzo Fujimoto.
   Photochemical regulation of DNAzyme activity using reversible DNA photo-cross-linking
   100th The Chemical Society of Japan, March 2020 in Chiba (Poster)
4. Yasuha Watanabe, Kenzo Fujimoto.
   Regulation of DNAzyme activity by reversible DNA photo-cross-linking toward for *in vivo* using.
   14th Bio-related Chemistry Symposium, September 2020 in Online. (Poster)
5. Yasuha Watanabe, Kenzo Fujimoto.
   Regulation of DNAzyme activity by reversible DNA photo-cross-linking toward for *in vivo* using.
   Hokuriku Chemical Society of Japan, November 2020 in Online. (Poster)
6. Yasuha Watanabe, Nanami Watanabe, Kenzo Fujimoto.
   High-sensitivity detection of Escherichia coli 16s rRNA 627-644 region using ultrafast RNA photo-cross-linking
   43th The molecular Biology society of Japan, December 2020 in Online. (Poster)
7. Yasuha Watanabe, Nanami Watanabe, Kenzo Fujimoto.
   Development of a FISH for the difficult-to-detect region of 16S rRNA using ultrafast RNA photo-cross-linking reaction.

Hokuriku Chemical Society of Japan, November 2021 in Online. (Poster, **Best poster award**)

Acknowledgement

Prof. Kenzo Fujimoto has my heartfelt gratitude for his unwavering support and advice in producing high-quality work, as well as for providing a well-equipped study environment that enabled me to complete my research on time.

I would also like to extend my heartiest thanks to Asst. Prof. Shigetaka Nakamura and laboratory member. We received a great deal of support in research consultations and daily life.